UNIVERSITY OF MILANO-BICOCCA

Ph.D. THESIS IN BIOMEDICAL TECHNOLOGIES

(XXVI CYCLE)

Coordinator: Prof. M. Del Puppo

_____

Synthesis and Development of Positron-Emitting Tracers, Labelled with Radiometals (^{68}Ga, ^{89}Zr, ^{90}Y and ^{177}Lu) and Carbon-11, and their Potential Use in Oncology

Supervisor:

Prof. Rosa Maria Moresco

Co-supervisor:

Prof. Hans-Jürgen Machulla

Student:

Elena Maria Andreolli

2013

Abstract

Study of altered metabolism as well as accurate initial diagnosis and determination of the extent of diseases continue to be a major challenge for contribution in understanding the modification that can result in appropriate treatment options, monitoring the effects of therapeutic interventions, and detecting disease after recurrence. Critical for the development of new tracers is the selection of appropriate targets.

Two different molecular targets have been taken into consideration and the thesis can be divided in two main projects:

1) Inflammation and cancer targeting with COX-2 selective inhibitor; the work foresaw the labelling of a COX-2 selective inhibitor with carbon-11 and the subsequent evaluation *in-vivo*.

2) Prostate cancer targeting with PSMA selective ligand; the work foresaw two subprojects:

a) coupling of DUPA-Pep with two different chelating agents and labelling with different radiometals for imaging (^{68}Ga and ^{89}Zr) and therapy (^{90}Y and ^{177}Lu);

b) labelling of mesoporous nanoparticles (MSNPs) for drug delivery into prostate cancer.

<u>Cyclooxygenases-2 (COX-2)</u> is an inducible enzyme involved in the conversion of arachidonic acid (AA) to prostaglandin H2 (PGH2) in the prostanoid biosynthesis. It is associated with cell activation and inflammation and its overexpression *in vivo* is associated with different pathologies (*e.g.* colorectal cancer). 1-(4-fluorophenyl)-3-(2-methoxyethyl)-2-methyl-5-(4-methylsulfonyl)phenyl)-1*H*-pyrrole (VA426) is a selective inhibitor of COX-2 provided by Anzini (University of Siena). The current work foresaw the labelling of VA426 with carbon-11 and its evaluation in an inflammation model. The synthesis of [^{11}C]VA426 was achieved by reacting [^{11}C]methyl iodide with an excess of the corresponding alcoholic precursor VA425 and NaH 60 % (1:10) in DMSO. The radiochemical yield was 21 ± 1.67 % (decay-corrected, based on [^{11}C]CH$_3$I) (n = 3) with a specific radioactivity of 90 ± 54 GBq/μmol (n = 3). The average time of synthesis from

end of bombardment including formulation was 30 min with 97.6 ± 2.6 % radiochemical purity. Preliminary investigation has been performed *in vivo* using BL/6 female mice. Mice treated with LPS, compared with the control, showed more intense uptake at the injection site of the toxin. In particular, it is possible to notice a major distribution in the liver and intestine. Further studies will be performed to evaluate the potential use of this tracer in colorectal cancer cell lines expressing COX-2.

Prostate-specific membrane antigen (PSMA) is a cell surface protein overexpressed in prostate cancer. Due to the specificity of PSMA expression, numerous urea-based ligands have been synthesized until now.

2-[3-(1,3-dicarboxypropyl)ureido]pentanedioic acid (DUPA) showed high specificity and selective tumor uptake. A derivative of DUPA (DUPA-Pep), derived from the linking of DUPA to two phenylalanine residues via 8-aminooctanoic acid (spacer), proved to be a successful imaging ligand with excellent potential for clinical studies.

The current study reports the coupling of DUPA-Pep with desferrioxamine (Df) and CHX-A´´-DTPA and the subsequent labelling with ^{68}Ga, ^{89}Zr for imaging (Df) and ^{90}Y, ^{177}Lu for therapy (CHX-A´´-DTPA), as new PSMA ligands. The labelling of Df-DUPA-Pep was performed at room temperature under neutral condition in 0.25 M HEPES buffer. In both radiosyntheses, the RCYs were higher than 95 % within 10 min, making dispensable any further purification and providing the radiotracers directly applicable for further utilization. Stability of the labelled peptide, in PBS and HS at 37 °C, revealed no decomposition or decreased amount of product as confirmed by radio-HPLC. K_D values and cellular uptake in PSMA-positive cell lines (LNCaP C4-2) were calculated and corresponded to 42.04 ± 4.76 and 29.84 ± 4.82 nM for the ^{68}Ga and ^{89}Zr labelled peptides, respectively. The inhibitor 2-PMPA completely abolished peptide binding, proving the peptide-specificity for PSMA. Study of biodistribution and tumor uptake were also performed in SCID mice implanted with PSMA-positive tumor xenografts. PET/CT images depicted a specific accumulation into the tumor. Further uptake was detected in kidney, bladder and spleen. An average tumor-to-tissue ratio of 26.75 ± 10.4 was

calculated in PSMA-positive tumors. PSMA-negative xenografts showed a tumor-to-tissue ratio of 1.15 ± 0.28.

Labelling of CHX-A''-DTPA-DUPA-Pep was also performed with both ^{68}Ga and ^{89}Zr at room temperature under neutral pH (0.25 M HEPES buffer), providing very high incorporation of ^{68}Ga within few minutes, with a high stability and K_D value at nanomolar concentration. The radiolabelling of the peptide with the therapeutic radiometals (^{90}Y and ^{177}Lu) was performed at room temperature in 0.5 M NH_4OAc buffer at pH 5.5. The incorporation of both radiometals was more than 90 % within 10 minutes. Further studies of stability have to be conducted in PBS and HS at 37°C to verify that the labelled peptide is stable in order to avoid side effects provoked by the free radiometals.

The labelling of MSNPs has been successfully performed with ^{89}Zr. Further experiments have to be made in order to increase the dispersibility into the suspension, through PEGylation. Tumor targeting can be evaluated by attaching DUPA-Pep to the particle surface.

Acknowledgements

Abbreviations

BFC, bifunctional chelator
2-PMPA, 2-(phosphonomethyl)pentanedioic acid
GCPII, glutamate carboxypeptidase II
DIPEA, *N,N*,diisopropylethylamine
DMSO, dimethyl sulfoxide
HS, human serum
NAAG, *N*-acetylaspartylglutamate
NAALADase, *N*-acetylated-α-linked acidic dipeptidase
PBS, phosphate buffered saline
PCa, prostate cancer
PET, positron emission tomography
PSMA, prostate-specific membrane antigen
RCP, radiochemical purity
RCY, radiochemical yield
SA, specific activity
SCID, severe combined immunodeficiency
SD, standard deviation
SPECT, single photon emission computed tomography
TEOS, tetraethoxysilane
TMOS, tetramethoxysilane
Δ, heating

Table of Contents

XIII

List of Figures

XVII

XVIII

List of Tables

List of Schemes

1 INTRODUCTION

1.1 Molecular Imaging

In the last years, the biomedical research has been characterized with development of new diagnostic technologies particularly advanced, indicated as "*Molecular Imaging*".

The concept and practice of *Molecular Imaging* is defined as the visualization, characterization and non-invasive measurement of biological processes at the molecular and cellular levels in humans and other living systems. *Molecular imaging* has attracted interest for decades and originated with targeted radiopharmaceutical. In the table 1 are shown the most common imaging techniques that include, apart from PET and SPECT, magnetic resonance imaging (MRI), MR spectroscopy (MRS), optical imaging and ultrasound imaging (Table 1) (Sinusas, 2008). These techniques, compared with the two first ones, are limited in term of sensitivity and spatial resolution. Moreover, in some cases there is a limit in depth penetration that precludes the visualization in clinical and preclinical models without supplemental approaches (*e.g.* catheter-based optical approaches).

Table 1. Characteristics of imaging techniques.

Imaging modality	Spatial resolution	Depth of penetration	Sensitivity (mol/L)	Molecular probe
PET	2 to 4 mm	No limit	10^{-10} to 10^{-12}	ng
SPECT	6 to 8 mm	No limit	10^{-5} to 10^{-6}	ng
Optical				
bioluminescence	3 to 5 mm	1 to 2 mm	10^{-15} to 10^{-17}	ng to µg
fluorescence	2 to 3 mm	< 1 mm	10^{-9} to 10^{-12}	ng to µg
FMT	1 to 3 mm	< 5 cm	10^{-6} to 10^{-12}	µg
MRI	50 to 250 mm	No limit	10^{-3} to 10^{-5}	µg to mg
X-Ray, CT	25 to 150 mm	No limit	-	mg
Ultrasound	30 to 500 mm	mm to cm	10^{-6} to 10^{-9}	µg to mg

PET indicates positron emission tomography; SPECT, single photon emission tomography; FMT, fluorescence molecular tomography

The emergence of *Molecular Imaging* is a result of the impressive development in chemistry, biology, physics and engineering, and the application of imaging probes and technologies in clinical medicine has been extensive since it allows diagnosing diseases,

prescribing treatment and non-invasively monitoring treatment effectiveness. Moreover, drug discovery in the pharmaceutical sciences has changed thanks to these more cost effective techniques to evaluate the efficacy of a drug candidate. This targeted imaging is defined in terms of the detection of an interaction between a probe and a target. Localization and quantification of the probe is directly related to the interaction of the probe with the target epitope or peptide. The main field of application of Single Photon Emission Computed Tomography (SPECT) and the Positron Emission Tomography (PET) are oncology, cardiology and neurology. However, severe efforts are dedicated also to psychiatric disorders and inflammation. Compared to its single-photon analogue, PET exhibits higher resolution (2–4 mm or lower compared to 6–8 mm for SPECT) and higher sensitivity (up to $\sim 10^{-12}$ M, compared to 10^{-6} M for SPECT) (Zeglis and Lewis, 2011). The resolution and sensitivity of PET are tied to the intrinsic properties of β^+ emission. Firstly, the resolution depends on the initial distance the β^+ travels before annihilation; this distance is dependent on the decay energy. Hence, lower energy β^+ emission is more desirable in PET in order to give better resolution. Secondly, high sensitivity is a result of the coincidence detection of two γ-rays (Ramogida and Orvig, 2013).

Differently from Nuclear Magnetic Resonance (NMR) and Computerized Axial Tomography (CAT), that typically provide morphologic and anatomic images, PET provides molecular information thus allowing to highlight the biological properties of an organ or apparatus and consequently the insurgence of a pathological condition as result of modifications in that function. For these reasons, rather than the PET instrument only, the integrated PET/CT scan (Computerized Tomography) has been developed in order to provide both anatomic and functional information, necessary to identify and characterize one or multiple cancer sites.

As described below, Fluoro-Deoxy-Glucose, also known as [^{18}F]FDG, is the mostly used radiopharmaceutical in oncology, as it permits a fairly good diagnosis of the staging and localization of tumors in the body. However, major uncertainties in image interpretation are reported particularly in the abdomen inspection, where there are no clearly identified anatomical structures. In such case, it is mandatory the integration of the

PET with the CT, in order to enable a more accurate identification of the anatomical structures and sites of tumors or metastases.

Besides the applications in oncology, PET and SPECT provided a significant contribution in the study and analysis of some important neurodegenerative diseases, such as Parkinson's disease, Alzheimer's disease and other Central Nervous System disorders. In fact, several diseases are correlated to functional alteration of the neurotransmission systems or to alterations of the cerebral receptor density.

Also in this case, PET and SPECT can be used for an early diagnosis of these pathologies, for the evaluation of disease's progression or of the effectiveness of a specific therapeutic strategy, facilitating a more appropriate therapeutic planning.

1.2 Positron Emission Tomography (PET)

PET is a nuclear medicine imaging technology that uses positron-labelled molecules in very low mass amounts (trace dose) to image and measure the function of biological processes with minimal disturbance. Measuring without disturbing the biological process is, of course, a fundamental and biologically important aspect of this tracer techniques (Phelps, 2000). This approach can give a better understanding of the biological characteristics of the examined pathology (*e.g.* tumors, cardiovascular and neurodegenerative diseases). The phenomenon of emitting a positron (β^+), which is defined as the antimatter particle of an electron, allows the unstable isotope to shed some of its unnecessary positive charge transforming the atom into a more stable atomic form. Once a positron has been emitted, it travels a small distance, dictated by the amount of energy the particle has been emitted with (0.5 - 2 mm), from its origin and then encounters an electron, which are plentiful in comparison to the number of positrons (Nolting, 2012). Annihilation occurs from this collision of matter and antimatter, which produces two gamma rays (γ-rays) of 511 keV that travel along a "line of coincidence" at nearly 180° out through the body (Czarnecki and Karshenboim, 1999). These two gamma rays (γ-rays),

detected as a coincident event of thousands of such coincident events by a series of detectors arranged into a circular ring, allow the reconstruction of a 3-dimensional image which contains information about radiotracer distribution and concentration in the body (Figure 1 and 2).

The PET detectors consist of an array of scintillation crystals made of bismuth germinate (BGO), lutetium oxyorthosilicate (LSO) or gadolinium silicate (GSO) and are optically coupled to several photomultipliers (Townsend, 2004).
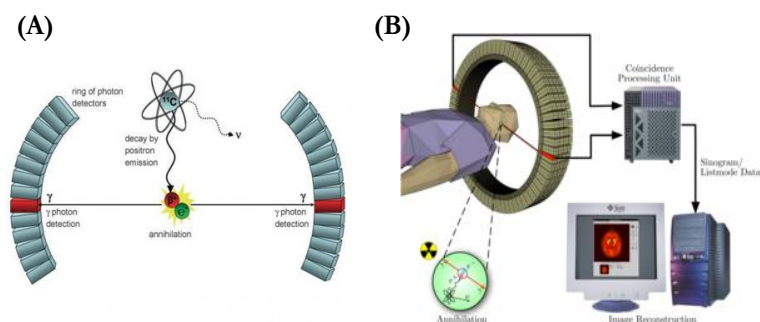
Figure 1. (A) The positron decay and annihilation and (B) detection of coincidence events and images reconstruction.

1.3 PET Radionuclides

Positron-emitting radionuclides are radioisotopes for diagnostic applications in PET and particular requirements need to be satisfied:

✓ half-life suitable with the biological process which is intended to study;

✓ easy and rapid production, in a reasonable activity;

✓ principle decay by positron emission (other types of emission are not useful for image generation and represent useless absorbed dose for patient *e.g.* electron capture).

Table 2 reports the traditional radioisotopes used. These radionuclides have been developed for incorporation into small molecules due to the attractive circumstance that are isotopes of elements naturally present in organic biomolecules and consequently the biological process studied is not disturbed (Pascali *et al.*, 1999).

Table 2. The most commonly used short-lived radionuclides in PET, their half-lives, nuclear reactions, target products, and decay product. (Holland *et al.*, 2010).

Radionuclide	Halflife	Nuclear Reaction	Target Material	Product	Decay Product
^{11}C	20.39 min	^{14}N$(p,\alpha)^{11}$C	$N_2(+O_2)$	$[^{11}C]CO_2$	^{11}B
			$N_2(+H_2)$	$[^{11}C]CH_4$	
^{13}N	9.97 min	^{16}O$(p,\alpha)^{13}$N	H_2O+EtOH	$[^{13}N]NH_3$	^{13}C
^{15}O	122.24 s	^{15}N$(p,n)^{15}$O	$N_2(+O_2)$	$[^{15}O]O_2$	^{15}N
^{18}F	109.77 min	^{20}Ne$(d,\alpha)^{18}$F	Ne$(+F_2)$	$[^{18}F]F_2$	^{18}O
		^{18}O$(p,n)^{18}$F	$[^{18}O]H_2O$	$[^{18}F]F^-$	

These positron-emitting nuclides can be generated in a cyclotron by irradiation of specific target materials, suitable for the production of the required radioisotope, with accelerated charged particles (*e.g.* protons, deuterons and alphas) with required energy range to produce the specific nuclear reaction (*e.g.* 8-19 MeV for ^{11}C, ^{13}N, ^{15}O and ^{18}F species, Figure 2). The target material is a stable isotope usually added with secondary component that allows to obtain a product easy to use in the next step of the radiosynthesis (*e.g.* ^{14}N$_2$ is the stable isotope for ^{11}C production; if the added component is oxygen, carbonic anhydride will be obtained ($[^{11}C]CO_2$) while in the case of hydrogen addition, carbon-11 will be obtained as methane ($[^{11}C]CH_4$)).
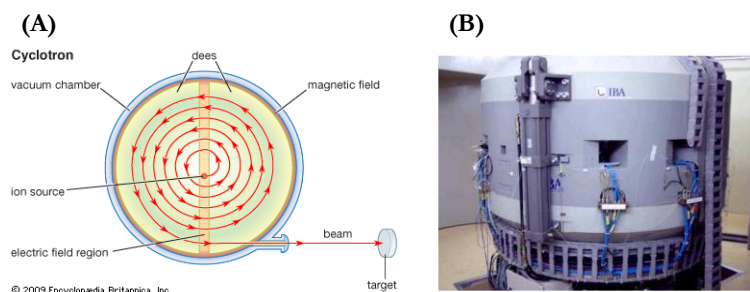
Figure 2. (A) Particles accelerated into the cyclotron; (B)18 MeV cyclotron (Cyclone 18/9 MeV, IBA).

Once produced, the radioisotope can be directly used as produced in the target or converted into another precursor that subsequently will be introduced into biomolecule precursors, as shown below in the case of carbon-11 (Figure 3) (Volterrani *et al.*, 2010).
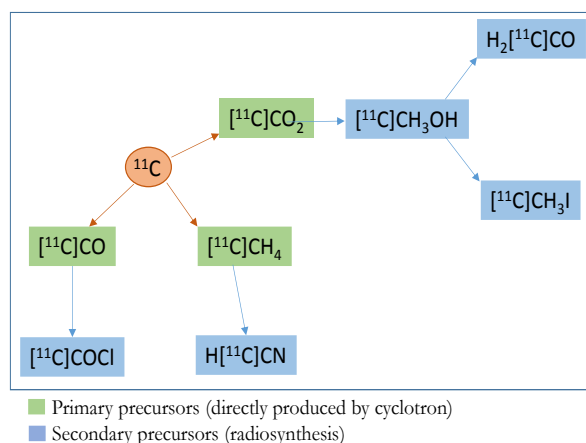
Figure 3: Primary and secondary precursors of carbon-11.

As mentioned before, the time scale of the biological process should be suitable with the half-life of the radionuclide used for tracer labelling. For example, oxygen-15 ($t_{1/2}$= 2.05 min) is the shortest-lived positron emitting isotope of oxygen and $[^{15}O]H_2O$ is used for short biological process in PET studies such as blood flow (Brunberg *et al.*, 1994). For clinical applications, fluorine-18 is the most widely used radioisotope due to its unique energy and emitting characteristics with relatively long half-life. Fluorine-18 can be incorporated into a large variety of organic compounds and forms strong covalent bond with carbon atom (Sandford *et al.*, 2007). The introduction of a fluorine atom into biological molecules to substitute hydroxyl group or hydrogen atom does not change the biological behaviour of the molecule due to its small size and little steric alterations in the molecule (Fletcher *et al.*, 2008). The development of biological targeting agents such as proteins, peptides, antibodies and nanoparticles, with a wide range of biological half-lives, requires the use of radionuclides with half-lives complementary with their biological properties. The table below reports a series of radionuclides and their physical characteristics, that have to be taken into consideration for choosing the suitable radionuclide for monitoring a defined biological process (Table 3) (Wadas *et al.*, 2010).

Table 3. Important positron emitters and their nuclear data.

Radionuclide	Half-Life	Decay Mode (%)	E_b^+ max (KeV)
Organic			
^{11}C	20,4 min	β^+ (99.8), EC (0.2)	960
^{13}N	9,96 min	β^+ (100)	1190
^{15}O	2,03 min	β^+ (99.9), EC (0.1)	1720
^{30}P	2,5 min	β^+ (99.8), EC (0.2)	3250
Analogue			
^{18}F	109.6 min	β^+ (97), EC (3)	635
^{75}Br	98 min	β^+ (75,5), EC (24,5)	1740
^{76}Br	16.1 h	β^+ (57), EC (43)	3900
^{73}Se	7.1 h	β^+ (65), EC (35)	1320
^{120}I	1.35 h	β^+ (64), EC (36)	4100
^{124}I	4.18 d	β^+ (25), EC (75)	2140
Metallic			
^{38}K	7.6 min	β^+ (100)	2680
^{62}Cu	9.7 min	β^+ (98), EC (2)	2930
^{64}Cu	12.7 h	β^+ (18), β^- (37), EC (45)	655
^{68}Ga	68.3 min	β^+ (90), EC (10)	1900
^{82}Rb	1.3 min	β^+ (96), EC (4)	3350
^{86}Y	14.7 h	β^+ (34), EC (66)	1300
^{94m}Tc	52 min	β^+ (72), EC (28)	2470
^{72}As	26 min	β^+ (88), EC (12)	2515
^{89}Zr	78.4 h	β^+ (23), EC (77)	900

1.4 Radiometals

Traditional PET isotopes, such as ^{18}F and the so-called "bionuclides" ^{11}C, ^{13}N and ^{15}O, have been developed for incorporation into small molecules; however, the use of these agents were limited due to their short half-lives and rapid clearance so only early time points were available for imaging, leaving the investigation of biological processes,

which occur over the duration of hours or days, difficult to explore. With the continuing development of biological targeting agents (*i.e.* proteins, peptides, antibodies and nanoparticles), a need arose to produce new radionuclides with half-lives compatible with the biological process under monitoring. As a result, the production and radiochemistry of radiometals such as Ga, Zr, Y, Lu and others have been studied, since they have the potential to combine their favourable decay characteristics with the biological characteristics of the targeting molecule and to become a useful radiopharmaceutical (Wadas *et al.*, 2010).

1.4.1   Gallium-68

^{68}Ga ($t_{1/2}$ = 67.71 min, β^+: 89 %, E_{β^+max}, 1.9 MeV; EC: 11 %, $E_{\gamma\,max}$: 4.0 MeV) is an important positron-emitting radiometal. An important characteristic of this positron-emitting radionuclide is its cyclotron-independent availability via the ^{68}Ge/^{68}Ga radionuclide generator system, which contains the parent radionuclide ^{68}Ge ($t_{1/2}$ = 270.95 days) that, by electron capture decay, produces the short-lived ^{68}Ga ($t_{1/2}$ = 67.71 min), which subsequently decays to stable ^{68}Zn. The parent radionuclide ^{68}Ge is accelerator produced on Ga_2O_3 targets by a (p,2n) reaction.
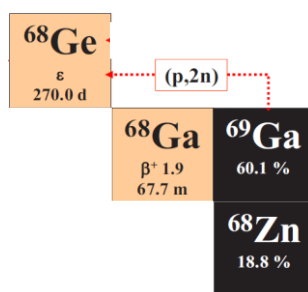
Figure 4. Production route and decay mode of ^{68}Ge and ^{68}Ga.

^{68}Ga is an excellent positron emitter, with 89 % positron emission. There are various generators that used organic and inorganic matrix; Schuhmacher and Maier-Borst prepared a pyrogallol-formaldehyde copolymer for elution with 5.5 M HCl, taking

advantage of the stable complex that Ge^{IV} forms with phenolic groups (Schuhmacher *et al.*, 1981). As inorganic matrix, it is worth to mention aluminium oxide (Al_2O_3) or zirconium oxide (ZrO_2), for elution with complexing agent like EDTA obtaining [^{68}GaEDTA]$^-$ complex (Greene *et al.*, 1961), tin dioxide-based and titanium dioxide-based matrix, for elution with diluted hydrochloric acid (1 M to 0.1 M) to obtain ^{68}Ga^{3+} (Cyclotron Co, Obninsk, Russia).

However, there are drawbacks, including ^{68}Ge breakthrough, large eluate volume, high HCl concentration and the presence of metallic impurities such as Zn^{2+}, Ti^{4+} and Fe^{3+} and/or organic residuals of matrix materials, which can lead to difficulties in synthesizing the ^{68}Ga radiopharmaceutical (Wadas *et al.*, 2010).

Thus, dedicated procedures to process the initial radionuclide generator eluate need to be applied to minimize the impurities and to increase the ^{68}Ga concentration.

Research groups have explored the purification protocols, among all anion- and cation-exchange microchromatography (Meyer*et al.*, 2004; Zhernosekov *et al.*, 2007) and fractionation (Breeman *et al.*, 2005).

1.4.1.1 *Aqueous and coordination chemistry Gallium-68*

The chemical equilibria in a solution are a crucial point for radiopharmaceuticals based on coordination complexes of metal ions, as it can affect their behaviour *in vivo*.

The only oxidation state of gallium in aqueous solution is +3. The aqueous chemistry of gallium is dominated by its strong tendency to hydrolyze; the hydrolysis can be represented by Equations 1-4:

$$[Ga]^{3+} \quad + H_2O \ = \ [Ga(OH)]^{2+} \ + H^+ \qquad (1)$$
$$[Ga(OH)]^{2+} \ + H_2O \ = \ [Ga(OH)_2]^{+} \ + H^+ \qquad (2)$$
$$[Ga(OH)_2]^{+} \ + H_2O \ = \ [Ga(OH)_3] \ + H^+ \qquad (3)$$
$$[Ga(OH)_3] \quad + H_2O \ = \ [Ga(OH)_4]^{-} \ + H^+ \qquad (4)$$
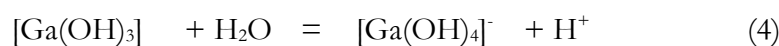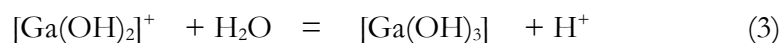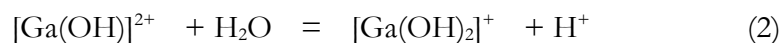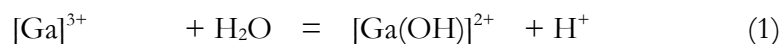
The fully hydrate (hexaaquo) Ga^{3+} ion is only stable under acidic conditions. Raising the pH, the predominant species is $[Ga(OH)_3]$ between pH $4.5 - 6$. At pH 4 $[Ga(OH)_2]^+$ is the main species in solution. At pH > 6 $[Ga(OH)_4]^-$ is predominant as shown in the figure below.
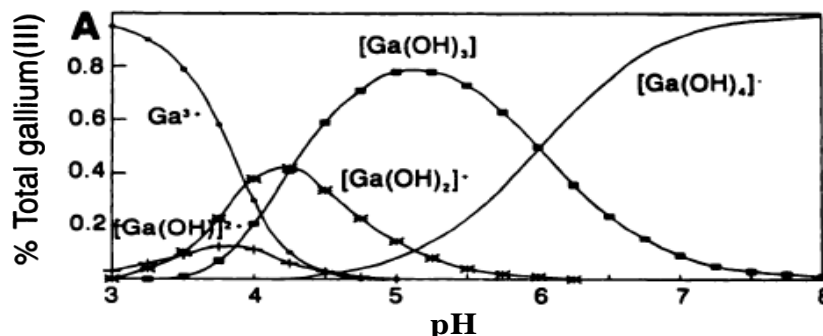
Figure 5. Speciation of a 10^{-9} M gallium(III) aqueous solution (Source: Jackson and Byrne, 1996).

At physiological pH 7.4, the predominant species is gallate $[Ga(OH)_4]^-$ and some $[Ga(OH)_3]$.

Based on Pearson´s Hard-soft Acid-base theory, Ga(III) is a hard acid, due to its high charge density. As a classic hard acidic cation, Ga(III) is strongly bound to ligands featuring multiple anionic oxygen donor sites, although it has also been shown to have good affinity for thiolates. Typically, chelators have been developed to sequester Ga(III) up to its maximum coordinate number of 6 in a pseudo-octahedral geometry.

An important chelating agent in physiological systems is the biological iron transporter transferrin (TF). TF occurs in plasma at a concentration of approximately $2x10^{-5}$ M and is critical for stability of potential gallium radiopharmaceuticals because of transchelation of the complexed gallium to the transferrin iron binding sites, which also show high affinity for Ga^{3+}. Therefore, radio-gallium chelator complexes must be sufficiently inert to transchelation to have efficacy for *in vivo* applications. Polydentate acyclic and macrocyclic chelators are suitable for stable complexation of Ga^{3+}. The

preferred coordination number is six although several chelates have been reported which are stable *in vivo* and have lower coordination number *i.e.* four or five.

1.4.2 Zirconium-89

Zirconium is a transition metal in Group IVB of the periodic table. ^{89}Zr ($t_{1/2}$ = 78.4 h, β^+: 23 %, $E_{\beta^+ max}$: 901 KeV; EC: 77 %, $E_{\gamma\ max}$: 909 KeV) was produced from the ^{89}Y$(p,n)^{89}$Zr nuclear reaction by proton bombardment of commercially available, high-purity (99.9 %, 0.1 mm thick) ^{89}Y-foil on a small cyclotron. It decays to the stable isotope ^{89}Y. ^{89}Zr was purified from the ^{89}Y target material by use of a hydroxamate resin. After oxidation of the ^{89}Zr to the M^{4+} oxidation state, it was separated from other possible metal impurities such as ^{89}Y, ^{88}Y, ^{65}Zr, ^{48}V and ^{56}Co using an anion exchange column chemically modified with hydroxamate groups. Hydroxamate was chosen because of its ability to form complexes with ^{89}Zr under highly acidic conditions, which allows the ^{89}Zr to be retained in the column while the other metal impurities are removed with highly concentrated HCl. Then, the purified ^{89}Zr can be eluted in high yield using 1 M oxalic acid (Meijs *et al.*, 1994, Verel *et al.*, 2003 and Holland *et al.*, 2009). [^{89}Zr]Zr-oxalate solution in 1.0 M oxalic acid can be then loaded onto an activated Waters Sep-Pak Light QMA (strong anion exchange cartridge), washed with trace selected water and then eluted using 1 M HCl to obtain [^{89}Zr]Zr-chloride (Holland *et al.*, 2009).

1.4.2.1 Aqueous Zirconium(IV) Coordination Chemistry

As a group 4 second row transition metal, zirconium forms an extremely acidic hydrated Zr^{4+} cation with a small radius of 59–89 pm (CN 4–9) (Shannon, 1976). Hydrated Zr(IV) likely exists only at high dilution in very acidic solutions and tends to form multiple monomeric, as well as polynuclear oxo/hydroxy species are believed to be present before onset of precipitation as the pH is raised (Wadas *et al.*, 2010). The extremely hard character

of Zr(IV) means it prefers to form complexes with multidentate ligands with hard donor atoms such as anionic oxygen from carboxylic acid or phosphinic acid residues, and prefers to form octadentate complexes. In the neutralized [^{89}Zr]Zr-oxalate preparation, Zr^{4+} is probably octachelated by four oxalates, resulting in an overall charge of -4. Moreover, Zr^{4+} forms an insoluble salt with the phosphate and precipitates in water. The high affinity of Zr^{4+} to phosphonate is also in line with the bone uptake results observed for [^{89}Zr]Zr-chloride when injected into mice. In fact, this affinity seems to be so strong that only a couple of percent of the bone activity is released and cleared from the body after 6 days (Abou *et al.*, 2011).

1.4.3   Yttrium-90

^{90}Y ($t_{1/2}$ = 64.1 h, β^-: 100 %, E_{β^-max}: 2.28 MeV) is a radionuclide generator product resulting from the decay of its 28 yr parent strontium-90 (^{90}Sr), which is produced in nuclear fission. It is often believed to be among the most useful of the radionuclides that have been considered for radioimmunotherapeutic applications, due to the following characteristics (Chinol and Hnatowich, 1987):

1.   half-life (64 hr) consistent with the rate of antibody accumulation in tumor;
2.   no accompanying gamma-ray radiation in its decay;
3.   beta rays of intermediate energy;
4.   stable daughter (^{90}Zr);
5.   simple chemistry and strong complexing with chelating agents.

^{90}Y of very high specific activity is required for the preparation of labelled peptides and antibodies used for targeted therapy and separation has to be performed from other species and from the long-lived parent. In fact, low level of ^{90}Sr contamination is essential for therapeutic application, cause ^{90}Sr localizes in the skeleton and has very low maximum permissible body burden of 74 KBq (2 µCi), due to its long half-life (U.S. Department of Commerce, 1959). In addition, other trace metals can interfere in the ^{90}Y antibody radiolabelling process, giving low radiolabelling yields. Separation methods involve

techniques such as precipitation (Salutsky and Kirly, 1955), solvent extraction (Wike *et al.*, 1990), ion exchange (Skraba *et al.*, 1978), extraction chromatography (Hsieh *et al.*, 1993), liquid membrane (Happel *et al.*2003) and electrochemical methods (Chakravarty *et al.*, 2008). Currently, ^{90}Y is obtained not from in-house generators, but from commercial sources and is separated by industrial manufacturers and supplied as a radiochemical in inorganic form to the radiopharmacies. ^{90}Y has been used successfully with several antibodies in radioimmuotherapy (RIT), but has a severe myelotoxicity. It is more appropriate in the treatment of larger tumor lesions and may not be suitable for smaller tumor or micrometastatic disease.

1.4.3.1   *Aqueous Yttrium(III) Coordination Chemistry*

Aqueous yttrium chemistry is often discussed together with that of the lanthanides because of their common tricationic state and similar ionic radii. Yttrium (III), 90-108 pm (CN 6-9), is significantly large and can readily reach high coordination numbers of 8 and 9 in its complexes. With a closed-shell electron configuration, it is also considered a harder acidic cation than Ga(III) (Wadas et al., 2010). In fact, the Y^{3+} metal ions show a hard acidic character and tend to form complexes with hard donor atom ligands. Therefore, the labelling of peptides has been performed using mainly polyaminocarboxylic ligands (Correia *et al.*, 2011).

1.4.4   *Lutetium-177*

^{177}Lu ($t_{1/2}$ = 6.73 d, β^-: 78.6 %, $E_{\beta^- max}$: 498 KeV; EC: 6.4 and 11 %, $E_{\gamma max}$: 113 and 210 KeV, respectively) is another radiometal applied for therapy but also for diagnosis since it owns a moderate gamma emission. There are currently two methods available to produce ^{177}Lu: direct and indirect. ^{177}Lu can be produced with relatively high specific activity directly by neutron capture of enriched Lutetium-176 (^{176}Lu(n,y)^{177}Lu). Because of the relatively

low (2.6 %) natural abundance, enriched lutetium-176 (*i.e.* >70 %) target material is required for this production route. Moreover, only about 20 % of the ^{176}Lu atoms are converted to ^{177}Lu and the long-lived impurity ^{177m}Lu (half-life = 160 days) is also produced in small quantities. As an alternative production route, carrier-free ^{177}Lu can be obtained from beta decay (indirect production) of Ytterbium-177 (half-life: 1.9 hr) produced by neutron capture of enriched Ytterbium-176 (^{176}Yb(n,y)^{177}Yb) (IAEA-TECDOC-1340, 2003). The advantage of this second reaction is that this production route avoids long-lived ^{177m}Lu. Chemical separation of the ^{177}Lu from the Yb target results in a high specific activity ^{177}Lu that can be used for radiotherapy (Ketring *et al.*, 2003). In the last few years, ^{177}Lu has been increasingly replacing ^{90}Y owing to the low energy of the β^- particles that results in the majority of the dose remaining localized in small areas. Thus, ^{177}Lu is associated with a reduced radiation exposure of the bone marrow and other normal organs so it is more appropriate for smaller, soft tumor and metastatic disease than ^{90}Y and in minimizing kidney dose. Moreover, the contemporary β^- and γ emission of ^{177}Lu makes it suitable both for therapeutic and diagnostic purposes.

1.4.4.1 *Aqueous Lutetium(III) Coordination Chemistry*

Lutetium belongs to the lanthanide group and, although Lu is the heaviest member of the lanthanides, the ionic radius of Lu^{3+} is expected to be comparable to that of Y^{3+} as the result of lanthanide contraction. In coordination number 6, the ionic radius of Lu^{3+} is 86.1 pm, ~ 4 pm smaller than that of Y^{3+}. Its most common oxidation state is +3, and it has a coordination number of 9. The behaviour of these two metals, yttrium and lutetium, is similar and lutetium tends to form complexes mainly with polyaminocarboxylic ligands (Correia *et al.*, 2011).

1.5 Chelating Agents

The utility of the previously described metallic radionuclides has necessitated the development of metal chelating agents to effectively provide a handle over their behaviour. These chelating agents have been termed "bifunctional chelating agents" (BFC) since they have a metal binding moiety function and a chemically reactive functional group. The former provides the sequestration of the metallic radionuclide while the latter offers the required chemistry for covalent attachment to a targeting vector of interest, such as small molecules peptides (octreotide), proteins (monoclonal antibody, Zevalin), or nano-particles.

There are several fundamental *criteria* that have to be consider in the design of bifunctional chelating agents for such applications. Foremost, the stability of the metal complex is one of the most important. Clearly, the consequences of loss or dissociation of the radionuclide from the complex are associated with toxicity in the case of therapeutics and poor image qualities for diagnostics (Brechbiel, 2008).

Fundamental coordination chemistry *criteria* are:
  i.   charge;
  ii. matching cavity size of the chelating agent with the ionic radius of the radionuclide;
  iii. appropriate chelate denticity;
  iv. donor binding groups of appropriate chemical character;
  v.   the rate of metal complex formation and the rate of dissociation.

Every radiometal is different regarding its own properties and coordination chemistry, so, unfortunately there is no bifunctional chelating agent suitable for all radionuclides (Brechbiel, 2008). Common chelates utilised in radiopharmaceuticals can be grouped into two classes:
  i.   acyclic (open chain);
  ii. macrocyclic (closed chain).

Generally, acyclic chelates are less kinetically inert than macrocyclic complexes, even when thermodynamic stability (KML) is comparable (Wadas *et al.*, 2010); however, recent

reports in the literature show good examples of acyclic chelators that exhibit both high thermodynamic stability with a specific metal and excellent kinetic inertness *in vitro* (Price *et al.*, 2012). Acyclic chelators typically have faster metal-binding kinetics compared to macrocyclic analogues, a significant advantage for shorter-lived isotopes.

Below, brief discussions of the most common chelators used in radiopharmaceutical applications are presented (Tables 4 and 5) (Ramonigida and Orvig, 2013).

Thereafter, validation of the suitability of bifunctional chelating agent for biological applications has to be executed. There are numerous properties that can be used to validate acceptability of a new bifunctional chelating agent, including:

   i.   thermodynamic stability constants;
   ii.   transchelation studies;
   iii. acid catalyzed dissociation constants;
   iv.   serum stability studies.

All of these properties do provide some information that can be used to suggest potential *in vivo* suitability. Serum stability can be a very useful tool and model that serves to predict and eliminate from contention those bifunctional chelating agents that are unsuitable for *in vivo* applications. None of these properties or models is predictive of actual *in vivo* stability of the metal complex. To assess real *in vivo* stability of the metal complex, the evaluation in an appropriate animal model is necessary (Brechbiel, 2008).

1.5.1   Acyclic chelators

Historically, one of the earliest reports of a bifunctional chelating agent conjugated to an antibody made use of a natural product, desferrioxamine (Df), for radiolabelling with [111]In (Pritchard *et al.*, 1976). Desferrioxamine is a well known chelator of Fe(III), and as such its derivation for use with In(III) and Ga(III) and also Zr(IV) has precedence. It has three hydroxamate groups for chelating metals and a terminal primary amine that can be used for conjugation to biomolecules. Due to the similarities between Fe(III) and Ga(III),

Df also forms gallium complexes of high thermodynamic stability and has proven to be useful for conjugation to peptides and small molecules. One application of Df lies in its ability to label Zr(IV); it is the most popular choice for zirconium radiochemistry.

Perk *et al.* recently introduced a new bifunctional chelating agent, *p*-isothiocyanatobenzyl-derivative of desferrioxamine B (Df-Bz-NCS), that enables an efficient and rapid preparation of [89]Zr-labelled biomolecules (Perk *et al.*, 2010). Radiolabelling studies using the trihydroxamate ligand desferrioxamine B (Df) gave 100 % radiochemical yields in <15 min at room temperature and *in vitro* stability measurements confirmed that [[89]Zr]Zr-Df is stable with respect to ligand dissociation in human serum for >7 days (Holland *et al.*, 2010). The complexation reaction between [[89]Zr]Zr-chloride or [[89]Zr]Zr-oxalate and the hexadentate tris-hydroxamate chelate Df is shown in Figure 6.
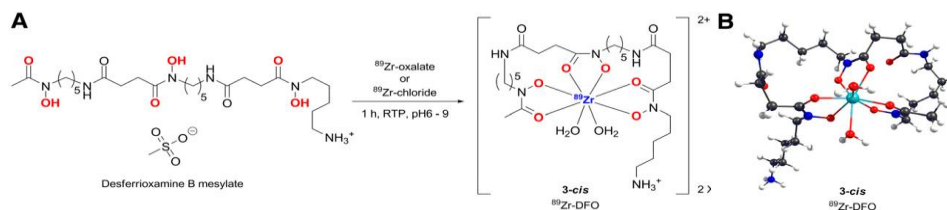
Figure 6. (A) Complexation reaction between $[^{89}Zr(C_2O_4)_4]^{4-}$ and Df. (B) DFT-optimized structure of 8-coordinate complex $[^{89}Zr(HDf)\text{-}cis\text{-}(H_2O)_2]^{2+}$ (3-cis). (Source: Holland *et al.*, 2010).

Small-animal PET imaging studies demonstrated that free [89]Zr(IV) ions administered as [[89]Zr]Zr-chloride accumulate in the liver whilst [[89]Zr]Zr-Df is excreted rapidly *via* the kidneys within <20 min (Holland *et al.*, 2009).

EDTA (N_2O_4) (ethylenediaminetetraacetic acid) and DTPA (N_3O_5) (diethylenetriaminepentaacetic acid) are the most commonly exploited acyclic chelators in radiopharmaceutical chemistry. EDTA derivatives were initially reported for use with ^{111}In and ^{90}Y, their limited stability forced a process to develop bifunctional DTPA derivatives that would provide a more appropriate coordination number. DTPA has been extensively used for labelling a variety of radiometals such as Cu(II) (CN 6, $\log K_{ML}$ = 21.4), Ga(III)

(CN 6, logK$_{ML}$ = 25.5), In(III) (CN 7, logK$_{ML}$ = 29.5), Y(III) (CN 8, logK$_{ML}$ = 22.0) and Zr(IV) (CN 8, logK$_{ML}$ = 35.8), being $K_{ML} = \frac{[ML]}{[M]\cdot[L]}$ (Wadas *et al.*, 2010).
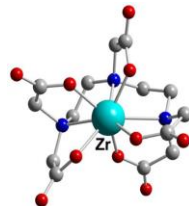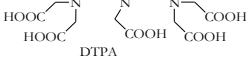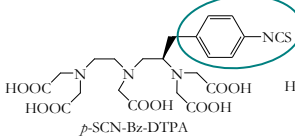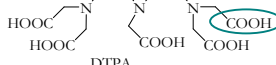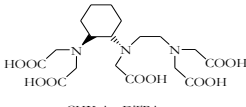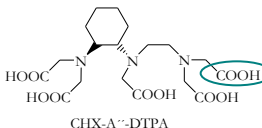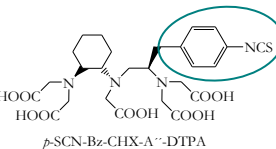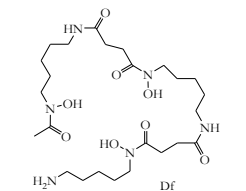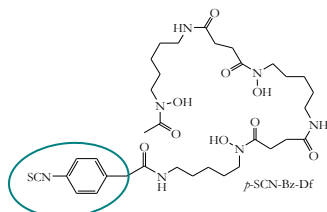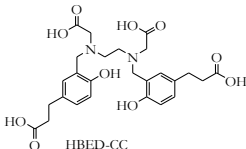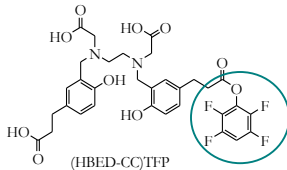
Figure 7. Structure of 8-coordinate complex Zr-DTPA. (Source: Wadas et al., 2010).

Its large binding sphere and hard oxygen donor set make it a good candidate for creating stable metal–ligand complexes with larger hard acidic cations. DTPA has been successfully incorporated into three FDA-approved radiopharmaceuticals (^{111}In based agents OctreoscanTM and ProstaScints, and ^{90}Y agent Zevalin) (Ramonigida and Orvig, 2013). More recently, a modified DTPA chelate, CHX-A´´-DTPA, has shown great promises for In(III), Y(III) and Bi(III) isotopes. CHX-A´´-DTPA incorporates a more rigid chiral cyclohexyl (CHX-A´) fragment into the backbone of DTPA in order to pre-organize the geometry of the donor atoms in hopes of improving kinetic inertness of the resulting metal complex.

Table 4. Selected acyclic chelators and their bifunctional analogues (coupling moiety highlighted in blue).

Chelate	Donor set	Metal ions (log K_{ML})	Bifunctional analogues
DTPA	N_3O_5	Cu(II) (21.4) Ga(III) (25.5) In(III) (29.5) Y(III) (22.0) Zr(IV) (35.8) Bi(III) (35.6)	*p*-SCN-Bz-DTPA, DTPA
CHX-A''-DTPA	N_4O_2	In(III) Bi(III) Ac(III) Lu(III) Y(III)	CHX-A''-DTPA, *p*-SCN-Bz-CHX-A''-DTPA
Df	O_6	Ga(III) (28.6) Zr(IV)	*p*-SCN-Bz-Df
HBED-CC	N_2O_4	Ga(III)	(HBED-CC)TFP

The aminophenolate chelator *N,N'*-bis(2-hydroxybenzyl)ethylenediamine-*N,N'*-diacetic acid (HBED) has a N_2O_4 donor set and its Ga(III) complex has a very high stability constant (logK_{ML} = 38). As a consequence, it has generated considerable interest as a bifunctional chelator. The derivative *N,N'*-bis[2-hydroxy-5-carboxyethyl)-benzyl]ethylene diamine-*N,N'*-diacetic acid (HBED-CC) and its tetrafluorophenyl ester derivative have been described to promote facile coupling to both scFV and anti-Ep-CAM diabodies. Using this BFC, these biomolecules could be labelled with ^{68}Ga to give specific activities of 142 GBq/µmol (Wadas *et al.*, 2010).

1.5.2 Macrocyclic chelators

The popular tri- and tetraaza-based amino carboxylate macrocyclic chelators NOTA (1,4,7-triazacyclononane-1,4,7-triacetic acid) and DOTA (1,4,7,10-tetraazacyclo-dodecane-1,4,7,10-tetraacetic acid), together with their bifunctional derivatives, form a class of "gold standards" that have been extensively used in the labelling of a variety of radiometals for imaging and therapy.
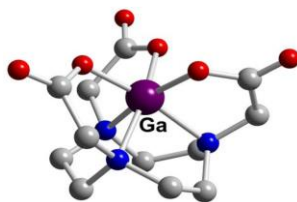
Figure 8. Structure of 6-coordinate complex Ga-NOTA. (Source: Wadas *et al.*, 2010).
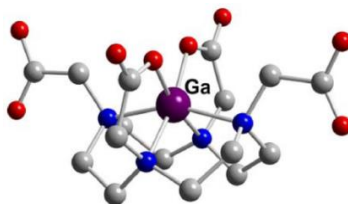
Figure 9. Structure of 6-coordinate complex Ga-DOTA. (Source: Wadas *et al.*, 2010).

NOTA and DOTA are BFCs, one of the pendant carboxylic acid arms can be used in a conjugation strategy to form a peptide bond with a biomolecule. This direct method alters the native binding sphere and donor-ability of the chelators. Alternatively, an extra carboxylic pendant arm is added (to form NODASA/NODAGA and DOTASA/DOTAGA) or a separate conjugation moiety (*p*-SCN-Bz) is incorporated at a position that will minimize the effect on the metal binding ability of the ligand (to form *p*-SCN-Bz-DOTA or *p*-SCN-Bz-NOTA). NOTA (N_3O_3) has the smaller binding pocket of the two; it is most commonly used for gallium(III) isotopes ($\log K_{ML} = 31.0$) (Correia *at al.*, 2011). NOTA has become particularly attractive for Ga^{3+} because of its ability to label gallium isotopes nearly quantitatively at room temperature and the high *in vivo* stability of the resulting complex. DOTA (N_4O_4) and its derivatives play an important role in clinical

applications as they form stable complexes with a variety of trivalent radiometals, such as ^{68}Ga (logK_{ML} = 21.3), $^{86/90}$Y (logK_{ML} = 24.3), ^{111}In (logK_{ML} = 23.9) (Wadas *et al.*, 2010), ^{177}Lu (logK_{ML} = 25.5) and divalent nuclide ^{64}Cu (logK_{ML} = 22.3) (Correia *at al.*, 2011). DOTA has been extensively used for labelling gallium isotopes and is the only clinically used BFC for ^{68}Ga, despite its less than optimal stability and need for heating to label quantitatively. The tetraazamacrocycle TETA (N_4O_4) (1,4,8,11-tetraazacyclotetradecane-1,4,8,11-tetraacetic acid) has been extensively used for Cu(II) radiopharmaceuticals, to bind copper to somatostatin peptides. Cu(II) shares a similar thermodynamic stability with TETA and DOTA (logK_{ML} = 21.9 and 22.3, respectively) although $[Cu(TETA)]^{2-}$ complexes are more kinetically inert compared to $[Cu(DOTA)]^{2-}$, but still suffer from radiocopper loss *in vivo* (Boswell *et al.*, 2008). The cross-bridged macrocyclic ligand CB-TE2A shows to bind copper with high stability; however, labelling CB-TE2A with Cu(II) isotopes requires rigorous heating (>90 °C) and prolonged reaction times (~1h), which is not favourable with thermally sensitive biomolecules (Shokeen and Wadas, 2011).

Table 5. Selected macrocyclic chelators and their bifunctional analogues (coupling moiety highlighted in blue).

Chelate	Donor set	Metal ions (log K_{ML})	Bifunctional analogues		
NOTA	N_3O_3	Cu(II) (21.6) Ga(III) (31.0) In(III) (26.2)	p-SCN-Bz-NOTA	n=1: NOTASA n=2: NOTAGA	NOTA (NO2A)
DOTA	N_4O_2	Cu(II) (22.3) Ga(III) (21.3) In(III) (23.9) Y(III) (24.4) Lu(III) (25.5) Zr(IV) Ac(III)	p-SCN-Bz-DOTA	n=1: DOTASA n=2: DOTAGA	DOTA (DO3A)
TETA	N_4O_4	Cu(II) (21.9) Ga(III) (19.7) In(III) (21.9) Y(III) (14.8) Lu(III) (15.3)	p-SCN-Bz-TETA	TETA	
CB-TE2A	N_4O_2	Cu(II) Ga(III) In(III)	p-SCN-Bz-TE2A	CB-TE2A	

1.6 Radiotracer characteristics

An ideal radiotracer needs to satisfy the following requirements to be administrated into patients:
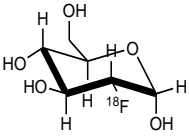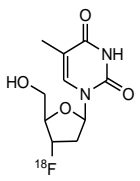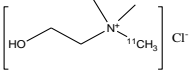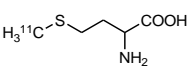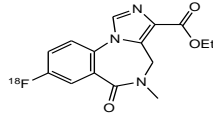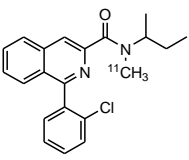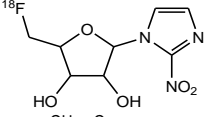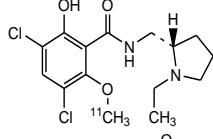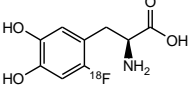
✓ easily relievable during the analysis;

- ✓ not interfering with functional process under investigation;
- ✓ high affinity and selectivity for the target;
- ✓ good permeability across the blood-brain barrier (BBB), critical for CNS study:
  - ○ passive diffusion for lipophilic tracer (1.5<logP<2) (Moerlein *et al.*, 1985);
  - ○ active transport carrier mediated;
- ✓ proper metabolic degradation, that does not produce undesired labelled metabolites, especially in target tissue, that can result in unwanted background signal;
- ✓ high signal to noise ratio;
- ✓ stereochemistry (enantiomerically pure labelled compound when required for the interaction);
- ✓ high specific activity, crucial for tracer addressed to specific molecular target (*e.g.* receptor, enzymes, etc.).

Basically, drugs are designed considering all the aforementioned characteristics and the applicability in PET for *in vivo* measurements occurs according to different mechanisms (Machulla, 2011):

i. binding (specific target; *e.g.* receptor, enzyme, antigens, etc.);

ii. metabolism:

    a. the tracer can follow the metabolic pathway of interest until it is metabolically incorporated ("metabolic trapping"), for which [^{11}C]choline ending in the synthesis of phospholipids is an example;

    b. another one is that of "blocked metabolism", for which [^{18}F]FDG is the classical example where the [^{18}F]substitution of the 2-O atom in glucose blocks further reactions after phosphorylation by hexokinase.

Table 6. Some of the main radiotracers for clinical application.

Radiotracer	Structure	Cellular target	Typical application
[18F]FDG		Glucose metabolism	Oncology, Neurology, Cardiology
[18F]NaF	Na-18F	Bone metabolism	Oncology
[18F]FLT		DNA synthesis (TK1)	Tumor cell proliferation
[11C]Choline		Choline kinase	Oncology
[11C]Methionine		Protein synthesis	Oncology
[11C]Flumazenil		CBR antagonist	Epilepsy
[11C]PK11195		TSPO antagonist	Inflammation
[18F]FAZA		Hypoxia	Oncology – response to therapy
[11C]Raclopride		D2 antagonist	Movement disorders
[18F]DOPA		Pre-synaptic dopamine receptor	Neuroendocrine tumor Movement disorders

In the tables 6 and 7 are reported some of the main radiotracers applied for clinical use. Apart from the classical radiotracers, tracers labelled with radiometals are gaining more and more importance thanks to the great efforts put in the development of new chelating agents. In clinical practice, DOTA is one of the main BFC used. In the table below two radiotracers for neuroendocrine tumors are reported ([68Ga]Ga-DOTATOC and [68Ga]Ga-DOTATATE), which include DOTA as chelating agent for 68Ga.

Table 7. Gallium based radiopharmaceuticals, with DOTA as BFC.

Radiotracer	Structure	Cellular target	Typical application
[68Ga]Ga-DOTATOC		Somatostin receptors (sst)	Neuroendocrine tumors (NETs)
[68Ga]Ga-DOTATATE		Somatostin receptors (sst)	Neuroendocrine tumors (NETs)

2 BACKGROUND

Concerning probes applied for specific targets imaging, two interesting and challenging targets are cyclooxygenase 2 (COX-2) and prostate-specific membrane antigen (PSMA), both applicable in oncological field. These probes may serve as agents for early detection, prognosis and intervention outcome measures.

COX-2 is an inducible enzyme, which plays an important role in inflammation, being the key enzyme required for prostanoid biosynthesis, important mediators of inflammation. Inflammation is a critical component of tumor progression. Many cancers arise from sites of infection, chronic irritation and inflammation. It is now becoming clear that the tumor microenvironment is a crucial participant in the neoplastic process, promoting proliferation, survival and migration. These insights are promoting new anti-inflammatory therapeutic approaches to cancer therapy. Moreover, the association of chronic inflammation with neoplasia combined with the correlation of elevated COX-2 levels with inflammation and premalignancy/cancer progression suggest that COX-2 is a useful imaging target (Ostrov and Contag, 2011). COX-2 is a challenging target because it is a cytoplasmatic enzyme located inside both immune cells and tumor cells. Thus, COX-2 probes have to cross the membrane to reach the target, besides being highly selective for COX-2 over COX-1. Actually, many molecules were synthesized up to now and just the fluorinated agent developed by Uddin *et al.* is under evaluation, proving the difficulty of an effective probes development.

On the other hand, PSMA is a cell surface protein overexpressed in prostate cancer. Due to the specificity of PSMA expression, numerous urea-based ligands have been successfully synthesized until now. In particular, DUPA-Pep, a glutamate-urea-glutamate molecule, showed very promising results. Different chelating agents have been applied (e.g. DOTA, NOTA) with this successful probe and [^{68}Ga]Ga-DOTA-DUPA-Pep gave excellent results in clinic. ABX recently purchased a precursor, bearing DUPA moiety and HBED-CC as chelating agent for ^{68}Ga.

This work aims to apply alternative chelating agents with Dupa-Pep. As the preferred labelling procedure for peptides involves a simple, fast and quantitative labelling step at room temperature, different chelator approaches are highly desired.

These chelators will allow the use of different radiometals, for both diagnostic and, more importantly, therapeutic purposes.

2.1 Cycloxygenases-2 (COX-2): inflammation and cancer

Prostaglandin endoperoxide H synthase (PGHS), also generically known as cyclooxygenase (COX), is the key enzyme required for the conversion of arachidonic acid (AA) to prostaglandin H2 (PGH2) in the committed step of prostanoid biosynthesis (Dong *et al.*, 2011). PGHS catalyses two different reactions, a cyclooxygenase (COX) reaction and a peroxidase (POX) reaction: the oxidation of AA to the hydroperoxy endoperoxide PGG2 and its subsequent reduction to the hydroxy endoperoxide PGH2, respectively. The PGH2 is transformed into the primary prostanoids, PGE2, PGF2, PGD2, PGI2, and TXA2 (Figure 10) (Vane *et al.*, 1998).
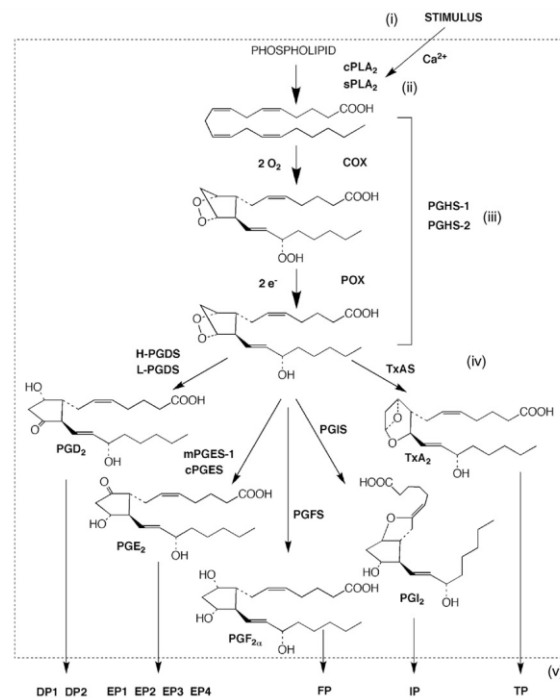
Figure 10. Pathways for prostaglandin synthesis and function (Source: Smith, 2008).

The two known COX isoforms are referred to as COX-1 and COX-2, for the order in which they were discovered (COX-1 discovered in 1971 by Vane and COX-2 discovered in the early 1990s) and are products of different genes. COX-1 expression is

induced during development in some cells, and COX-1 mRNA and COX-1 protein are very stable. As a consequence, COX-1 protein levels remain relatively constant. COX-2 mRNA and protein have relatively short half-lives, so COX-2 is usually present transiently during early stages of cell replication or differentiation and is associated with cell activation and inflammation. COX-2 degradation is programmed to auto-limit the amount of this isoform, and COX-2 overexpression *in vivo* is associated with pathologies, such as colon cancer (Smith, 2008). Thus, basically, COX-1 is constitutively expressed, whereas COX-2 expression is inducible. They share a similar three-dimensional fold and the catalytic mechanism is conserved between isoforms, thus, the major difference between isoforms is in their observed expression patterns.

Table 8. Biochemical and pharmacological properties of COX-1 versus COX-2. (Source: Smith, 2008).

Properties	PGHS-1 (COX-1)	PGHS-2 (COX-2)
Structure	Homodimers; 60 % sequence identity within species	
Catalysis	Similar catalytic mechanism and similar KM and VMAX values for AA; PGHS-1 exhibits cooperativity with AA	
Peroxide requirement	Both isoforms require peroxides for activity; PGHS-2 requires a ten -fold lower concentration than PGHS-1	
Substrate preferences	AA»EPA; not active with esters; AA oxygenation inhibits by EPA and other fatty acids	AA~esters>EPA; AA is preferred substrate when other fatty acids are present
Expression	Constitutive; developmentally regulated by SP1 promoter elements and an AP1 intronic element	Inducible; six known promoter-response elements differently operative in various cells
Function	Immediate, pulsatile burst of PG formation in response to hormones	Continuous, slow generation of PGs following induction by growth factors, cytokines
Pathologies associated with overexpression	Cardiovascular (*e.g.* low dose aspirin used as anti-platelet therapy)	Inflammation, pain, colon cancer
Pharmacology	Inhibited by common NSAIDs (*e.g.* aspirin, ibuprofen, naproxen)	Inhibited by common NSAIDs and coxibs (*e.g.* celecobix, rofecoxib)

In 2002, the group of Daniel Simmons characterized and cloned a COX enzyme in dog brain, different from COX-1 and COX-2 enzymes. This COX enzyme was a variant of COX-1 and derived from the same gene; it was designated as COX-3. Preferential expression of COX-3 in the brain and heart has been reported (Chandrasekharan *et al.*, 2002). The distinctive characteristic of COX-3 as compared to COX-1 and COX-2 is its greater sensitivity to acetaminophen. COX-3 is considered to play a key role in the biosynthesis of prostanoids known to be important mediators in pain and fever (Zarghi and Arfaei, 2011).

2.1.1 Structure and mechanism of action

The cyclooxygenases (COX-1 and COX-2) are membrane-associated, heme-containing homodimers (Vecchio and Malkowski, 2011). The enzymes are embedded in the luminal monolayer of the endoplasmic reticulum and inner membrane of the nuclear envelope (Eisinger *et al.*, 2008) and each isoform consists of two separate, but functionally linked active sites. The crystal structures of the COX isoforms are quite structurally homologous and consistent with a high sequence identity (*ca.* 60 %); the overall structures of COX-1 and COX-2 are highly conserved. The COX monomer consists of three structural domains:

1. N-terminal epidermal growth factor (EGF)-like domain of 50 amino acids at the N terminus;

2. membrane binding domain (MBD) of about 48 amino acids in length, which anchors the protein to one leaflet of the lipid bilayer;

3. large C-terminal globular catalytic domain (about 460 amino acids) with the COX active site, which accommodates the substrate or the inhibitors, and the peroxidase one, which contains the heme cofactor.

These sites are distinct but functionally and structurally interconnected. The peroxidase reaction occurs near the protein surface while the cyclooxygenase reaction occurs in a hydrophobic channel in the core of the enzyme (Garavito *et al.*, 2002).
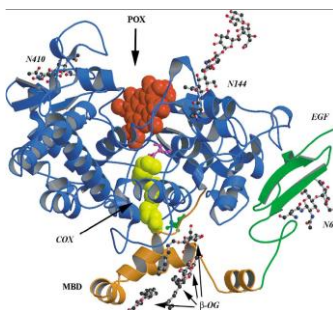
Figure 11. Ribbon drawing of the ovine PGHS-1 monomer with bound arachidonic acid (AA). The color scheme indicates the epidermal growth factor domain (green), the MBD (gold), the globular catalytic domain (blue), the hemes (red), AA (yellow) in the COX active site (Source: Garavito *et al.*, 2002).

Figure 12 (b) represents the two active sites of COXs – the COX site with AA bound and the POX site having a heme group with an alkyl hydroperoxide (ROOH) bound. The carboxyl group of AA is ligated by Arg120. The COX reaction is initiated by POX activity (d). ROOH oxidizes the heme to Compound I and is reduced to an alcohol. Oxidation of the heme leads to oxidation of Tyr385 in the COX site to the tyrosyl radical of Intermediate II. This radical abstracts the C-13 hydrogen from AA. The product is an arachidonyl radical with its electron stabilized in a resonance structure at C-11 (a). The arachidonyl radical reacts with oxygen to form the 11-hydroperoxyl radical; after cyclization, rearrangement and insertion of another O_2 at C-15, the bicyclic endoperoxide PGG_2 is formed. Reduction of the C-15 peroxyl group by the peroxidase (POX) activity of COXs yields PGH_2 (Smith, 2008).
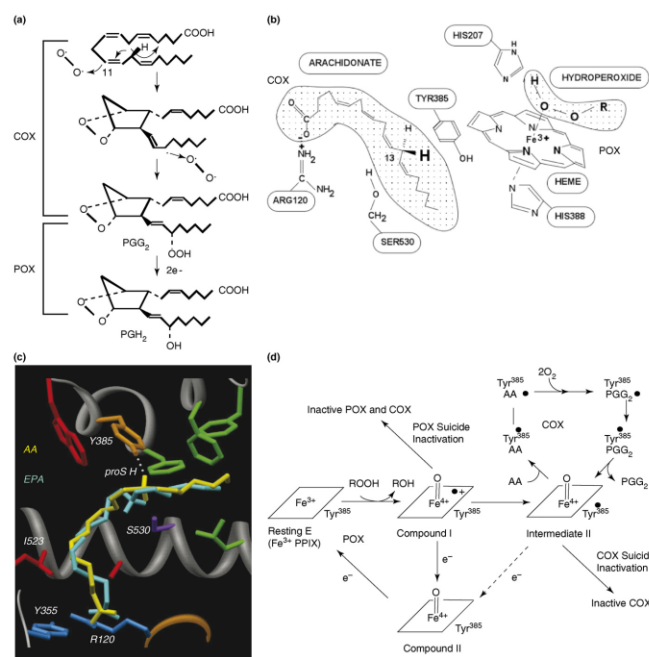
Figure 12. Prostaglandin endoperoxide H synthase reactions and reaction mechanism. (a) shows the two reactions catalyzed by PGHSs. (Source: Smith, 2008).

The biosynthetic activity of both isoforms can be inhibited by non-steroid anti-inflammatory drugs (NSAIDs) and coxibs through the binding to the hydrophobic COX site and interference with AA binding. When aspirin binds COXs, through an ionic

interaction between the carboxylate and the Arg120 residue adjacent to the active site, it acetylates the COX site at Ser530 in irreversible way, and the resulting Ser-O-acetyl group interferes with the proper positioning of AA, leaving the peroxidase activity of the enzyme unaffected.

2.1.2 Physiological and pathological functions of COX-1 and COX-2

The COX isozymes have roles in a wide range of physiological and pathological functions. COX-1 is primarily responsible for the physiological functions of the prostaglandins, whereas COX-2 produces the "bad" prostaglandins during inflammatory processes. The main findings supporting this hypothesis are, firstly, that the prostaglandins that mediate inflammation, fever and pain are produced solely via COX-2, and secondly, that the prostaglandins important in gastrointestinal and renal function are produced solely via COX-1. In this theory context, the physiological roles of COX-1 have been deduced from the deleterious side effects of NSAIDs in the gastrointestinal and renal system, which while inhibiting PG biosynthesis at inflammatory sites, also inhibit constitutive biosynthesis, due to their lack of selectivity with respect to inhibition of COX-1 and COX-2 (Dannhardt and Laufer, 2000). Thus, COX-1 provides PGs in the stomach and intestine to maintain the integrity of the mucosal epithelium and its inhibition leads to gastric damage, haemorrhage, and ulceration.

However, there are evidences of other COXs' roles in pathologies that include, for COX-1, thrombosis and for COX-2, neurological disorders like Alzheimer's and Parkinson's diseases and various cancers (Garavito *et al.*, 2002). COX-2 affects many processes that have been implicated in different stages of carcinogenesis. These include xenobiotic metabolism, cell proliferation, angiogenesis, apoptosis, immune function and tumor invasiveness (Zarghi and Arfaei, 2011).

2.1.3   NSAIDs and COXIBs

Non-steroidal anti-inflammatory drugs NSAIDs are among the most widely used therapeutics. These drugs have analgesic, anti-pyretic and anti-inflammatory activities and they represent a suitable treatment in various inflammatory diseases such as arthritis, rheumatisms as well as relieving the pains of everyday life. The targets of these drugs are the COX activities of COXs and their function at biochemical level is to prevent PG biosynthesis. From a historical viewpoint, the first NSAID with therapeutic benefits was aspirin and it still represents, with ibuprofen and naproxen, the most commonly used NSAIDs. Classical NSAIDs inhibit the COX activities of both isoforms. A subset of NSAIDs called coxibs (<u>COX</u>-2 specific <u>inhib</u>itor<u>s</u>) inhibit the COX activity of COX-2 and not of COX-1 (Smith, 2008). All NSAIDs compete with arachidonate for binding to the cyclooxygenase active site but each molecule exhibits one of the three kinetic modes of inhibition (Smith *et al.*, 2000):

1. rapid, reversible binding (*e.g.* ibuprofen);
2. rapid, lower affinity reversible binding followed by time-dependent, higher affinity, slowly reversible binding (*e.g.* flurbiprofen);
3. rapid, reversible binding followed by covalent modification (acetylation) of Ser530 (*e.g.* aspirin).
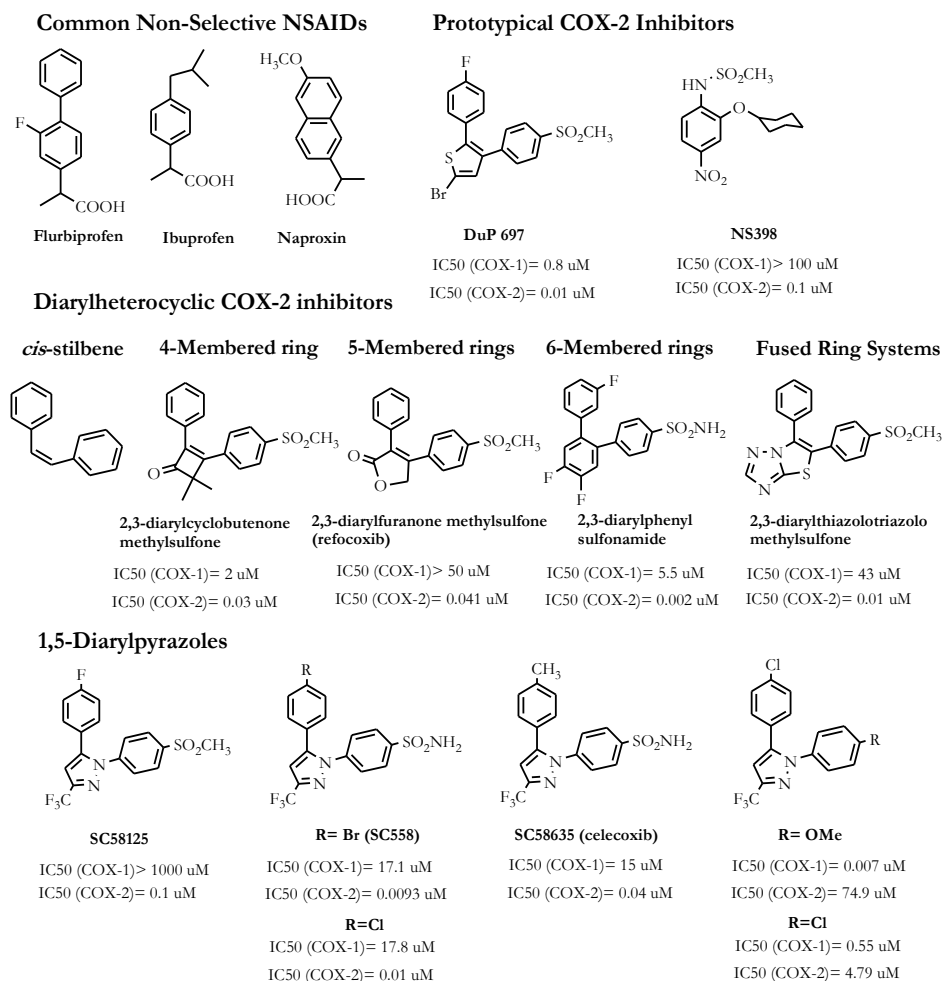
Figure 13. Structures of representative nonselective and Cox-2-selective NSAIDs (Source: DeWitt, 1999).

A single amino acid residue in the arachidonic acid binding channel is critical for inhibitor selectivity: there is an isoleucine at position 523 in COX-1 and a valine (smaller by a single methyl group) in COX-2 (Dannhardt and Laufer, 2000). Thus, the COX site of COX-2 has a 20 % larger volume than the one of COX-1 (Smith *et al.*, 2000) and the smaller valine molecule in COX-2 leaves a gap in the wall of the channel, giving access to a side-pocket, which is thought to be the site of binding of many selective drugs. The bulkier isoleucine at 523 in COX-1 is large enough to block access to the side-pocket (Hawkey, 1999). This change is compounded by the substitution of Ile434 in COX-1 with Val434 in COX-2. The combination of these two differences at position 523 and 434 in

COX-2 causes a movement of Phe518 that further increases the size of the side pocket, which is a pre-requisite for COX-2 drug selectivity, as shown in Figure 14 (Smith *et al.*, 2000).
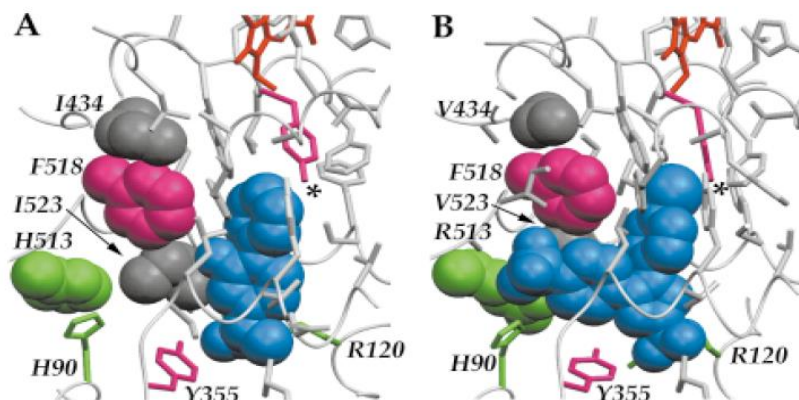
Figure 14. NSAID (blue) binding to the cyclooxygenase active sites of COX-1 versus COX-2. (A) Flurbiprofen bound to COX-1. (B) The COX-2 inhibitor SC-588 bound to COX-2. Access to the additional side pocket is made easier by the I434V change in COX-2, which allows Phe518 to move out of the way when drugs bind in this pocket (Smith *et al.*, 2000).

These findings allowed the synthesis of a large number of COX-2 selective compounds, as shown in the series based on flurbiprofen. Progressive modification and extension of flurbiprofen's methyl group resulted in molecules that were increasingly selective in their ability to bind COX-2 in the side-pocket, but too bulky to fit within the COX-1 channel (Hawkey, 1999).

Contrary to the classic NSAIDs, this new class of enzyme inhibitors lacks the carboxylic group, thus selective inhibitors of COX-2 do not bind to Arg120 as classical NSAIDs (aspirin), but have a different orientation within the enzyme without formation of a salt bridge in the hydrophobic channel of the enzyme. This is probably due to the larger effective size of COX-2 central channel, which reduces steric and ionic crowding by the charged Arg120 (Smith *et al.*, 2000). Finally, the substitution of His513 in COX-1 to Arg513 in COX-2 alters the chemical environment of the side pocket. This substitution results in a stable positive charge that can interact with polar moieties entering the pocket. For example, Arg513 appears to interact with 4-methylsulfonyl or 4-sulfonamoylphenyl

substituents of diarylheterocyclic COX-2 inhibitors. In general classification, selective COX-2 inhibitors belong to two major structural classes (Zarghi and Arfaei, 2011):

1. **Tricyclics** (also known as ortho-diaryl heterocycles or carbocycles): 1,2-diarylsubstitution on a central hetero or carbocyclic ring system (4-, 5-, or 6-membered cores or fused ring system) with a characteristic methanesulfonyl, sulfonamido, azido, methanesulfonamide;

2. **Non-tricyclics**: acyclic central systems such as olefinic, iminic, azo, acetylenic and α,β-unsaturated ketone structures; they include non-tricyclic with a 2-, or 3-membered central template.

In the figure below are reported some of the most known Coxibs.

(a) Celecoxib

(b) Refocoxib

(c) Eterocoxib

(d) DuP-697
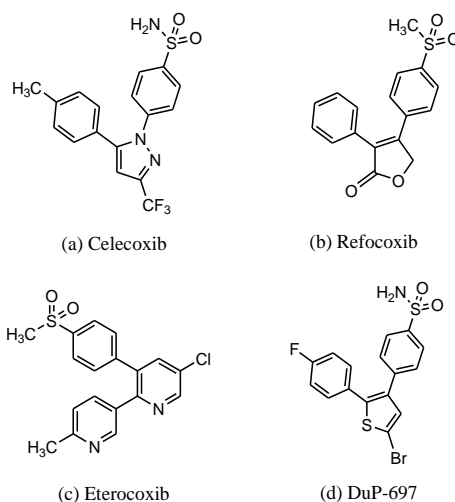
Figure 15. Coxibs characterized by tricyclic structures.

2.1.4 Potential COX-2 tracers

As above mentioned, COX-2 is associated with inflammation and it also plays a prominent role in the initiation and progression of various diseases and pain. It is well documented its overexpression in many human cancer entities such as colorectal, gastric, and breast cancer. In addition, it is present in high level also in cardiac and cerebral

ischemia, AD, PD. For these reasons, study on the *in vivo* COX-2 expression would have significant potential in differential diagnosis, monitoring of disease progression and evaluation of therapeutic interventions. Currently, assessment of COX-2 expression levels and/or activity can only be achieved by laborious analyses *ex vivo*. Moreover, instability of COX-2 mRNA and protein leads to further difficulties in terms of the intervals between tissue sampling and time of analysis (de Vries *et al.*, 2008). In this line, non-invasive monitoring of COX-2 functional expression by means of nuclear molecular imaging techniques like positron emission tomography (PET) provides unique opportunities to obtain data on COX-2 expression levels during disease progression and the potential role of COX-2 in diseases. In search for a suitable PET tracer for COX-2 imaging, several selective COX-2 inhibitors have been labelled, including [^{18}F]SC58125, [^{18}F]desbromo-DuP-697, [^{11}C]celecoxib and [^{11}C]rofecoxib (McCarthy *et al.*, 2002; DeVries *et al.*, 2003 and 2008; Prabhakaran *et al.*, 2005).

(a) ^{11}C-Celecoxib

(b) ^{11}C-Refocoxib

(c) ^{18}F-SC-58125

(d) ^{18}F-desbromo-DuP-697
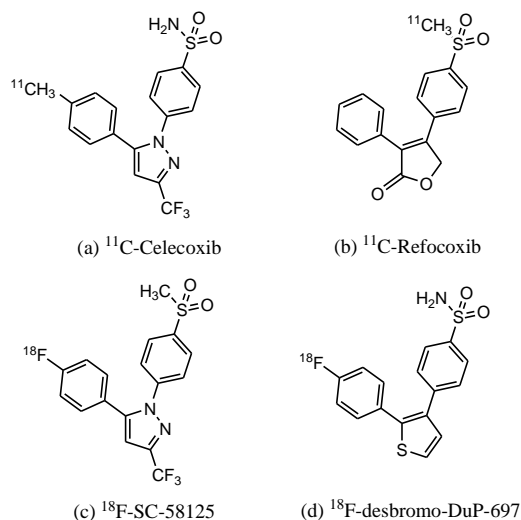
Figure 16. Chemical structures of radiolabelled COX-2 inhibitors.

The celecoxib analogue [^{18}F]SC58125 showed an uptake in COX-2 expressing activated macrophages *in vitro* but did not show any specific binding to COX-2 in healthy rats and baboon (McCarthy *et al.*, 2002). [^{18}F]Desbromo-DuP-697 appeared to display COX-2-related specific uptake in rats (DeVries *et al.*, 2003), but a PET study in pigs did

not show any specific binding (DeVries *et al.*, 2008). Recently, a new fluorinated derivative of celecoxib was developed by Uddin *et al.*, which may be a useful probe for early detection of cancer and for evaluation of the COX-2 status of premalignant and malignant tumors (Uddin *et al.*, 2011). Hence, all the work done demonstrates the challenging of *in-vivo* imaging of COX-2 expression level and continuous efforts are required for developing applicable radiotracers.

2.2 *Prostate-specific membrane antigen (PSMA): Prostate Cancer*

Prostate cancer (PCa) is one of the major causes of mortality and morbidity in Western society today (the second in the United States) (Kularatne *et al.*, 2009a).

Current diagnosis is typically achieved by digital rectal exam, blood prostate-specific antigen (PSA) testing or prostate biopsy (Hillier *et al.*, 2009). Since the introduction of serum PSA screening, prostate cancer incidence rates have increased dramatically as a consequence of the number of men being treated for the disease (Hankey *et al.*, 1999). However, 20 % to 30 % of men with prostate cancer have serum PSA levels within the reference range, resulting in false negatives (Catalona *et al.*, 1991), whereas others have elevated serum PSA levels due to conditions other than prostate cancer, *i.e.* benign prostatic hyperplasia or prostatitis, resulting in false positives and unnecessary biopsies (Tricoli *et al.*, 2004).

Therefore, accurate initial diagnosis and determination of the extent of disease continues to be a major challenge for selecting appropriate treatment options, monitoring the effects of therapeutic interventions, and detecting disease after recurrence. For this reason, non-invasive detection of prostate cancer or metastases still remains a challenge in the field of molecular imaging (Hao *et al.*, 2010).

Currently, the most commonly used Positron Emission Tomography (PET) probe, $2\text{-}^{18}\text{F-fluoro-2-deoxy-D-glucose}$ ($^{18}\text{F-FDG}$), is useful for identification of localized prostate cancer only in a small percentage of patients, presenting tumor lesions characterized by poorly differentiated phenotype (Belloli *et al.*, 2009). Moreover, the

prostate is in the close proximity of the bladder, where the FDG is cleared, and the prostate cancer cells are inherently not glucose avid (Shreve *et al.*, 1996). To date, various PET tracers have been introduced for prostate cancer imaging based on different molecular mechanisms.

To mention a few, ^{11}C- or ^{18}F-labelled choline, that is incorporated into tumor cells by an active carrier-mediated transport mechanism and then it is phosphorylated by choline kinase, an enzyme that is often upregulated in human cancers, to produce phosphoryl ^{11}C-choline (Hara *et al.*, 1998). These radiotracers have shown promising results in detecting primary and metastatic prostate cancer, but with inconsistent findings in densely sclerotic bone lesions (Hara *et al.*, 1998) although false-positive PET scans were also reported (15 %-47 % of patients), due to its uptake in inflammatory lesions, thus underscoring the necessity for confirmatory tissue biopsy. ^{11}C- or ^{18}F-labelled acetate is actively incorporated into newly synthesised lipids of malignant cells with highly active basal lipid metabolism associated with the cell membrane (Soloviev *et al.*, 2008); it was reported with potential to detect local recurrences and regional lymph node metastases (Oyama *et al.*, 2002). 3´-^{18}F-fluorothymidine ([^{18}F]FLT) is an analogue of the nucleoside thymidine (deoxythymidine) and the concentration of FLT nucleotides in the cells is proportional to thymidine kinase I (TK1) activity and therefore to cellular proliferation (Shields *et al.*, 1998); it was used for monitoring the therapeutic effect of androgen ablation therapy in prostate cancer (Oyama *et al.*, 2004);

Each radiotracer has its benefits and detriments, with no single agent ideal *i.e.* easy to synthesize, little metabolism and demonstrating tumor-specific uptake in all PCa phenotypes. So, the development of imaging and therapeutic agents remains a challenge and, for this purpose, a cell surface glycoprotein, the prostate-specific membrane antigen (PSMA) is one of the most favourable targets (Olson *et al.*, 2007).

2.2.1 Prostate-specific membrane antigen (PSMA)

Glutamate carboxypeptidase II (GCPII) is a membrane zinc metallopeptidase expressed in numerous tissues such as central and peripheral nervous system, prostate, kidney, small intestine and tumor-associated neovasculature (Berger *et al.*, 1995). The GCPII form expressed in the central nervous system, also known as NAALA-Dase, is responsible for the hydrolysis of *N*-acetyl-L-aspartyl-L-glutamate (NAAG) into *N*-acetyl-L-aspartate (NAA) and L-glutamate (Robinson *et al.*, 1987), and is thought to be implicated in various pathologic conditions associated with altered glutamatergic signal transmission (Doble, 1999).
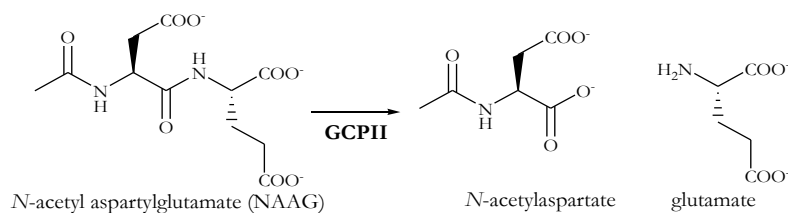
Scheme 1. NAAG degradation by GCP II.

Several derivatives of 2-(phosphonomethyl)-pentanedioic acid (2-PMPA), a potent and selective inhibitor of GCPII, have been described as selective inhibitors and, among those, (S)-2-(4-iodobenzylphosphonomethyl)-pentanedioic acid (GPI-18431) exhibits an IC_{50} value of 30 nM (Mester *et al.*, 2006). Below, the crystal structure of the fully glycosylated extracellular domains (residues 44–750) of GCPII in complex with GPI-18431 as reported by Mesters *at al.*.
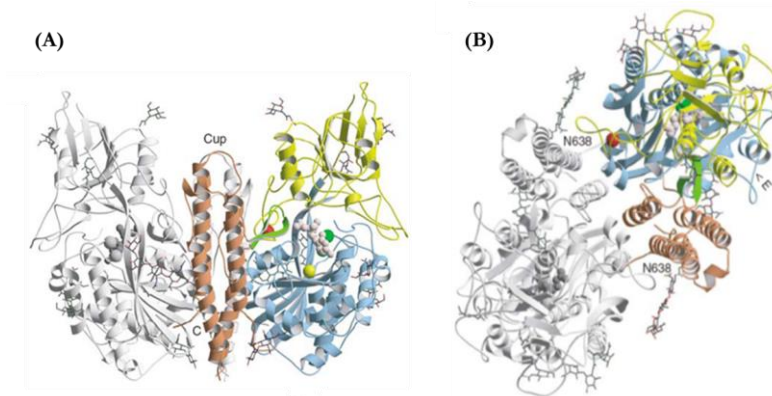
Figure 17. Structure of GCPII. Three-dimensional structure of the dimer. The GPI-18431 inhibitor is shown as small beige balls. The position of the structure relative to the membrane is shown in (A). (B) provides a view into the 'cup' of the dimeric enzyme. The entrance to the catalytic site is indicated ('E'). (Source: Mester *et al.*, 2006).

The prostate form, termed prostate-specific membrane antigen (PSMA), is overexpressed in almost all PCa cells, whose expression level has been shown to increase as the stage and grade of the tumor progresses but has limited extra-prostatic expression (Kularatne *et al.*, 2009a). PSMA is a type 2 transmembrane-glycoprotein and consists of a large, globular extracellular localized domain (ED, amino acids 45-750), a hydrophobic transmembrane domain (TM, amino acids 20 to 44) and an endocytic intracellular targeting motif (CD, amino acids 1 to 19, binding site) (Figure 18) (Rajasekaran *et al.*, 2005).
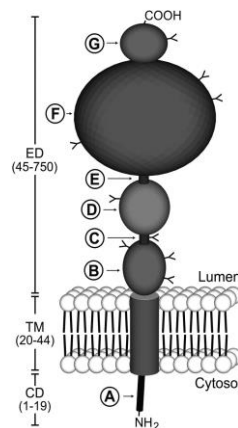
Figure 18. Integral structure of prostate specific membrane antigen (PSMA).

Normally detected in prostate epithelium, PSMA is considerably higher expressed in localized and metastatic prostate cancer (Ghosh and Heston, 2004). Internalization of PSMA via clathrin-coated pits reveals the opportunity of intracellular delivery of cytotoxic drugs or radionuclides (Goodman *et al.*, 2007). Due to the specificity of PSMA over expression exclusively in PCa, tremendous efforts have been made to discover potent inhibitors and numerous PSMA-specific tracers.

[111]In-Capromab pendetide (ProstaScint) is a commercially available monoclonal antibody (MAb) that binds to the intracellular domain of the PSMA and has been approved by FDA for diagnostic imaging of prostate cancer. It has limited use because the MAb binds primarily to necrotic parts of the tumor and may not detect any viable malignant tumor cells (Chopra). Moreover, it has been cited for complexities associated with its administration and the interpretation of the images obtained (Ponsky *et al.*, 2002). On the contrary, radiolabelled small molecule drugs have an advantage over MAbs because they are inexpensive to produce, can easily penetrate solid tumors, and, due to their pharmacokinetic properties, are superior for use in the detection (by imaging techniques) and therapy of cancerous tumors (Chopra). On the basis of these facts, a series of low molecular weight inhibitors of PSMA were recently synthesized and evaluated until now (Foss *et al.*, 2005; Kularatne *et al.*, 2009; Kularatne *et al.*, 2009; Ikeda *et al.*, 2010; Chen *et al.*, 2011; Malik *et al.*, 2011, Al-Momani *et al.*, 2012). Most of these small-molecules have been synthesized based on glutamate-urea-R species, where R corresponds to one or more α-amino acids and among all, DUPA, a high affinity inhibitor of PSMA, has shown promising results.

2.3 DUPA

DUPA, 2-[3-(1,3-dicarboxypropryl)ureido]pentanedioic acids, is a glutamate-urea-glutamate molecule developed by Kularatne and co-workers.
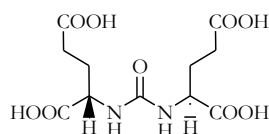
Figure 19. Structure of 2-[3-(1,3-dicarboxypropryl)ureido]pentanedioic acids (DUPA-Pep).

Although the function of PSMA in PCa cells still remains unknown, the fact that PSMA and NAALA-Dase are the same protein allowed Kularatne's group to conduct an *in silico* docking study, using a high resolution crystal structure of the ectodomain of NAALADase in complex with one of its higher affinity inhibitors (GPI-18431). In this study, DUPA was found to share the greatest number of docking interactions with GPI-18431, as shown in the figure below, reported by Kularatne *et al.*, 2009.
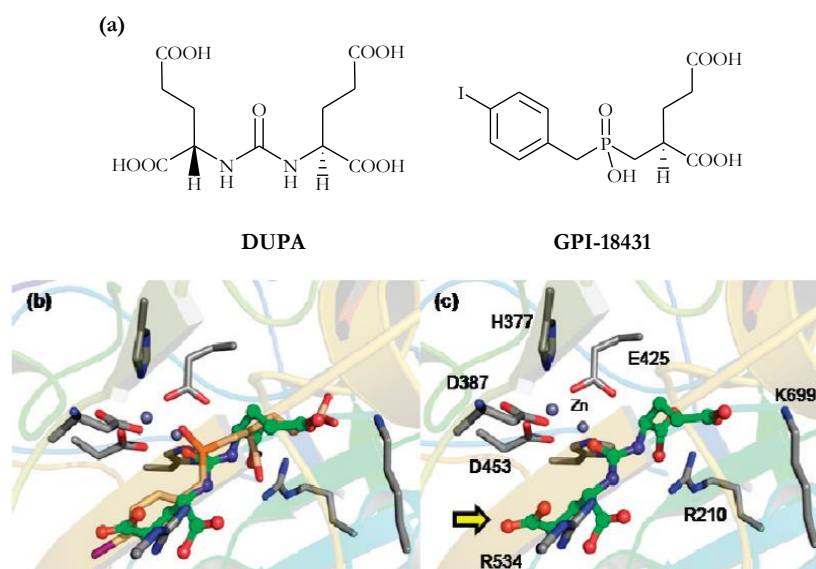
Figure 20. (a) Structures of DUPA and GPI-18431. Superimposition of (b) docked DUPA (green) with GPI-18431 (brown) and (c) docking interactions of DUPA (green) with residues in the active site of NAALADase. Yellow arrow indicates γ'-carboxylic acid of DUPA. (Source Kularatne *et al.*, 2009b).

Looking at the binding mode, the oxygen atom of the urea moiety in DUPA was found to directly coordinate with the zinc atom(s) in the active site and also the three carboxylic groups are required for binding within the binding pocket of PSMA.

48

Moreover, during the design of radioimaging agents, the group synthesized and tested different structures and found that the linking of DUPA to the chelating moiety with a spacer containing two phenylalanine residues at appropriate position (via an 8-aminooctanoic acid spacer) created an imaging ligand with excellent potential for clinical studies (Figure 21) (Kularatne *et al.*, 2009b).
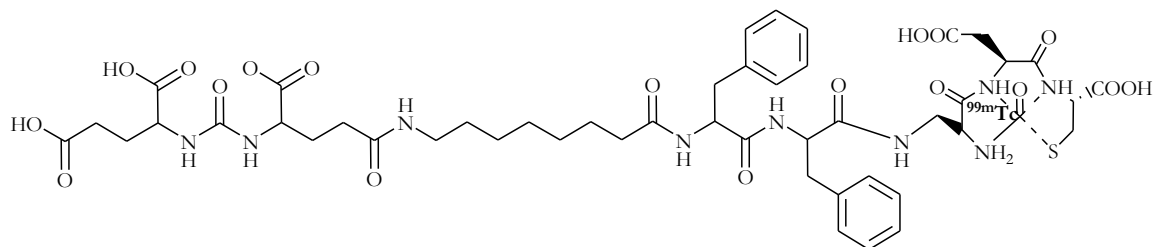
Figure 21. Structures of PSMA-targeted radiotracer, DUPA-^{99m}Tc.

This compound showed a high affinity and specificity to PSMA (K_D = 14 nM) (Kularatne *et al.*, 2009a). According to this promising molecule, other structures have been synthesized, labelled and tested, confirming the encouraging data and suggesting their potential in imaging prostate cancer and future application in therapy.

2.4 Nanocarriers

A major challenge to a successful cancer chemotherapy is how to achieve specific drug accumulation at tumor sites. Conventional chemotherapeutic agents are distributed non-specifically in the body where they affect both cancerous and normal cells, thereby limiting the dose achievement within tumors and also resulting in systemic toxicity and undesired side effects (Danhier *et al.*, 2010). In order to improve the chemotherapy, tremendous research efforts have been devoted to the development of tumor targeted nanocarriers for the controlled delivery of anticancer drugs. Various nanocarrier platforms, including liposomes, nanoparticles, polymeric micelles and nanogels, have been developed in order to deliver anticancer drugs to tumor tissues by taking advantage of the

enhanced permeability and retention effect (EPR), whereby the endothelial cells of the blood vessel walls possess large fenestrations, or gaps, between cells as compared to normal healthy tissue, which have tight junctions. The EPR effect allows small nanocarriers to extravasate the endothelial barrier and accumulate in the tumor tissues, while leaving the healthy surrounding tissue largely untouched (Maeda *et al.*, 2001).
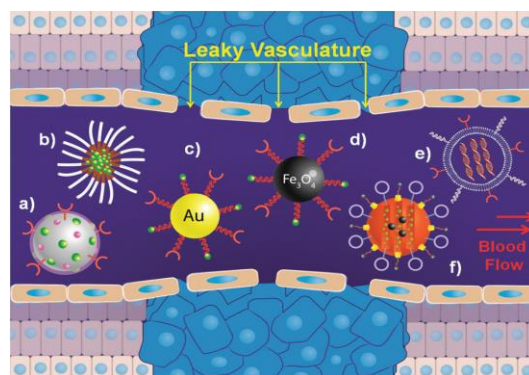
Figure 22. A multifunctional (a) polymeric nanogel, (b) polymeric micelle, (c) gold nanoparticle, (d) iron oxide nanoparticle, (e) siRNA ensconced in a liposome delivery vector, and (f) a stimuli-responsive capped mesoporous silica nanoparticle are shown. (Source Li *et al.*, 2012).

These nanocarriers are often functionalized with poly(ethyleneglycol) (PEG) polymers (Li *et al.*, 2012). Surface modifications with PEG offer several unique features, including the enhancement of the nanocarrier dispersion in physiological conditions, the prolongation of the nanocarrier circulation time in blood, due to the inhibition of opsonization, and the facilitation of preferential accumulation at the tumor sites by the EPR effect (Zhang *et al.*, 2012). However, the EPR effect is often not enough efficient to eradicate the side effects of cytotoxic drugs and to selectively exert the anticancer therapy in cancer cells (Peer *et al.*, 2007). In order to further enhance the targeting ability of nanocarriers to cancer cells, a promising strategy is to functionalize the surface of nanocarriers using targeting agents that can selectively bind to over-expressed antigens or receptors on the surface of cancer cells, increasing specificity and uptake of drugs (Zhang *et al.*, 2012). The targeting agents normally include small nutrient molecules such as mannose or folic acid, bio-oligomers like peptides and bio-macromolecules such as protein

and antibodies (Vivero-Escoto *et al.*, 2010). All of the above mentioned designs take advantage of the overexpression of cellular receptors for these moieties due to the special metabolic and nutritional demands of certain types of cancer cells.

An ideal drug delivery system should be stable under a long circulation period, and can keep loaded drugs unreleased during the circulation in the bloodstream or in normal tissues. Once having reached tumor tissues and after being taken up by cancer cells by passive and active targeting, the system should release the drugs rapidly in response to the local environment (Zhang *et al.*, 2012).

2.4.1   Mesoporous silica nanoparticles (MSNPs)

Mesoporous silica nanoparticles (MSNPs) have attracted great attention for their high potential as carriers for drug delivery systems (DDS) and probes for bioimaging owing to their dispersibility, biocompatibility, and easy surface modification incorporating various functionalities. Since the discovery of MCM-41 by Mobil scientists (Beck *et al.*, 1992), significant research progress has been made in controlling and modifying the properties of mesoporous silica materials (controlled particle size, morphology, porosity, chemical stability). The high surface area-to-volume ratio allows increased surface functionalization, while the great porosity allows to house appreciable amounts of cargo and multiple payloads, with different drugs or with both diagnostic and therapeutic agents, without destabilization of the silica framework.

In addition, the research group of Lin of the Iowa State University have discovered that surface functionalized mesoporous silica nanoparticle (MSN) materials can be readily internalized by animal and plant cells without posing any cytotoxicity issue *in vitro* (Radu *et al.*, 2004). These new developments provide the possibility of designing a new generation of drug/gene delivery systems and biosensors for intracellular controlled release and imaging applications.

2.4.1.1   *Synthesis of MSNPs*

These nanoparticles are formed through base-catalyzed sol–gel condensation around hexagonally packed micelle structures, formed by cationic surfactants as the templating agent (Kresge *et al.*, 1992; Grün *et al.*, 1997). The sol–gel process utilizes the organosilane precursors (TMOS, TEOS, etc.), which, by means of hydrolysis and condensation reactions,

Hydrolysis:$\qquad\qquad$ $OH^- + Si(OR)_4 - Si(OR)_3OH + RO^-$ $\qquad\qquad$ (1)

Condensation:$\qquad\quad$ $SiO^- + Si(OH)_4 - Si–O–Si + OH^-$ $\qquad\qquad$ (2)
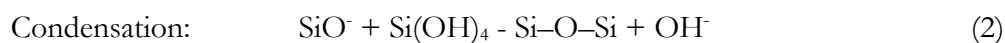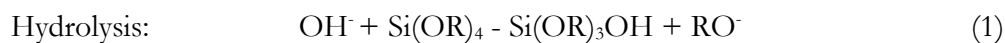
leads to the formation of a new phase (sol). The small colloidal particles within the sol then condense into the gel phase.

In a typical synthesis of the 100 nm MCM-41 type mesoporous silica nanoparticles, one of the most popular mesoporous material, the silica source, tetraethylorthosilicate (TEOS), is added into a heated basic (pH 11) aqueous solution of the templating surfactant, cetyltrimethylammonium bromide (CTAB). 100 nm diameter nanoparticles (Figure 23 a) are formed through base-catalyzed sol–gel condensation around the hexagonally packed micelle structures (Figure 23 b). After aging, the resulting nanoparticles are refluxed in acidic alcohol to decrease the interactions between the surfactant and the silica frame, and remove the templating agent from the mesopores (Li *et al.*, 2012).
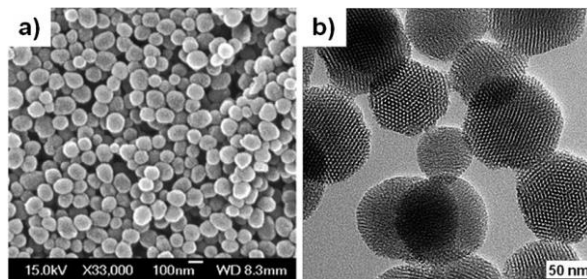
Figure 23. SEM image of MCM-41 mesoporous silica nanoparticles(Source Li *et al.*, 2012).

Various functional moieties can be introduced into the MSNPs, either through covalent bonding or electrostatic interactions, providing high level of versatility and many mechanized features to the mesoporous silica materials, that play a crucial role in the cargo loading and in achieving controllable cargo delivery.

2.4.1.2   *Release controlled cargo delivery*

Major research on MSNPs has so far focused on the development of controlled cargo release by applying mechanical controls over the pore openings in response to external or internal *stimuli*, that can lead to MSNPs-based controlled release systems (Zhang *et al.*, 2012). The ease of introducing various organic functional groups, either through covalent bonding or electrostatic interactions, provides high level of versatility and many mechanized features to the mesoporous silica materials, that could be functionalized with stimulus-esponsive mechanically interlocked molecules (MIMs) to yield mechanized silica nanoparticles (MSNPs).

Different *stimuli* have been taken into account for the design of more robust theranostic delivery systems and are well depicted in Figure 24 from a recent review by Zink and coworkers of the University of California, NanoSystems Institute, USA. These MIMs can be designed in such a way that they either change shape or shed off some of their parts in response to a specific *stimulus*, such as changes in redox potential, alterations in pH, irradiation with light, or the application of an oscillating magnetic field, allowing a theranostic payload to be released from the nanopores to a precise location at the appropriate time (Ambrogio *et al.*, 2011).

Figure 24. Pore opening control motifs designed for MSNPs, showing pore blocking and unblocking by (a) the formation and breaking of covalent bonds; (b) the shrinking and swelling of polymer chains; (c) attachment and removal of bulky groups; (d) threading and dethreading of a cyclic torus molecule with a bulky stopper; (e) shuttling of a cyclic molecule; (f) cis-trans photoisomerization of the azobenzene propels the cargo molecules out of the mesopores. (Source: Li *et al.*, 2012).
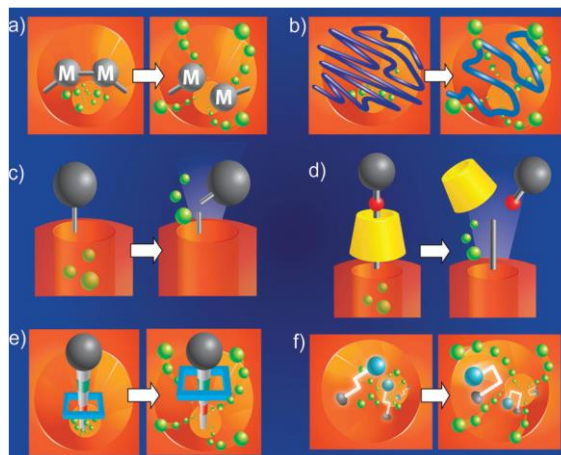
2.4.1.3 Applications

The main applications of MSNPs are the delivery of hydrophobic drugs within the bloodstream (*e.g.* anti-cancer drugs), the increase of cellular uptake by chemically modifying the MSNPs with moieties that selectively bind cell surface receptors overexpressed in diseased organs and tissues, and the controlled release thanks to mechanically interlocked molecules (MIMs). Before MSNPs can be effectively applied as drug delivery systems, their cellular uptake and cytotoxicity properties have been investigated by various research groups that have demonstrated that cell uptake and cellular toxicity of the MSNPs depend on the particle's size, shape, surface charge and functional groups (Vivero-Escoto *et al.*, 2010; Wu *et al.*, 2011). Thus, to be clinically successful, these nanoparticles should be tumor selective, nontoxic and exhibit favourable targeting and clearance profiles (Benezra *et al.*, 2011)

3 AIMS

The aim of this thesis is the development of new molecules specific for two different targets, cyclooxygenase-2 (COX-2) and prostate-specific membrane antigen (PSMA), for diagnosis and therapy of the associated diseases.

Cyclooxygenase-2 (COX-2) is involved in the body's response to inflammation and pain. Moreover, it is also overexpressed in many human cancers (*e.g.* colorectal cancer) and involved in various neurodegenerative diseases (*e.g.* AD, PD). Non-invasive monitoring of *in-vivo* COX-2 expression may provide the opportunity to follow its expression level during disease manifestation and progression. The aim of this part of the thesis is to label with carbon-11 a specific COX-2 inhibitor (VA426), which showed a COX-2 IC_{50} within nanomolar concentration range, to investigate the biodistribution of this compound in different models and to evaluate the potential use as COX-2 radiotracer.

Prostate-specific membrane antigen (PSMA), the second target under investigation, is a valid target for prostate cancer diagnosis and therapy due to its high expression in prostate carcinoma. DUPA-Pep, a glutamate-urea-glutamate based molecule, is a known specific ligand of this target. The aim of this second part of the thesis is to investigate DUPA-Pep coupling with two chelating agents (Df and CHX-A´´-DTPA) and subsequent labelling with different radiometals, for both diagnostic and therapeutic applications. One of the main advantages of these chelating agents is the ability to label conjugated biomolecules at room temperature, avoiding unexpected heat-based side reactions. It was intended also to measure K_D values, to verify the stability in PBS and HS, and to study the biodistribution of these compounds in mice bearing PSMA-positive tumor xenografts.

Moreover, ^{89}Zr labelling of Mesoporous Nanoparticles, coupled with Desferal, has been investigated. This is an initial part of a bigger research project which will foresee the coupling of these nanoparticles with DUPA moiety to selectively deliver MSNPs, with the loaded theranostic cargo, at the disease's specific sites.

4   EXPERIMENTAL

GENERAL METHODS

All chemicals and solvents for organic synthesis were commercially available and used without further purification. They were purchased from ABX, Applichem, Fluka, J.T.Baker®, MACROCYCLICS, Merck, Phenomonex, S.A.L.F., Sigma Aldrich, Waters. Precursor VA425 and standard VA426 were kindly provided by Anzini (University of Siena).

<u>^{1}H and ^{13}C nuclear magnetic resonance</u> spectra were recorded using a 300 MHz Brucker Avance spectrometer at ambient temperature. Chemical shifts (δ) are quoted in parts per million (ppm) and are referenced to the residual solvent peak. Coupling values (*J*) are given in hertz (Hz). Spin multiplicities are given as s (singlet), d (doublet), dd (double doublet), t (triplet), dt (double triplet), m (multiplet).

<u>Analytical thin layer chromatography (TLC)</u> was performed using Merck TLC Silica gel 60 RP-18 F_{254}S (on Aluminium sheets 5 x 7.5 cm), with visualization of the compounds by UV light (254 nm).

<u>High performance liquid chromatography (HPLC)</u> analyses and preparative separations were performed with a system consisting of P680 HPLC Pump and UCD170U Dionex, Raytest Gabi and analytical and preparative Phenomonex Gemini 5u C18 (250x4.6 mm, 5 micron; 250x21.10mm, 5 micron) for DUPA-Pep project and with a Waters system for COX-2 project, consisting of a 515 isocratic pump, rheodyne manual injection valve, a 486 Tunable Absorbance ultraviolet detector operated at 254 nm, and a Bioscan Geiger–Müller radioactivity detector and analytical ACE 5u C18 (5µm; 250x4.6 mm I.D.; CPS).

The radiosynthesis of [^{11}C]VA426 was performed using a fully automated synthesis module PET tracer Synthesizer, Nuclear Interface (Datentechnik GmbH, Munster, Germany). HPLC semipreparative purification was performed with a system consisting of an isocratic pump Sykam mod. S1021, UV-detector K-2001 Knauer, operated at 254 nm, Bioscan Geiger–Müller radioactivity detector and a semipreparative reversed-phase column Platinum C18 EPS (10µm; 250x7.0 mm I.D.; Grace).

[^{90}Y]Y-Cl$_3$ and [^{177}Lu]Lu-Cl$_4$, in 0.04 M HCl, were purchased from Eckert Ziegler and Isotope Technologies, respectively. ^{68}Ge/^{68}Ga generator was obtained from IDB Holland BV.

4.1 Synthesis of [^{11}C]VA426

[^{11}C]CO$_2$ was converted to [^{11}C]CH$_3$I by treatment with lithium aluminum hydride followed by hydriodic acid, using an automated synthesis system. [^{11}C]CH$_3$I was trapped in a solution of precursor VA425 (2.0 mg, 5.4 μmol) and NaH 60 % dispersion in mineral oil (2.0 mg, 51 μmol) in DMSO (300 μL) at 80 °C. Then, the mixture was left at 80°C for 2 min and then cooled at 30°C. After cooling, the mixture was diluted with H$_2$0/EtOH (6/4) (1 ml) and injected onto a semipreparative HPLC column (Platinum C18 EPS 10μm; 250 x 7.0 mm I.D.; Grace) using a mobile phase of H$_2$0/EtOH (6/4) at a flow rate of 4 ml/min with UV detection at 254 nm. The [^{11}C]VA426 retention time was 13.5 min. The desired fraction was collected for 1 minute (*ca.* 4 ml) in a flask and diluted with NaCl 0.9 % to get a final volume of 10 ml. The total synthesis time from EOB was 30 min. The decay-corrected radiochemical yield was 21 ± 1.67 % (n = 3) based on [^{11}C]CH$_3$I with a specific radioactivity of 90 ± 54 GBq/μmol (n = 3), with an average final activity of 2.01 ± 0.17 GBq (n=3). The chemical identity of [^{11}C]VA426 was confirmed by co-injection with reference standard VA426 in analytical HPLC (ACE 5 C-18 5 μm; 250 x 4.6 mm I.D.; Cps); mobile phase: CH$_3$CN/phosphate 0.025 M (70/30); flow rate: 1 mL/min; UV detection: 254 nm; retention time: 6.0 min) and it showed the same retention time on the UV and the radioactive chromatograms. Both the chemical purity, analysed at 254 nm, and the radiochemical purity were greater than 95 %.

4.2 Animal Studies

C57 BL/6 mice of ~20 g weight were used for this study. All the procedures involving the animals and their care were conducted in conformity with the relative institutional guidelines, which comply with relevant national (no. 116, G.U., suppl. 40, 18/2/1992, no. 8, G.U., 14/7/1994) and international laws and policies (EEC Council

Directive 86/609, OJ L 358,1, Dec 12, 1987; Guide for the Care and Use of Laboratory Animals, US National Research Council, 1996).

Peritoneal inflammation was caused in animal (n=1) by intraperitoneal (*i.p.*) administration of 10 mg/Kg of Lipopolysaccharides (LPS) from Escherichia coli 055:B5 (Sigma). Briefly, LPS was dissolved in vehicle (Phosphate Buffered Saline PBS, Euroclone) and then immediately injected in mouse abdomen. Control mouse was injected *i.p.* with PBS vehicle.

PET Imaging studies were performed 24 hours after LPS administration, using the YAP-(S)-PET scanner (ISE, Pisa, Italy) with a field of view (FOV) of 4 x 4 cm of diameter.

Animals were anesthetized with 1 % isoflurane in air, positioned supine on the PET scanner bed with abdomen centred in field of view and injected in the tail vein with 5.5 $\pm$ 0.5 MBq of [^{11}C]VA426. Radioactivity concentration was measured starting immediately after tracer injection up to 60 minutes, according to the following schedule: 4 frames of 2.5 minutes each, 2 frames of 5 minutes each and 4 frames of 10 minutes each (Total 60 minutes). The images obtained from PET studies were corrected for radioactivity decay, calibrated and radioactivity concentration data were expressed as percentage of injected dose per gram of tissue weight (% ID/g). Regions of Interest (ROIs) were performed drawing circular ROIs on lungs and liver of both LPS and PBS mice. Muscle was used as reference region.

4.3 Preparation of Zirconium-89

4.3.1 Preparation of the hydroxamate resin column

Accell Plus CM cation exchange medium (300 Å, 0.35 mmol/g ligand density; Waters) (1 g) was suspended in 8 mL of water traceSELECT®in a Falcon tube (15 mL, VWR). Then, 75 µL of 3 M HCl, 1 mL of a TFP solution (200 mg/mL in MeCN, 1.2 mmol) and 384 mg of solid EDAC (2 mmol) were added (final pH 5.7–6.0). The suspension was mixed on a vertical lab rotator for 1 h at room temperature. Further 3 M HCl (aq.) (100 µL), TFP (1.0 mL, 1.20 M in MeCN) and EDAC (385 mg, 2.0 mmol) were added (pH 5.8 – 6.1). The reaction was mixed at room temperature for 2 – 3 h. The resin

was then collected by filtration and washed with water (3 x 25 mL) and MeCN (3 x 25 mL) to remove any unreacted TFP and EDAC and the 1-(2-(dimethylamino)ethyl)-3-methylurea by-product. The hydroxylamine hydrochloride (695 mg, 10 mmol) was dissolved with 1 mL of 1 M NaOH and 2 mL of MeOH, followed after 15 min by the addition of 25 – 50 μL of 1 M NaOH to reach pH 5.3–5.4. This solution was added to the activated resin in a 15 mL Falcon tube, and the reaction (pH 5.0 – 5.2) was mixed by inversion at room temperature for 18 h. The product was then collected by filtration and washed with water (5 x 25 mL) and MeCN (5 x 25 mL) and dried *in vacuo* to give 0.988 g of a white powder. Then, a reservoir (Exctract Clean™ 1.5 ml Reservoir 100 pk) was filled with 100 mg of resin to perform the purification of ^{89}Zr.

4.3.2 Purification of ^{89}Zr from the ^{89}Y target material and preparation of [^{89}Zr]ZrCl$_4$

The irradiated ^{89}Y-foil target (approx. 0.36 g, 25 x 25 mm, 0.127 mm thick, 99.9 %, Alfa Aesar®) was transferred to a Wheaton (10 mL), dissolved by the addition of 4 x 0.5 mL fractions of 6 M HCl (aq.) and diluted with 5 ml of water traceSELECT®. The solution was then transferred to the hydroxamate column, previously activated with 5 ml MeCN, 10 ml NaCl 0.9 % and 2 ml HCl 2 M, under pump negative pressure applied by use of a polyetheretherketone (PEEK) tube connected to the reservoir through an adaptor cap. This mechanism also facilitated minimal radiation exposure. After loading the ^{89}Zr activity, the column was washed with 2 M HCl (aq.) (6 mL) and water traceSELECT® (6 mL) to remove the soluble Y(III) ions and other impurities. After blowing air through the column to remove the solvent, the ^{89}Zr activity was slowly eluted with 1.0 M oxalic acid (2 x 0.5 mL). The [^{89}Zr]Zr-oxalate was then loaded on a QMA cartridge, previously activated with 6 ml MeCN, 10 ml NaCl 0.9 % and 10 ml water traceSELECT®. The cartridge was then washed with water traceSELECT® (50 mL). The activity was then recovered using 1M HCl (0.5 ml) as [^{89}Zr]ZrCl$_4$. Finally, the excess of acid was neutralized by adding the appropriate volume of Na$_2$CO$_3$ (aq.) (2 M in water traceSELECT®) (*ca.* 100 μl) and the pH was adjusted to 7-8. The activity in each step was measured by dose calibrator.

4.4 Preparation of Gallium-68

^{68}Ga was eluted from the TiO$_2$-based commercially available ^{68}Ge/^{68}Ga generator (IDB Holland BV, $t_{1/2}$ of ^{68}Ge and ^{68}Ga = 270 days and 68 min, respectively) with *ca.* 2 ml of 1M HCl (aq.) and collected into a vial containing 1 ml of HCl 30 % (9.5 M, Suprapure®, Merck). This solution was then loaded onto a reservoir (Exctract Clean™ 1.5 ml Reservoir 100 pk) filled with 100 mg Dowex 1 x 8 (Fluka), a strong basic anion exchange resin. The resin was activated with 1 ml ethanol absolute pure *Ph. Eur.*, USP (AppliChem), 1 ml water traceSELECT® (Fluka) and 1 ml 4M HCl (aq.).

Once ^{68}Ga was adsorbed, the resins was washed with 2 ml of 4M HCl (aq.) and flushed with 5 ml air. Elution of the ^{68}Ga from the reservoir was achieved with 2 x 100 μl of water traceSELECT®, both flushed with 1 ml air. Finally, the excess of acid was neutralized by adding the appropriate volume of Na$_2$CO$_3$ (aq.) (2 M in water traceSELECT®) (*ca.* 100 μl) and the pH was adjusted to 7-8.

4.5 Synthesis of Df-DUPA-Pep

1-Amino-5,8-dibenzyl-4,7,10,19,24-pentaoxo-3,6,9,18,23,25-hexaazaoctacosane-22,26,28-tricarboxylic acid trifluoro-acetate ("DUPA-Pep" Trifluoroacetate, ABX) (15.84 mg, 20 nmol) was dissolved in dimethylsulfoxide (DMSO; 1 ml) and *N,N*-diisopropylethylamine (DIPEA; 6 μl, 80 nmol) and 1-(4-isothiocyanatophenyl)-3-[6,17-dihydroxy-7,10,18,21-tetraoxo-27-(*N*-acetylhydroxylamino)-6,11,17,22-tetraazaheptaeicosine]thiourea (*p*-SCN-Deferroxamine, MACROCYCLICS) (15.7 mg, 20 nmol) were added. The reaction was then mixed by a vertical lab rotator overnight and then purified by preparative HPLC using C18 column (Gemini 5u C18, 250 x 21.10 mm, 5 micron, Phenomonex) with a gradient elution carried out as follows: at 0-6 min 15 % MeCN in H$_2$O (0.1 %TFA), at 6-8 min from 15 to 35 % MeCN in H$_2$O (0.1 % TFA), at 8-30 min from 35 to 45 % MeCN in H$_2$O (0.1 % TFA) and then at 30-40 min 55 % MeCN in H$_2$O (0.1 % TFA), at a flow rate of 10 mL/min under UV detection (λ: 220, 254 nm) to give Df-DUPA-Pep, retention time *ca.* 22.5 min, (23.8 mg, 16 nmol, 80 %) as a colorless solid after lyophilization.

^{1}H NMR (300 MHz, DMSO-d$_6$) δ 1.27 (m, 30H); 1.64 (m, 2H); 1.85 (m, 7H); 2.03 (m, 2H); 2.19 (m, 6H); 2.43 (m, 2H); 2.60 (dd, *J*=13.64, 9.10 Hz, 1H); 2.77 (dd, *J*=13.64, 10.61 Hz, 1H); 2.91 (m, 8H); 3.18 (m, 2H); 3.39 (m, 10H); 4.01 (m, 2H); 4.40 (m, 2H); 6.29 (m, 2H); 7.13 (m, 11H); 7.26 (dd, *J*=23.24, 9.10 Hz, 4H); 7.61 (s, 2 H); 7.79 (m, 5H); 7.98 (m, 2H); 9.35 (s, 1 H); 9.53 (s, 2 H).

^{13}C NMR (300 MHz, DMSO-d$_6$) δ 20.31 (CH$_3$); 23.44 (CH$_2$); 23.54 (CH$_2$); 25.09 (CH$_2$); 25.99 (CH$_2$); 26.02 (CH$_2$); 26.09 (CH$_2$); 26.26 (CH$_2$); 27.50 (CH$_2$); 28.17 (CH$_2$); 28.29 (CH$_2$); 28.35 (CH$_2$); 28.48 (CH$_2$); 28.77 (2 CH$_2$); 29.06 (2 CH$_2$); 29.82 (3 CH$_2$); 31.59 (3 CH$_2$); 35.13 (CH$_2$); 37.20 (CH$_2$); 37.76 (CH$_2$); 37.95 (CH$_2$); 38.36 (CH$_2$); 38.38 (CH$_2$); 38.47 (CH$_2$); 46.72 (2 CH$_2$); 46.78 (CH$_2$); 47.02 (CH$_2$); 47.03 (CH$_2$); 51.58 (CH); 52.06 (CH); 53.60 (CH); 53.96 (CH); 126.09 (C6(Phenylalanin)); 126.25 (C6 (Phenylalanin)); 127.88 (2 C2 Phenyl(Desferal)); 128.03 (2 C3 Phenyl(Desferal)); 129.09 (4 C6 (Phenylalanin)); 129.16 (4 C3 (Phenylalanin)); 137.56 (C1, C6 Phenyl(Desferal)); 137.91 (2 C1 (Phenylalanin)); 157.23 (HN-(C=O)-NH); 170.09 (C=O-CH$_3$); 170.96 (C=O); 171.13 (C=O); 171.27 (2 C=O); 171.91 (C=O); 172.12 (CO$_2$H); 173.71 (3 C=O); 174.12 (2 CO$_2$H); 174.22 (2 C=S).

ESI-HRMS (*m/z*): calcd for C$_{72}$H$_{107}$N$_{15}$O$_{19}$S$_2$, 1550,84; found, (M+H)$^+$ 1550,73; (M-H)$^-$ 1548,73.

4.5.1 Synthesis of [*89Zr]Zr-Df-DUPA-Pep*

[89Zr]ZrCl$_4$ in neutral aqueous solution (25 μL; 3-5 MBq) was added to a freshly prepared solution of Df-DUPA-Pep, dissolved in DMSO (1 mg/mL), and 0.25 M HEPES buffer (pH 7.5, 500 μL) for a total volume between 526-575 μL and a final pH of 7.5. Different amounts of peptide (1, 5, 10, 25 and 50 μg; 0.6, 3, 6, 15 and 30 nM) were used for studying the dependence between concentration of peptide and RCY. The reaction was carried out at room temperature for 60 min. At different reaction times (1, 5, 10, 30 and 60 min), 1 μL aliquots were withdrawn and analyzed by radio-TLC on RP-18 thin layer plates.

4.5.2 Synthesis of [⁶⁸Ga]Ga-Df-DUPA-Pep

[^{68}Ga]GaCl$_3$ activity in neutral aqueous solution (10-15 μL; 8-12 MBq) was added to freshly prepared solution of Df-DUPA-Pep, dissolved in DMSO (1 mg/mL), and 0.25M HEPES buffer (pH 7.5, 500 μL) for a total volume between 511-535 μL and a final pH of 7.5. Different amounts of peptide (1, 5 and 20 μg; 0.6, 3 and 13 nM) were used for studying the dependence of the RCY on the concentration of peptide. The reaction was carried out at room temperature for 10 min. At different reaction times (1, 5 and 10 min), 1 μL aliquots were withdrawn and analyzed by radio-TLC on RP-18 thin layer plates.

4.5.3 Stability Studies

The radiochemical stability was determined by mixing the radiotracer ([^{89}Zr]Zr-Df-DUPA-Pep or [^{68}Ga]Ga-Df-DUPA-Pep) with both human serum (HS) and PBS buffer and incubating maintained at 37°C for 48 h. The total volume was 1.2 mL (950 μL of serum or buffer and 250 μL of product solution). The activity used for each test was 12 MBq and 5 MBq for ^{68}Ga and ^{89}Zr, respectively. 200 μL of the mixture were withdrawn at every time point and the samples were analysed by radio-TLC and radio HPLC. 1 μl was spotted twice on a RP-18 TLC strip and the remaining sample was used for HPLC. RP-18 TLC strip was developed in Trisodium Citrate dihydrate buffer (0.1 M, pH 5). Once the solvent front reached the end of the strip, the TLC plate was removed from the solvent and analysed by phosphoimager. In the HPLC analysis, the samples in PBS were directly injected while the ones in serum underwent a work up, before being injected, as described below: an equal volume of EtOH (200 μL) was added to the samples to precipitate serum proteins. Subsequently, the samples were centrifuged for 10 min at 10000 rpm. The surnatant was then ultra filtered for 10 min at 10000 rpm using Amicon ultra centrifugal filter, 3KDa NMWL (Millipore), and the filtrate was analyzed by RP-HPLC.

4.5.4 In vitro Studies

LNCaP C4-2 cells (American Type Culture Collection "ATCC", Rockville, MD) were grown in RPMI 1640 supplemented with 20 % Ham´s F12 medium, 5 % FCS (fetal calf serum), 1 % Penicillin and Streptomycin, 5 μg/ml insulin, 12.5 μg/ml adenine, 6.825

pg/ml T3, 5 μg/ml apotransferrin and 0.25 μg/ml biotin (called T-Medium) at a temperature of 37 °C, in an environment containing 5 % CO_2. Prior to use, the cells were washed in 1X PBS buffer solution, trypsinized in 0.05 % Trypsin/0.02 % EDTA solution (3 - 5 min), suspended in 10 ml medium into a falcon tube with 40 ml PBS and then centrifuged (2000 rpm/5 min). The surnatant was removed and the cells were resuspended in a total volume of 6 ml medium and counted. After counting, the cells were transferred in well-plates (5 x 10^5 cells/plate) and put into the incubator at a temperature of 37 °C for 2 days and then the medium was changed to fresh and 2-PMPA was added as inhibitor in a part of the plates. Decreasing concentration of labelled Df-DUPA-Pep (both with ^{89}Zr or ^{68}Ga) were added in both well-plates, with and without inhibitor, and incubated at 37°C for 1 h. After incubation, the surnatant was removed, the cells were washed two times with PBS (1 ml) and then destroyed by NaOH (1 M, 1 ml) and taken out; all these samples were counted in a gamma counter. The cell-binding characteristics of the labelled peptide was determined using Prism 5 (GraphPad).

4.5.5 In vivo Studies

Prostate carcinoma cell lines LNCaP C4-2 (PSMA positive cells) and PC3 (PSMA negative cells) (American Type Culture Collection, Rockville, MD) were grown in 10 % FCS RPMI Medium, T-Medium and PC-Medium, respectively, at a temperature of 37 °C in an environment containing 5 % CO_2. The cells were trypsinized, counted, and suspended in BD Matrigel^{TM} (BD Biosciences). In 12 weeks old male SCID mice xenografts were developed in the scapular region. Therefore, 0.15 mL suspension containing 1-2 x 10^6 cells of the PSMA-positive cell line LNCaP C4-2 was injected subcutaneously on the left shoulder. After 7-18 d, tumor xenografts had developed, with a maximum diameter of 1 cm. The PSMA-negative PC3 cells were implanted in SCID mice in an identical manner on the right shoulder. 0.12 mL of [^{68}Ga]Ga-Df-DUPA-Pep or [^{89}Zr]Zr-Df-DUPA-Pep, formulated in 0.9 % NaCl solution, were injected into tumor-bearing mice through the tail vein. The radioactivity injected was between 2-12 MBq for the ^{68}Ga and less than 1 MBq for ^{89}Zr, due to the different half-life (~68 min and ~78 h, respectively). Accumulation of the radiolabelled peptide was measured in PET/CT at

various time points (1 to 3 h for ^{68}Ga and up to 24 h for ^{89}Zr). PET studies were performed using the Biograph$^{\text{TM}}$ PET·CT (Siemens Healthcare, Germany). Whole-body imaging studies (one bed positions, total acquisition time 5 min per mouse) were carried out on mice anesthetized with 1.5 - 1.7 % isoflurane (Abbott)/oxygen gas mixture. ^{68}Ga cylinder phantoms were imaged each day for normalization and quantitative analysis.

The energy window for PET acquisition of ^{68}Ga and ^{89}Zr was set between 435 keV and 650 keV. The imaging data were reconstructed using the Fourier rebinned ordered subsets expectation maximization method with scatter correction (linear background subtraction) and with Time of Flight. A point spread function reconstruction with Time of Flight was also done. The reconstructed images were processed and analyzed using Syngo.Via Software (Siemens Healthcare, Germany). After the acquisition, the animals were sacrificed and the major organs as well as the tumors were recovered. Blood samples were also obtained at the time of sacrifice. The blood and tissue samples were weighed and activity was counted in the γ-counter. The background corrected relative activity (cpm) of tissue samples was expressed as a percentage of the injected dose per gram (% ID/g).

4.6 Synthesis of CHX-A´´-DTPA-DUPA-Pep

1-Amino-5,8-dibenzyl-4,7,10,19,24-pentaoxo-3,6,9,18,23,25-hexaazaoctacosane-22,26,28-tricarboxylic acid trifluoro-acetate ("DUPA-Pep" Trifluoroacetate, ABX) (10 mg, 12.5 nmol) was dissolved in dimethylsulfoxide (DMSO; 1 ml) and *N*,*N*-diisopropylethylamine (DIPEA; 15 μl, 90 nmol) and *N*-[(R)-2-Amino-3-(p-isothiocyanato-phenyl)-propyl]-trans-(S,S)-cyclohexane-1,2-diamine-*N*,*N*,*N*',*N*'',*N*''-pentaacetic-acid (*p*-SCN-Bn-CHX-A´´-DTPA·3HCl, MACROCYCLICS; 7 mg, 11 nmol) were added. The reaction was then mixed by a vertical lab rotator overnight and then purified by preparative HPLC using C18 column (Gemini 5u C18, 250 x 21.10 mm, 5 micron, Phenomonex) with a gradient elution carried out as follows: at 0-3 min 20 % MeCN in H_2O (0.1 % TFA), at 3-15 min from 20 to 40 % MeCN in H_2O (0.1 % TFA) and then at 15-30 min 40 % MeCN in H_2O (0.1 % TFA), at a flow rate of 7 mL/min under UV detection (λ: 220, 254nm) to give CHX-A´´-DTPA-DUPA-Pep, retention time *ca.* 23.2 min, (12 mg, 8.6 nmol, 70 %) as a colorless solid after lyophilization.

^{1}H NMR (300 MHz, DMSO-d$_6$) δ 1.18 (m, 14H); 1.66 (m, 4H); 1.97 (m, 8 H); 2.24 (m, 2H); 2.66 (m, 1H); 2.83 (m, 1H); 2.98 (m, 6H); 3.2 (m, 4H); 3.37 (m, 4H); 3.55 (m, 7H); 4.07 (m, 5H); 4.46 (m, 3H); 6.35 (m, 2H); 7.26 (m, 14H); 7.77 (m, 2H); 8.03 (m, 3H); 9.64 (s, 1H); 12.64 (s, 5H).

^{13}C NMR (300 MHz, DMSO-d$_6$) δ 25.09 (2 CH$_2$); 26.26 (1 CH$_2$); 27.48 (2 CH$_2$); 28.26 (2 CH$_2$); 28.28 (2 CH$_2$); 28.35 (1 CH$_2$); 28.48 (1 CH$_2$); 29.06 (1 CH$_2$); 29.82 (1 CH$_2$); 31.59 (1 CH$_2$); 35.12 (1 CH$_2$); 36.99 (1 CH$_2$); 37.16 (2 CH$_2$); 37.74 (1 CH$_2$); 37.90 (2 CH$_2$); 38.46 (3 CH$_2$); 48.25 (2 CH$_2$); 51.58 (2 CH); 52.07 (1 CH); 53.61 (2 CH); 53.94 (2 CH); 126.09 (C6 (Phenylalanin)); 126.27 (C6 (Phenylalanin)); 127.89 (2 C2 Phenyl(Desferal)); 128.03 (2 C3 Phenyl(Desferal)); 129.08 (4 C6 (Phenylalanin)); 129.16 (4 C3 (Phenylalanin)); 137.53 (C1, C6 Phenyl(Desferal)); 137.92 (2 C1 (Phenylalanin)); 155.33 (2 C=O); 157.23 (HN-(C=O)-NH); 158.24 (2 C=O); 170.96 (2 COOH); 171.13 (COOH); 172.14 (2 COOH); 173.70 (COOH); 174.11 (2 COOH); 174.22 (C=S).

ESI-HRMS (*m/z*):

MALDI calcd for C$_{65}$H$_{89}$N$_{11}$O$_{21}$S$_1$, 1391; found, (M+H)$^+$ 1392.60177.

4.6.1 Synthesis of [^{89}Zr]Zr-CHX-A´´-DTPA-DUPA-Pep

[^{89}Zr]ZrCl$_4$ in neutral aqueous solution (16 µL; 3.95-4.01 MBq) was added to a freshly prepared solution of CHX-A´´-DTPA-DUPA-Pep, dissolved in DMSO (2 mg/mL), and 0.25 M HEPES buffer (pH 7.4, 500 µL) for a total volume between 529-566 µL and a final pH of 7.4. Different amounts of peptide (25, 50 and 100 µg; 18, 36 and 72 nM) were used for studying the dependence of RCY on peptide concentration and time (n=3). The reaction was carried out at room temperature for 60 min. At different reaction times (1, 5, 10, 30 and 60 min), 1 µL aliquots were withdrawn and analyzed by y-counter measurements of TLC (0.1 M citrate-buffer; pH 5).

4.6.2 Synthesis of [^{68}Ga]Ga-CHX-A´´-DTPA-DUPA-Pep

[^{68}Ga]GaCl$_3$ in neutral aqueous solution (13 µL; 9.3-9.6 MBq) was added to freshly prepared solution of CHX-A´´-DTPA-DUPA-Pep, dissolved in DMSO (2 mg/mL), and 0.25 M HEPES buffer (pH 7.4, 500 µL) for a total volume between 513.5-563 µL and a

final pH of 7.4. Different amounts of peptide (1, 10, 25, 50 and 100 µg; 0.7, 7.3, 18, 36 and 72 nM) were used for studying the dependence of RCY on peptide concentration and time (n=3). The reaction was carried out at room temperature for 60 min. At different reaction times (1, 5, 10, 30 and 60 min), 1 µL aliquots were withdrawn and were analyzed by radio-TLC on RP-18 thin layer plates (0.1 % TFA/MeOH (30/70)).

4.6.3 Synthesis of [^{90}Y]Y-CHX-A´´-DTPA-DUPA-Pep

[^{90}Y]YCl$_3$ solution in 0.04 M HCl (20 µL; 3.7-3.8 MBq) was added to a freshly prepared solution of CHX-A´´-DTPA-DUPA-Pep, dissolved in DMSO (2 mg/ml) and 0.5 M NH$_4$OAc buffer (pH 5.5, 500 µL) for a total volume between 533-570 µL and a final pH of 5.5. Different amounts of peptide (25, 50 and 100 µg; 18, 36 and 72 nM) were used for studying the dependence of RCY on peptide concentration and time (n=3). The reaction was carried out at room temperature for 60 min. At different reaction times (5, 10, 30 and 60 min), 1 µL aliquots were withdrawn and analyzed by radio-TLC on RP-18 thin layer plates (0.1 % TFA/MeOH (30/70)).

4.6.4 Synthesis of [^{177}Lu]Lu-CHX-A´´-DTPA-DUPA-Pep

[^{177}Lu]LuCl3 solution in 0.04 M HCl (5 µL; 6.3-6.7 MBq) was added to freshly prepared solution of CHX-A´´-DTPA-DUPA-Pep, dissolved in DMSO (2 mg/ml), and 0.5 M NH4OAc buffer (pH 5.5, 500 µL) for a total volume between 510-555 µL and a final pH of 5.5. Different amounts of peptide (10, 25, 50 and 100 µg; 7.2, 18, 36 and 72 nM) were used for studying the dependence of RCY on peptide concentration and time (n=3). The reaction was carried out at room temperature for 60 min. At different reaction times (5, 10, 30 and 60 min), 1 µL aliquots were withdrawn and analyzed by radio-TLC on RP-18 thin layer plates (0.1 % TFA/MeOH (30/70)).

4.6.5 Stability study

The radiochemical stability was determined by mixing the radiotracer ([^{68}Ga]Ga-CHX-A´´-DTPA-DUPA-Pep) with both human serum (HS) and PBS buffer and incubating maintained at 37°C for 48 h. The total volume was 1.2 mL (950 µL of serum or buffer and 250 µL of product solution). The activity used was 11 MBq. 200 µL of the

mixture were withdrawn at every time point and the samples were analysed by radio-TLC and radio HPLC. 1 µl was spotted twice on a RP-18 TLC strip and the remaining sample was used for HPLC. RP-18 TLC strip was developed in Trisodium Citrate dihydrate buffer (0.1 M, pH 5). Once the solvent front reached the end of the strip, the TLC plate was removed from the solvent and analysed by phosphoimager. In the HPLC analysis, the samples in PBS were directly injected while the ones in serum underwent a work up, before being injected, as described below: an equal volume of EtOH (200 µL) was added to the samples to precipitate serum proteins. Subsequently, the samples were centrifuged for 10 min at 10000 rpm. The surnatant was then ultra filtered for 10 min at 10000 rpm using Amicon ultra centrifugal filter, 3KDa NMWL (Millipore), and the filtrate was analyzed by RP-HPLC.

4.6.6 In vitro Studies

LNCaP C4-2 cells (American Type Culture Collection "ATCC", Rockville, MD) were grown in RPMI 1640 supplemented with 20 % Ham´s F12 medium, 5% FCS (fetal calf serum), 1 % Penicillin and Streptomycin, 5 µg/ml insulin, 12.5 µg/ml adenine, 6.825 pg/ml T3, 5 µg/ml apotransferrin and 0.25 µg/ml biotin (called T-Medium) at a temperature of 37°C, in an environment containing 5% CO_2. Prior to use, the cells were washed in 1X PBS buffer solution, trypsinized in 0.05% Trypsin/0.02% EDTA solution (3-5 min), suspended in 10 ml medium into a falcon tube with 40 ml PBS and then centrifuged (2000 rpm/5 min). The surnatant was removed and the cells were resuspended in a total volume of 6 ml medium and counted. After counting, the cells were transferred in well-plates (5 x 10^5 cells/plate) and put into the incubator at a temperature of 37°C for 2 days and then the medium was changed to fresh and 2-PMPA was added as inhibitor in a part of the plates. Decreasing concentration of labelled CHX-A´´-DTPA-DUPA-Pep (both with ^{68}Ga or ^{177}Lu) were added in both well-plates, with and without inhibitor, and incubated at 37°C for 1 h. After incubation, the surnatant was removed, the cells were washed two times with PBS (1 ml) and then destroyed by NaOH (1 M, 1 ml) and taken out; all these samples were counted in a gamma counter. The cell-binding characteristics of the labelled peptide was determined using Prism 5 (GraphPad).

4.7   Labelling of Df-MSNPs with ^{89}Zr

[^{89}Zr]ZrCl$_4$ in neutral aqueous solution (*ca.* 100 MBq, the amount depending on the radioconcentration) was added to a sospension of Df-MNSPs (100 μg in 100 μl DMSO) and NH$_4$OAc-buffer 0.25 M (pH = 7.8, 1 ml). The reaction was mixed by a vertical lab rotator.

5   RESULTS AND DISCUSSIONS

5.1 COX-2 inhibitor

The first project foresaw the labelling with carbon-11 of a COX-2 inhibitor molecule and, thus, the evaluation of the new labelled compound for the potential imaging of COX-2 expression. In scheme 2 is reported the labelling reaction.
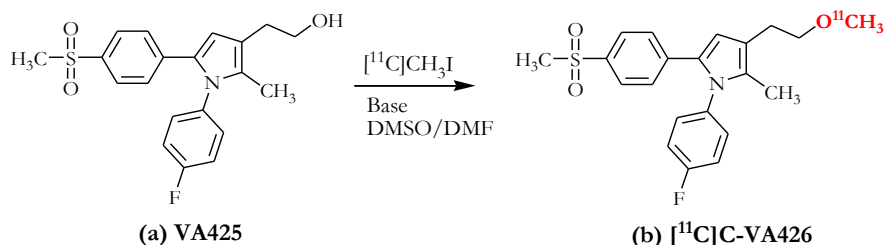
Scheme 2. ^{11}C-methylation reaction for labelling VA426.

The precursor (a), together with the standard compound (b), has been provided by Anzini (University of Siena), following the procedure reported by Anzini *et al.*, 2008. 1-(4-fluorophenyl)-3-(2-methoxyethyl)-2-methyl-5-(4-methylsulfonyl)phenyl)-1*H*-pyrrole showed a highly selective and potent COX-2 inhibitory activity. COX-2 IC_{50} is 0.018 μM, comparable to the IC_{50} of refocoxib (0.012 μM; Almansa *et al.*, 2003) and the selectivity, expressed as IC_{50}COX-1/ IC_{50}COX-2, is >5555 (Anzini *et al.*, 2008).

5.1.1 ^{11}C- methylation via Wet-phase method

Carbon-11 is produced as [^{11}C]carbon dioxide via ^{14}N(p,α)^{11}C nuclear reaction, starting from highly pure nitrogen (N60, 99.9999 % pure, Air Liquide), with 0.5 % O_2, as target material. Once produced, the radioisotope can be directly used as produced in the target, or converted into another precursor that subsequently will be introduced into biomolecule precursors. In both, wet- and gas-phase, the precursor used is [^{11}C]methyl iodide; the main difference is the synthetic pathway. In the wet-phase, the adopted method used is the reduction of [^{11}C]carbon dioxide to [^{11}C]methanol by use of lithium aluminium

hydride followed by the conversion of the generated [^{11}C]methanol into [^{11}C]methyl iodide with hydriodic acid, as shown in the scheme below (Comar *et al.*, 1974).

$$[^{11}C]CO_2 \xrightarrow{\ LiAlH_4/THF\ } [^{11}C]CH_3OH \xrightarrow{\ HI\ } [^{11}C]CH_3I$$

Scheme 3. Formation of ^{11}CH$_3$I via reduction by LiAlH$_4$.

A fully automated synthesis system (PET tracer Synthesizer, Nuclear Interface), controlled by the software Tracerlab FX C (GE) is used (Figure 25).

(A)   **(B)**
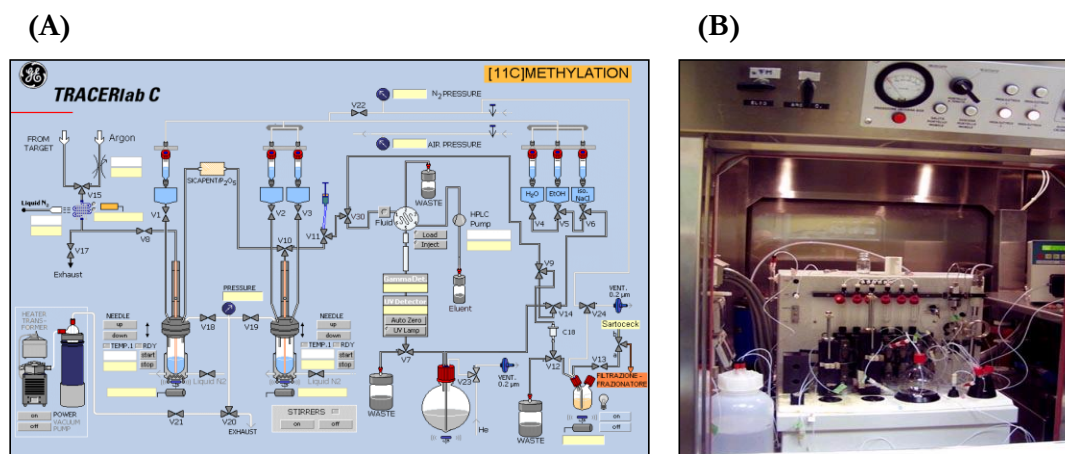
Figure 25. (A) TRACERlab C System Flow Path and (B) hot cell with automated synthesizer.

5.1.2 ^{11}C- methylation via Gas-phase method

An alternative to the lithium aluminium hydride method is the gas-phase halogenation of [^{11}C]methane with iodine (Prenant and Crouzel, 1991). [^{11}C]carbon dioxide was converted into [^{11}C]methane in the presence of Ni catalyst (Shimalite-Ni). [^{11}C]methane was reacted with elemental iodine at 760 °C into a quartz tube to get [^{11}C]methyl iodide.

$$I_2 \rightarrow 2I^{\bullet}$$

$$I^{\bullet} + [^{11}C]CH_4 \rightarrow [^{11}C]CH_3^{\bullet} + HI$$

$$[^{11}C]CH_3^{\bullet} + I_2 \rightarrow [^{11}C]CH_3I + I^{\bullet}$$
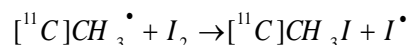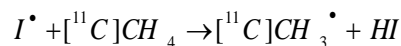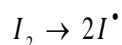
Scheme 4. Formation of $^{11}CH_3I$ via radical reaction.

The [^{11}C]methyl iodide was trapped on the Porapak Q trap at room temperature and the unchanged [^{11}C]methane was recirculated. When the radioactivity in the Porapak Q trap reached the maximum (3 - 5 min), recirculation was stopped and the trap was heated to 200°C to release the [^{11}C]methyl iodide trapped into suitable solvent or reaction mixture. In alternative, [^{11}C]methyl triflate ([^{11}C]CH₃OTf) can be produced by passing gaseous [^{11}C]methyl iodide through a column of silver triflate (AgOTf) at 200°C and then into the reactor. In the figure below the process screen and the module are reported, with particular emphasis on the recirculation system.

(A)   **(B)**
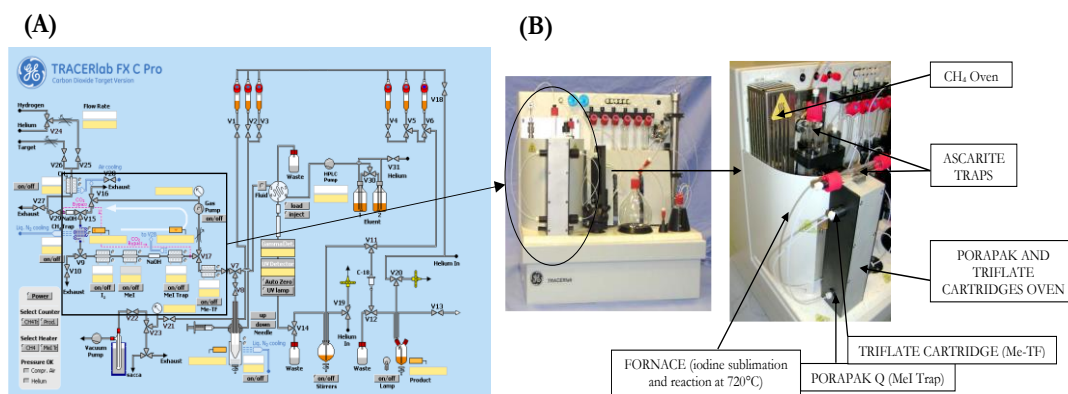
Figure 26. (A) TRACERlab FX C Pro System Flow Path and (B) automated synthesizer.

5.1.3   *Semipreparative and analytical HPLC methods*

In the development of new tracers, a suitable method for identification of the chemical compounds present in the reaction mixture and for quantification of the cold

mass in the final formulation is required. Therefore, an analytical chromatographic method has been set up and the optimized conditions are reported below.

Table 9. Analytical HPLC condition.

CROMATOGRAPHIC ANALYTICAL METHOD		
Column	ACE 5 C-18 (5µm; 250x4,6mm I.D.; Cps)	
Flow	1 ml/min	
UV detector	254 nm (WATERS™486 Tunable Absorbance)	
Mobile phase	**Compound**	**Retention time (min)**
CH₃CN/Phosphate 0.025 M (70/30)	VA425	3.8
	CH₃I	4.5
	VA426	6.1
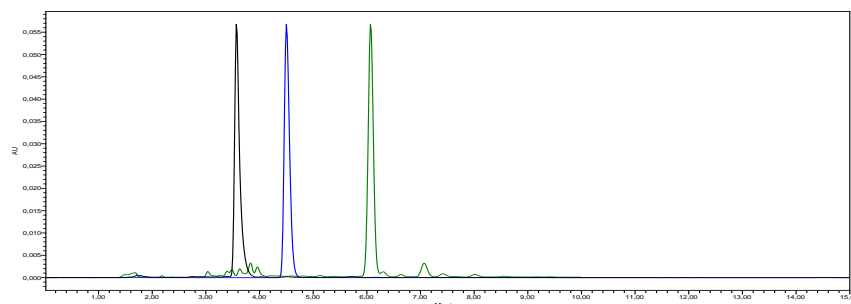
Figure 27. Overlay chromatograms of precursor VA425 (black), methyliodide (blue) and standard VA426 (green).

Furthermore, a calibration curve has been constructed for quantification of VA426, in the range of 1-18 nmol/ml, with R^2 0.9998, in order to calculate the specific activity of [^{11}C]VA426, defined as the amount of radioactivity per unit mass (GBq/µmol or Ci/µmol).

5.1.4 Labelling optimization

Various labelling reactions were performed with both synthesis module (wet- and gas-phase) and different methylating agents ($[^{11}C]CH_3I$ and $[^{11}C]CH_3OTf$). Different solvents, bases and reaction conditions were tested. Preliminary experiments were conducted by recovery of the crude mixture, without any further purification, and subsequent injection into analytical HPLC, using the previously described method. Thus, it was possible to evaluate whether the desired labelled compound was present in the mixture and, in such case, in which percentage with respect to the other radioactive species. The table below reports the conditions used and the percentage $[^{11}C]VA426$ compared to the total activity injected, being $\dfrac{P.A.}{T.A.}(\%)$ the ratio between the active peak area of the $[^{11}C]VA426$ and the area of all the other active peaks present in the chromatogram.

Table 10. Reaction conditions with TRACERlab FX C Pro (gas-phase), using as methylating agent $[^{11}C]CH_3I$.

Solvent	Base	Equivalent Prec./Base	Temp. during CH_3I transfer	Reaction condition	$\dfrac{P.A.}{T.A.}(\%)$
DMSO	TBAOH (55 %)	1/1.0	25°C/2min	80°C/5min	3.1
DMSO	TBAOH (55 %)	1/1.5	25°C/2min	80°C/5min	13.1
DMF	TBAOH (55 %)	1/1.5	25°C/2min	80°C/5min	14.4
DMF	K t-butoxide	1/1.5	80°C/3min	80°C/1min	4.3

Table 11. Reaction conditions with PET-Tracer Nuclear Interface (wet-phase).

Solvent	Base	Equivalent Prec./Base	Temp. during CH_3I transfer	Reaction condition	$\frac{P.A.}{T.A.}(\%)$
DMF	TBAOH (55 %)	1/1.5	80°C/3min	80°C/1min	3.1
HMPA	TBAOH (55 %)	1/1.5	80°C/3min	80°C/2min	---
DMF	K t-butoxide	1/3.0	80°C/3min	80°C/2min	28
DMF	K t-butoxide	1/6.0	80°C/3min	80°C/2min	32.4
DMSO	K t-butoxide	1/6.0	80°C/3min	80°C/2min	---

Experiments conducted using wet-phase method gave best results, even if not satisfactory. Thus, it was decided to perform further experiments using wet-phase module and changing the base. In fact, the bases used till now were not strong enough to abstract the hydrogen from the primary alcohol of VA425. Due to the weak acidity of the alcoholic precursor, stronger base should be necessary for allowing the methylation by [^{11}C]CH$_3$I. It was decided to test sodium hydride (NaH, 60% dispersion in mineral oil) and, in the meanwhile, to set up a purification method by semipreparative HPLC and solid-phase extraction, to isolate [^{11}C]VA426 from the reaction mixture and prepare it in a suitable final formulation. The first column tested was semipreparative ACE 5 C18 (5µm; 250x10 mm I.D.; CPS) and the developed method foresaw the separation of precursor and standard using CH$_3$CN/Phosphate 0.05 M (6/4) as mobile phase at a flow rate of 4 ml/min. Under these conditions, VA425 and VA426 were eluted at 6.8 (k' 1.0) and 12.9 min (k' 2.7), respectively. Once recovered the desired fraction, the compound had to be loaded onto a cartridge to remove organic solvent and salt, washed and recovered. Due to the lipophilicity of VA426, SepPak tC18 Plus, a silica-based bonded phase with strong hydrophobicity, was chosen and a recovery test was performed before introducing this step into the radiosynthesis process. A solution of VA426 in CH$_3$CN/ Phosphate 0.05 M (6/4) (725 nmol/ml in 10 ml) was loaded onto a SepPak tC18 Plus, previously activated with 5 mL ethanol and 10 mL water, and washed with 10 ml water. The fractions collected during the loading and the washing steps were both injected into analytical HPLC, to verify that VA426 was retained onto the cartridge. Less than 1.5 % of the initial amount was

present in the chromatograms. The recovery was done in two different steps: 0.7 ml of ethanol were used for the first recovery and, subsequently, 1 ml of ethanol. 0.7 ml of ethanol elution guarantees a recovery of 78 %, increasing just 6 % with the following 1 ml (Table 12). Thus, less than 1 ml ethanol is enough for recovering most of the VA426 loaded onto SepPak tC18 Plus.

Table 12. Recovery results using SepPak t C18 Plus.

Sep-Pak tC18 Plus	Starting solution	Loading	Washing	Recovery 1	Recovery 2
	VA426		**H₂O**	**EtOH**	**EtOH**
Volume (ml)	10	7	10	0.7	1
Concentration (nmol/ml)	72.50	1.20	0.15	808.94	43.91
Amount (nmol)	725	8.40	1.53	566.30	43.91
Recovery (%)		**1.16**	**0.21**	**78**	**6**

Using 2 mg of precursor and 10 equivalent of base, the radiochemical yield was 23.05 ± 5 % (decay corrected yield, based on $[^{11}C]CH_3I$, n=2), considering just the chromatographic purification. In these tests, the precursor, dissolved in DMSO (300 μl), was mixed with the base for 5 min. Once the reactor was set up into the module, the reaction conditions were as follows:

1. Temperature reactor 2 during activity transfer ($[^{11}C]CH_3I$): 80°C;
2. Reaction condition: 80°C for 2 minutes;
3. Purification via semipreparative HPLC, as before described.

In the table and figure below are reported the results obtained and the radio-chromatogram of a synthesis; the retention time of the peak corresponding to $[^{11}C]VA426$ was 13.4 min.

Table 13. Summary of results obtained using NaH 60 % solid dispersion and semipreparative purification with ACE.

$[^{11}C]CH_3I$ in Re2	Capintec	Reaction Conditions	Final Volume	RCY (d.c.)	RCP (%)	pH
14.5 ± 6.4 GBq	1.5 ± 0.2 GBq	2 mg precursor 2 mg NaH 60% (10) 300 ul DMSO	ca. 3 ml	23.1 ± 7.8 %	90 ± 0.1	$8,6 \pm 0.2$

n=2

Figure 28. HPLC chromatograms (up: radio; down: UV) of purification by semipreparative reversed-phase column ACE 5 C18 (5µm; 250x10 mm I.D.; CPS).

The subsequent HPLC quality control showed a not satisfying radiochemical purity (RCP) (90 %) and overlaid UV- and radio-chromatograms are reported below (the baseline of the radioactive channel showed a step due to the presence of high activity in the first minute of acquisition, that was removed during running sample).
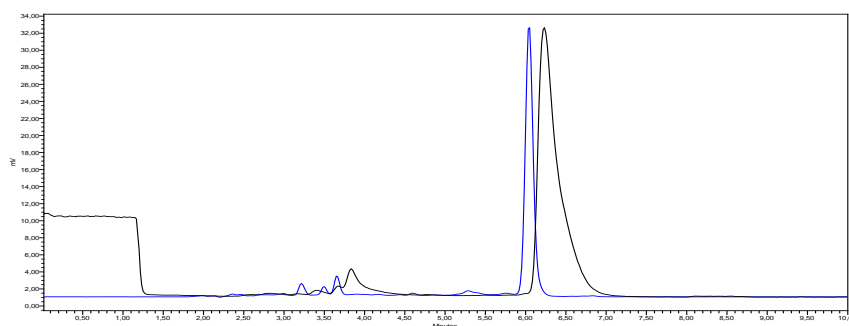
Figure 29. Overlaid HPLC chromatograms (black: radio; blue: UV) of quality control by analytical reversed-phase column ACE 5 C18 (5µm; 250x4.6 mm I.D.; CPS).

Sep-Pak purification was tested on the batch of [^{11}C]VA426 and the RCP increased to 97 %, as shown in the chromatogram.
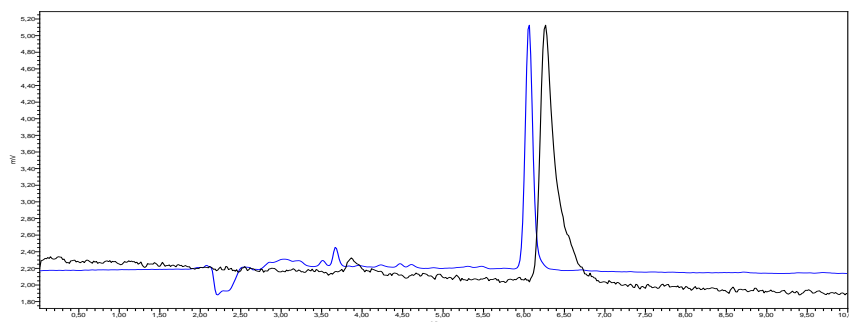
Figure 30. Overlaid HPLC chromatograms (black: radio; blue: UV) of quality control by analytical reversed-phase column ACE 5 C18 (5µm; 250x4.6 mm I.D.; CPS) after purification on cartridge.

In order to confirm that [^{11}C]VA426 was not washed away during the loading and the washing steps, also these fractions were injected and the chromatograms confirmed that just the impurities were washed away and that the desired compound was retained onto the cartridge.
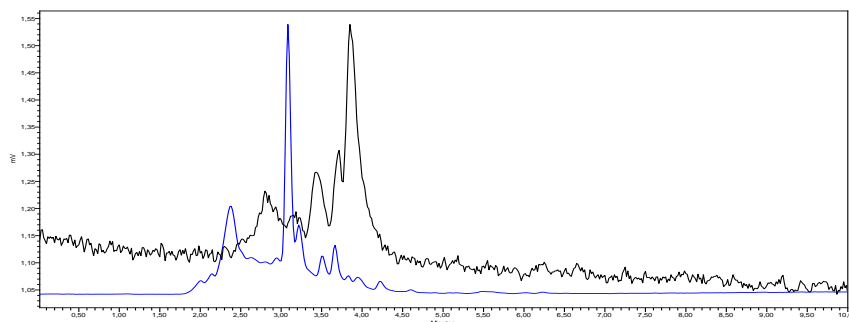
Figure 31. Overlaid HPLC chromatograms (black: radio; blue: UV) of loading step on cartridge by analytical reversed-phase column ACE 5 C18 (5µm; 250x4.6 mm I.D.; CPS).

Thus, cartridge purification was also included in the automated synthesis, to eliminate the active impurities and formulate the desired compound. The fraction containing [^{11}C]VA426, eluted from HPLC, was diluted with 20 mL water for injection and passed over a solid phase extraction column (SepPak tC18 Plus, preconditioned with 5 mL ethanol and 10 mL water for injection). After washing the column with 15 mL water for injection, the desired compound was eluted from the cartridge by 0.7 ml ethanol, followed by 10 ml isotonic saline solution into the collect vial. Table 14 shows the obtained results (RCY decay corrected, based on [^{11}C]CH$_3$I).

85

Table 14. Summary of the results obtained using semipreparative column ACE and SepPak tC18 Plus for purification.

[^{11}C]CH$_3$I in Re2	Capintec	Reaction Conditions	Final Volume	RCY (d.c.)	RCP (%)	pH
17.3 ± 9.1 GBq	0.8 ± 0.6 GBq	2 mg precursor 2 mg NaH 60% (10) 300 ul DMSO	10.7 ml	12.7 ± 1.0 %	94.3 ± 3.0	6.7 ± 0.6

n=3

Surprisingly, the quality control was not satisfactory, showing again a low radiochemical purity.
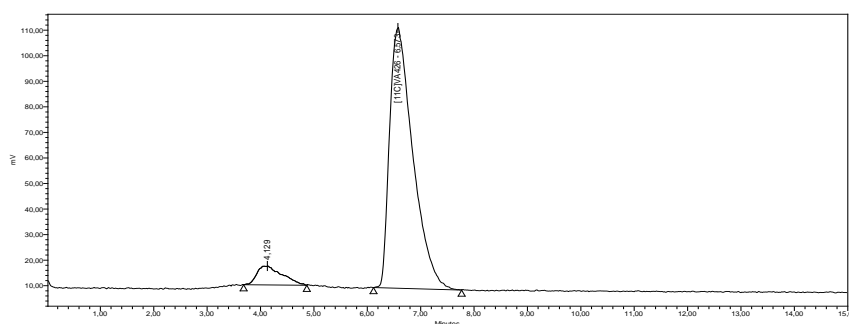
Figure 32. HPLC radio-chromatograms of quality control by analytical reversed-phase column ACE 5 C18 (5μm; 250x4.6 mm I.D.; CPS).

The retention time of the unknown impurity corresponds to the precursor's retention time, as shown in the overlaid chromatograms reported below. Thus, the impurity is likely to be the precursor labelled at the sulphone position, where the methyl group could be substituted with the radioactive one, as shown in scheme 5. Indeed, also in the semipreparative chromatogram, there was a radioactive peak in correspondence of precursor run time, in almost 50:50 ratio with the peak corresponding to [^{11}C]VA426. The HPLC purification was not effective and the subsequent SPE was not able to efficiently separate and purify the final compound from its labelled precursor.
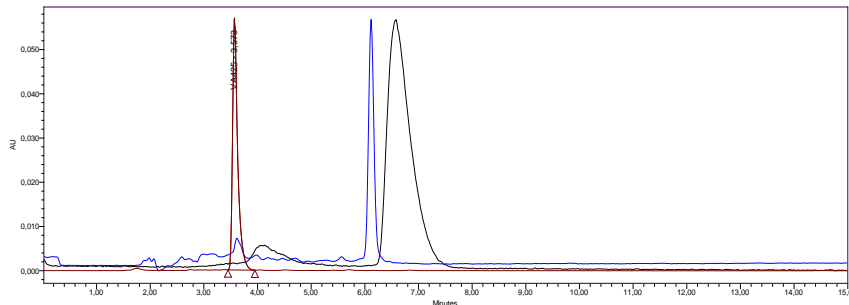
Figure 33. Overlaid HPLC chromatograms of precursor (purple) and quality control of [^{11}C]VA426 (black: radio; blue: UV) by analytical reversed-phase column ACE 5 C18 (5µm; 250x4.6 mm I.D.; CPS).

(a) VA425   **(b) [^{11}C]C-VA425**
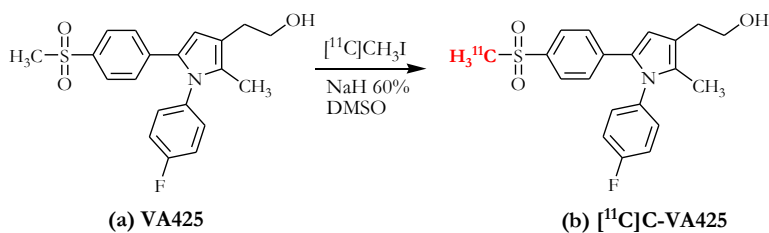
Scheme 5. Side reaction for the formation of [^{11}C]VA425.

In order to reduce the ratio between [^{11}C]VA425/[^{11}C]VA426 and to drive the reaction through the methylation of the alcohol instead of the substitution at the sulphone, less equivalents of base have been used. A suspension of 1 M of NaH in DMSO was prepared, still using NaH 60 % solid dispersion, in absence of a glove box for handling in inert atmosphere the base. Adopting the same reaction condition (2 mg precursor, 300 µl DMSO), 2 equivalents of NaH were added. The RCY was very low (<1 %), resulting in a final activity of 0.14 GBq (4 mCi). Interestingly, the ratio was not changed, suggesting that also using less amount of base, the reaction could not be driven through a highest formation of [^{11}C]VA426. Thus, a more efficient purification was needed and different columns were tested.

First, Polar C18 (Phenomenex) has been tested. Different mixtures of acetonitrile/phosphate at low pH have been examined, to guarantee the presence of the precursor in a single state (non dissociated, ROH), and CH$_3$CN/Phosphate 0.05 M (55/45) pH 4 at a flow of 5 ml/min was found to be suitable. Retention times of precursor

and reference compound were 7.5 min and 14.5 min, respectively. [11C]VA426 was synthesised applying the same conditions used in the previous tests, apart from the semipreparative purification, that was changed in favour of the new method. The desired peak was collected from the column and diluted into water for Sep-Pak tC18 Plus cartridge purification and formulation, in the same conditions described before.
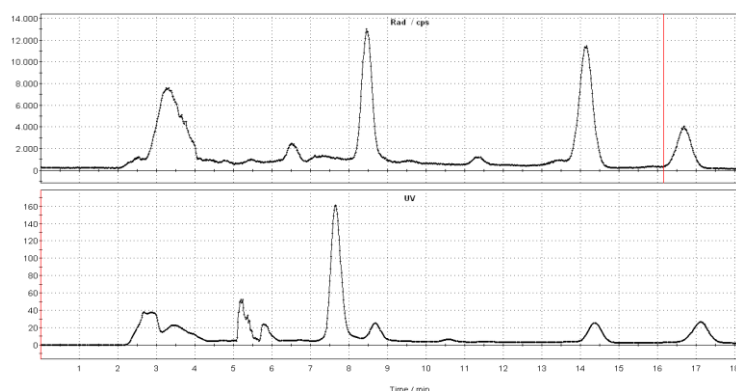
Figure 34. HPLC chromatograms for quality control of [11C]C-VA426 using reversed-phase column Polar (Phenomenex).

The HPLC quality control showed again both radioactive peaks, [11C]VA425 and [11C]VA426, with a better RCP even if not satisfactory (95.1 %).

Table 15. Results obtained using Polar semipreparative column for purifying [11C]C-VA426.

[11C]CH$_3$I in Re2	Capintec	Reaction Conditions	Final Volume	RCY (d.c.)	RCP (%)	pH
23 GBq	1.26 GBq	2 mg precursor 2 mg NaH 60% (10) 300 ul DMSO	10.7 ml	12.9 %	95.1 %	6.5
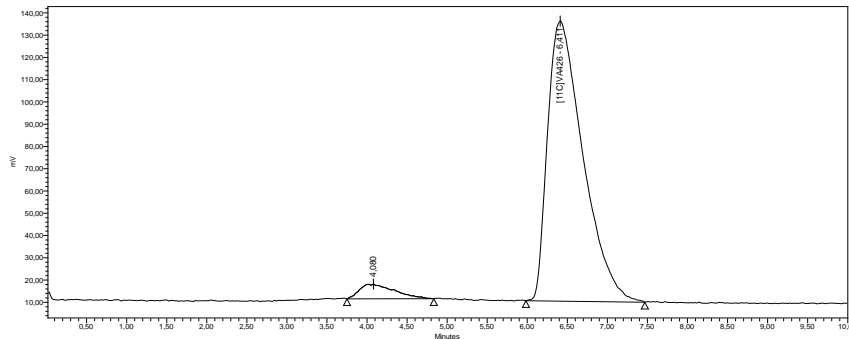
Figure 35. HPLC radio-chromatograms for quality control of [^{11}C]VA426 using analytical reversed-phase column ACE 5 C18 (5µm; 250x4.6 mm I.D.; CPS).

Another column for semipreparative purification, Platinum C18 EPS (10µm; 250x7.0 mm I.D.; Grace), was examined in order to increase the RCP, using two different mobile phases, either $H_2O/EtOH$ (6/4) or H_2O/CH_3CN (6/4). $H_2O/EtOH$ (6/4) was the first mobile phase tested at a flow rate of 4 ml/min and, under these conditions, the retention time of [^{11}C]VA426 was *ca.* 13.5 min. The semipreparative chromatograms of the purification are reported below.
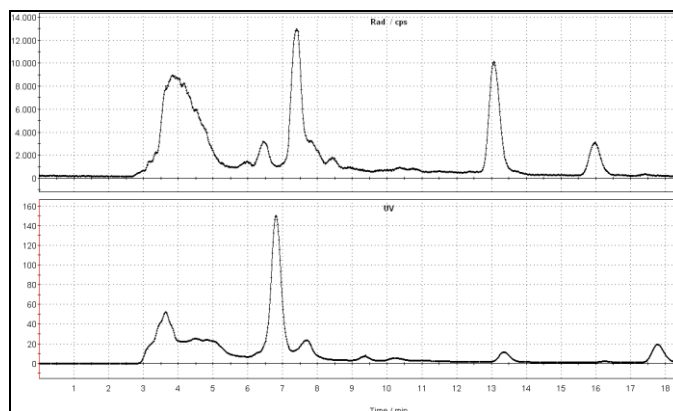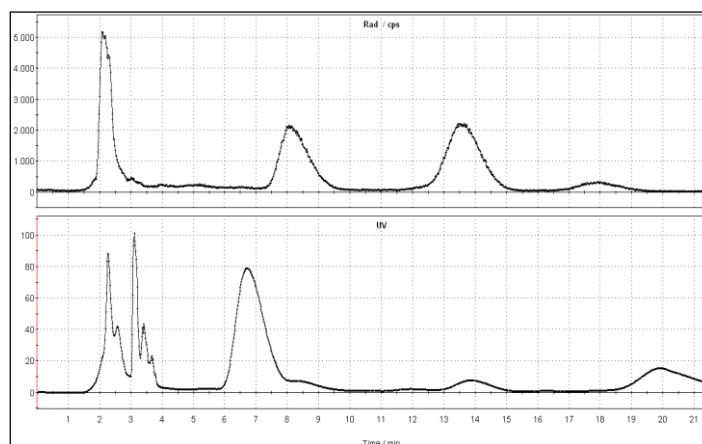

Figure 36. HPLC chromatograms (up: radio; down: UV) of purification by semipreparative reversed-phase column Platinum C18 EPS (10µm; 250x7.0 mm I.D.; Grace).

In the preliminary tests, the final product was directly recovered from the column without further formulation, for a total volume of 8 ml (2 minutes recovery), in order to

verify the RCP. Using this condition, the RCP increased up to more than 95 %, as shown in the quality control chromatograms.
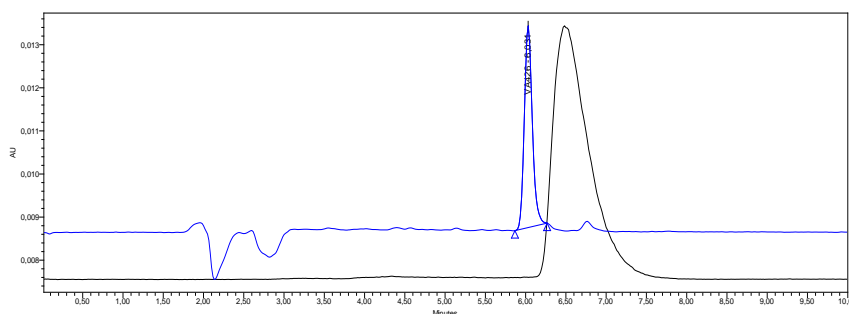
Figure 37. Overlaid HPLC chromatograms (black: radio; blue: UV) of quality control of [^{11}C]VA426 purified by semipreparative reversed-phase column Platinum C18 EPS (10μm; 250x7.0 mm I.D.; Grace).

Also H_2O/CH_3CN (6/4) mobile phase, at a flow rate of 5 ml/min, was tested but, in this case, the RCP was again less than 95 %. The results obtained using the different purification conditions are summarized in the table below.

Table 16. RCP obtained with different conditions for purifying [^{11}C]C-VA426.

Column	Flow (ml/min)	Mobile Phase	RCP (%)
ACE	4	CH_3CN:Fosf. 0.05M (6/4)	92.6±3.2
POLAR	5	CH_3CN/Fosf. 0.05M (55/45) pH 4.0	95.1
PLATINUM	4	EtOH/H_2O (4/6)	98.9±1.1
	5	CH_3CN/Fosf.0.05M (4/6)	96.7±2.2

Therefore, it was decided to purify [^{11}C]VA426 using Platinum with EtOH/H_2O (4/6) as eluent, which gave the best results in terms of RCP. The fraction of the desired compound was collected from the semipreparative column for just 1 minute, in order to have a total volume of 4 ml from the column, and consequently 1.6 ml of ethanol. Then, the collected fraction was diluted with NaCl 0.9 % solution to a final volume of 10 ml.

The total percentage of ethanol was less than 20 %, which is the maximum percentage of ethanol for intravenous bolus injection (Strickley, 2004). The overall synthesis took 30 minutes and the results are reported below.

Table 17. Results obtained using Platinum semipreparative column for purifying [^{11}C]VA426.

[^{11}C]CH$_3$I in Re2	Capintec	Reaction Conditions	Final Volume	RCY (d.c.)	RCP (%)	pH
16.8 ± 6.1 GBq	1.7 ± 0.8 GBq	2 mg precursor 2 mg NaH 60% (10) 300 ul DMSO	10 ml	26.3 ± 6.9 %	97.6 ± 2.9	6,9 ± 0.2

n=6

In the first syntheses, the specific activity (SA) was less than 37 GBq/µmol – 1 Ci/µmol (7.4 GBq/µmol - 0.2 Ci/µmol), which was the established lower limit suitable for tracer specific for saturable targets. Thus, the ascarite traps used to purify the cyclotron target gas and the module carrier helium were changed in the attempt to improve this parameter. After optimization, the specific activity increased up to 90 ± 54 GBq/µmol (2.42 ± 1.46 Ci/µmol), with an average final activity of 2.01 ± 0.17 GBq (54.20 ± 4.71 mCi) (n=3). In addition, standard methods for determination of half-life and radionuclidic purity were also applied.

Different filters were tested for sterile filtration. The first test was performed with the initial formulation (1 ml ethanol and 9 ml NaCl 0.9 %, formulation A) and the obtained results are reported below.

Table 18. Results obtained with different filters for sterile filtration.

Filters	Init. Conc (nmol/ml)	Conc. after Filtration (nmol/ml)	Retained (%)
Acrodisc (PVDF)	20.5	10.7	52.2
Millex GV (PVDF)	55.6	30.4	**45.3**
Sartorius (cellulose acetate)	55.5	4.3	92.3

The better results were obtained with Millex GV filter (0.22 μm, PVDF, 13 mm, ethylene oxide sterilized), even if the percentage of tracer retained was almost 50 % and thus not applicable due to the low final activity achieved. The improvement in the synthetic pathway and the subsequent change in the final formulation (16 % ethanol, formulation B) led to a new sterile filtration test. Millex GV was selected, since it was proved to be the better one in the previous test. The amount of tracer retained on Millex GV decreased by increasing the percentage of ethanol in the formulation, due to the poor solubility of the molecule in the final formulation A. Going up to less than 20 % of ethanol, and in particular to 16 %, the percentage of retained tracer decreased to 10.8 %.

Table 19. Results obtained with Millex GV with two different formulations.

Formulation	Millex GV		
	Init. Conc (nmol/ml)	Conc. after Filtration (nmol/ml)	Retained (%)
A (10 % EtOH)	55.6	30.4	45.3
B (16 % EtOH)	13.9	12.4	**10.8**

5.1.5 Preclinical

Preliminary investigation was performed *in vivo* using BL/6 female mice to monitor the biodistribution and clearance of the new tracer [^{11}C]VA426. For this purpose, the animals have been injected *i.p.* with 10 mg/Kg of lipopolysaccharide (LPS) in order to create a peritoneal inflammation (Carter *et al.*, 2012). Control animals have been treated with the vehicle (PBS). 24 hours after injection, the animals were studied by [^{11}C]VA426-PET. Mice treated with LPS, compared with the control, showed more intense uptake at the site of injection of the toxin. In particular, it was possible to notice a major distribution in the liver and intestine, as shown in the figure below. Further protocols have been planned, in order to verify the specificity and potential use of this tracer for colorectal cancer, since recent epidemiologic studies have shown a 40-50 % reduction in mortality

from colorectal cancer in individuals who take NSAIDs drugs on a regular basis compared with those not treated with these agents (Tsujii *et al.*, 1997).
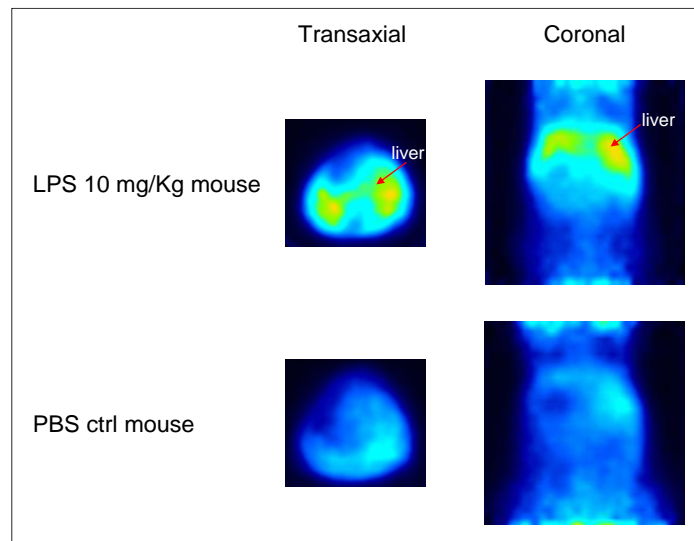
Figure 38. PET images of BL/6 mice injected with [^{11}C]VA426, via 60 minutes acquisition after tracer's injection.

5.2 Radiometals preparation

5.2.1 Preparation of [^{89}Zr]ZrCl$_4$

^{89}Zr was produced from the ^{89}Y$(p,n)^{89}$Zr nuclear reaction by proton bombardment of commercially available, high-purity ^{89}Y-foil (25 mm × 12.5 mm × 0.127 mm, approx. 0.33 g, 3.70 mmol; 99.9 %, Alfa Aesar$^{®}$) on a PETtrace cyclotron (GE). Yttrium is a lanthanide group metal and has only one stable isotope, ^{89}Y, an element that does not require enrichment because of its natural abundance of 100 %. In these studies, the radionuclidic purity of the isolated ^{89}Zr fractions was found to be > 99.9 %. The radionuclidic purity of the product was determined by gamma-spectrometry using a Ge/Li-detector (Berthold) controlled and analyzed by *Maestro* software. No significant amount of ^{88}Zr and ^{88}Y were detected (Figure 39).
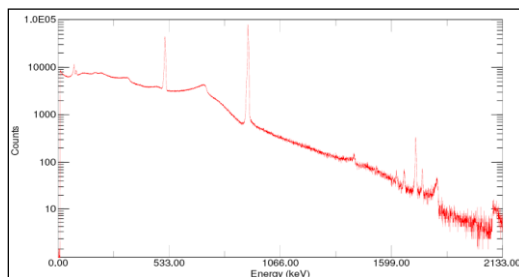
Figure 39. Zirconium-89 γ-ray spectrum.

Table 20. Decay data of ^{89}Zr.

Radiation Type	Energy (KeV)	Radiation intensity (%)
β$^+$	395,5	22,74
Auger-L	1,91	79
Auger-K	12,7	19,47
γ annihilation	511	45,48
γ	909,15	99,04
γ	1620,8	0,07
γ	1657,3	0,11
γ	1713	0,75
γ	1744,5	0,12

The intact commercially available yttrium foil (approx. 0.36 g, 25 x 25 x 0.127 mm, 99.9 %, Alfa Aesar®) was cut in two pieces (25 x 12.5 mm each), mounted in a target holder of high purity alumina (two aluminium plates with beam window) and placed into the shielding box that was moved into the cyclotron room, as shown in Figure 40. After that, an automatic system placed the target holder with the foil into a custom-made water-cooled target body mounted with a 11° angle of incidence (Figure 41).
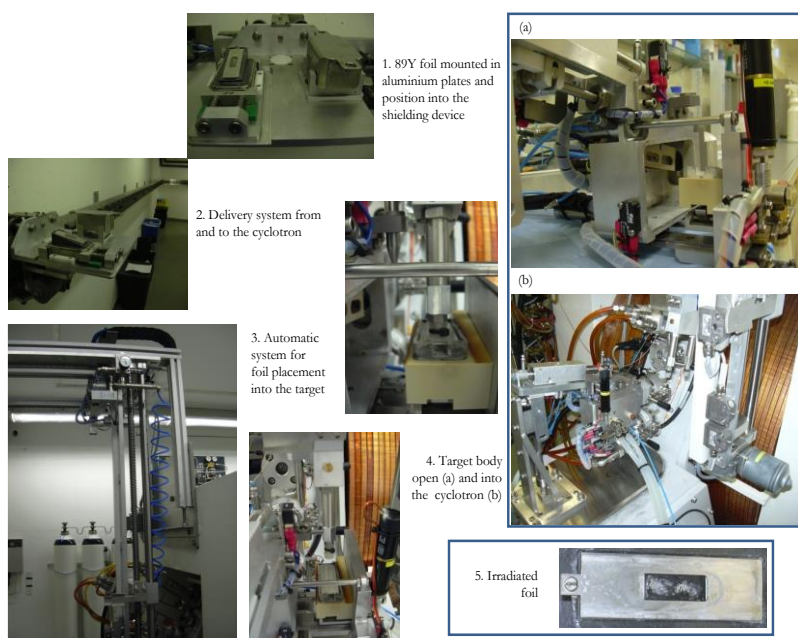
Figure 40. Automatic system for Yttrium foil positioning into the target body and delivery from and to the cyclotron.

Figure 41. Target body with the aluminium plates in open and closed mode (left and right, respectively) with the window for the entrance of the proton beam during the irradiation into the cyclotron.

The optimal beam energy for the production of ^{89}Zr was between 4-14 MeV. The replacement of the original cyclotron target foil (havar, 25 μm) by a thicker havar foil of 50 μm led to an additional proton energy degradation of approximately 1 MeV (estimation). Under these pre-conditions, a typical ^{89}Zr production protocol foresaw a proton irradiation for 1 h with resulting beam energy of approximately 14 MeV and a beam current of 7 μAh. The average yield was 33 ± 8 MBq/μAh, resulting in batches of 175-287 MBq of ^{89}Zr. In fractionated irradiations of 6 h at 7 μA, up to 1 GBq of ^{89}Zr was obtained. In a single fractionated irradiation of 12 h with 10 μA, 1.7 GBq of ^{89}Zr were obtained. The purification and preparation of [^{89}Zr]ZrCl$_4$ was done similarly to the known procedure described by Holland *et al.*, 2009. Briefly, ^{89}Zr was isolated as [^{89}Zr]Zr-oxalate by using a solid-phase hydroxamate resin with >80 % recovery of the radioactivity. In order to remove the potentially toxic oxalic acid from the next steps, [^{89}Zr]Zr-oxalate solution in 1.0 M oxalic acid was loaded onto an activated Waters Sep-pak Light QMA, strong anion exchange cartridge, washed with 50 mL trace select water and eluted with 500 μl of 1.0 M HCl (aq.). Finally, the excess of acid was neutralized by adding the appropriate volume of Na$_2$CO$_3$ (aq.) (1 or 2 M in trace select water) (100–250 μl) and the pH adjusted to 7-8.
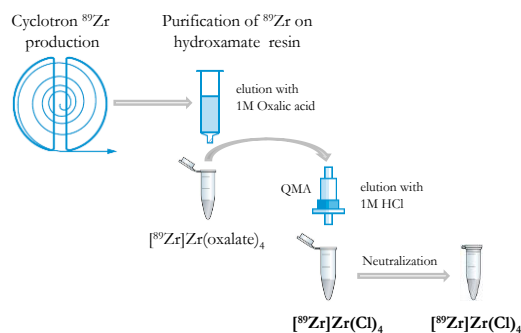
Figure 42. Production and purification of ^{89}Zr.

To facilitate minimal radiation exposure during the preparation and purification of ^{89}Zr, a system was implemented to reduce the handling processes and consequently the time exposure of the personnel. The loading and washing steps were carried out placing the cartridge onto a system connected to a pump which created a negative pressure,

allowing the operator to stay at a reasonable distance during these steps, thus reducing the absorbed dose (see below).
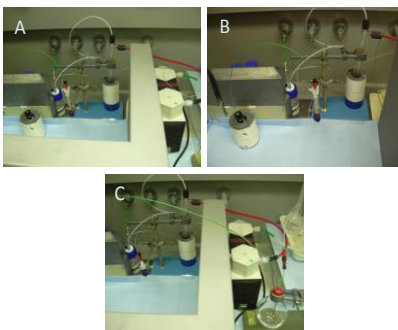
Figure 43. A, B) Activity loading on the hydroxamate resin under negative pressure; C) QMA washing with 50 ml water traceSELECT® after [^{89}Zr]Zr-oxalate under gas flow and pump aspiration.

The table below reports the recovery obtained during the purification of ^{89}Zr.

The recovery of [^{89}Zr]Zr-oxalate was > 85 %, with the best result (97 %) achieved in the experiment with the highest activity (1,1 GBq). The final recovery of the entire preparation, including the [^{89}Zr]Zr-oxalate conversion in [^{89}Zr]Zr-chloride, was >80 %. The final reported volume had different values due to the changing of the molarity of the solution of Na_2CO_3 used for neutralization (from 1 M to 2 M).

Table 21. Recovery for every single step and final recovery of the initial foil activity.

Recovery Zirconium-89 Preparation							
Foil Activity (MBq)	^{89}Zr-oxalate (MBq)	Recovery (%)	^{89}ZrCl$_4$ (MBq)	Recovery (%)	Final Activity (MBq)	Final Volume (µl)	Final Recovery (%)
377	304	80,6	282	92,8	278	700	73,7
211	181	85,8	166	91,7	165	700	78,2
327	274	83,8	270	98,5	260	750	79,5
434	378	87,1	372	98,4	360	750	83,0
289	256	88,6	251	98,1	253	750	87,5
518	456	88,0	434	95,2	419	600	80,9
452	398	88,1	390	98,0	377	600	83,4
1141	1110	97,3	1040	93,7	1030	615	90,3
	Mean (%)	**87,4**	**Mean (%)**	**95,8**		**Mean (%)**	**82,1**

5.2.2   Preparation of [^{68}Ga]GaCl$_3$

The preparation and purification of [^{68}Ga]GaCl$_3$ was done similarly to the known procedure described by Meyer *et al.*. Briefly, ^{68}Ga was eluted from a TiO$_2$-based ^{68}Ge/^{68}Ga generator with ca. 2 ml of 1M HCl (aq.) and collected into a vial containing 1 ml of HCl 30 % (9,5 M, Suprapure®, Merck). This solution was then loaded onto a strong anion exchange resin (100 mg Dowex 1 x 8), preactivated with 1 ml ethanol, 1 ml trace select water and 1 ml 4 M HCl (aq.). At hydrochloric acid concentrations > 5.5 M, Ga^{3+} ions form the negatively charged [GaCl$_4$]$^-$ complex and the ^{68}Ga was adsorbed onto the resin, while all the other cationic impurities were not retained. The resin was then washed with 2 ml of 4 M HCl (aq.) and flushed with air, to blow off most of the strong hydrochloric acid. Elution of the ^{68}Ga from the microcolumn was achieved with 2 x 100 µl of trace select water, which led to decomposition of the tetrachloro complex and release of ^{68}Ga as ^{68}Ga^{3+} aq. The pH of the effluent solution (about 200 µl) was usually in the order of 2.0. Finally, the excess of acid was neutralized by adding the appropriate volume of Na$_2$CO$_3$ (aq.). In the initial experiments, 1 M Na$_2$CO$_3$ in trace select water was used (100–250 µl) resulting in a high final volume; thus, in order to increase the radioconcentration, the molarity was increased (2 M) with a maximum volume used of 100 µl. The overall time for the concentration process was less than 15 min.

Table 22. Recovery for every single step and final recovery of the initial activity.

Recovery Gallium-68 Preparation							
Eluted Activity (GBq)	Cartridge (MBq)	Retention (%)	⁶⁸GaCl₃ (MBq)	Recovery (%)	Final Activity (MBq)	Final Volume (μl)	Final Recovery (%)
1,25	872	69,8	644	73,9	576	390	46,1
1,25	815	65,2	651	79,9	594	430	47,5
1,23	742	60,3	607	81,8	545	450	44,3
1,29	833	64,6	607	72,9	585	275	45,3
927	592	63,9	482	81,4	449	375	48,4
939	738	78,6	620	84,0	515	340	54,8
685	552	80,6	461	83,5	446	300	65,1
1,11	668	60,2	524	78,4	514	300	46,3
893	469	52,5	375	80,0	353	300	39,5
1,11	762	69,3	565	74,1	550	300	50,0
	Mean (%)	66,50	**Mean (%)**	79,00		**Mean (%)**	48,74

5.3 DUPA Peptide

Recently, due to the very promising results reported by Kularatne and co-workers, analogues of DUPA-Pep were synthesized, applying different chelating agents or prosthetic groups for the introduction of radionuclides, but maintaining the structural features which had shown to be essential for the binding to PSMA, that were the two phenylalanine residues tethered to DUPA-Pep via an 8-aminooctanoic acid spacer. Below are reported the structures of these new compounds (Malik *et al.*, 2011; Malik *et al.*, 2012).
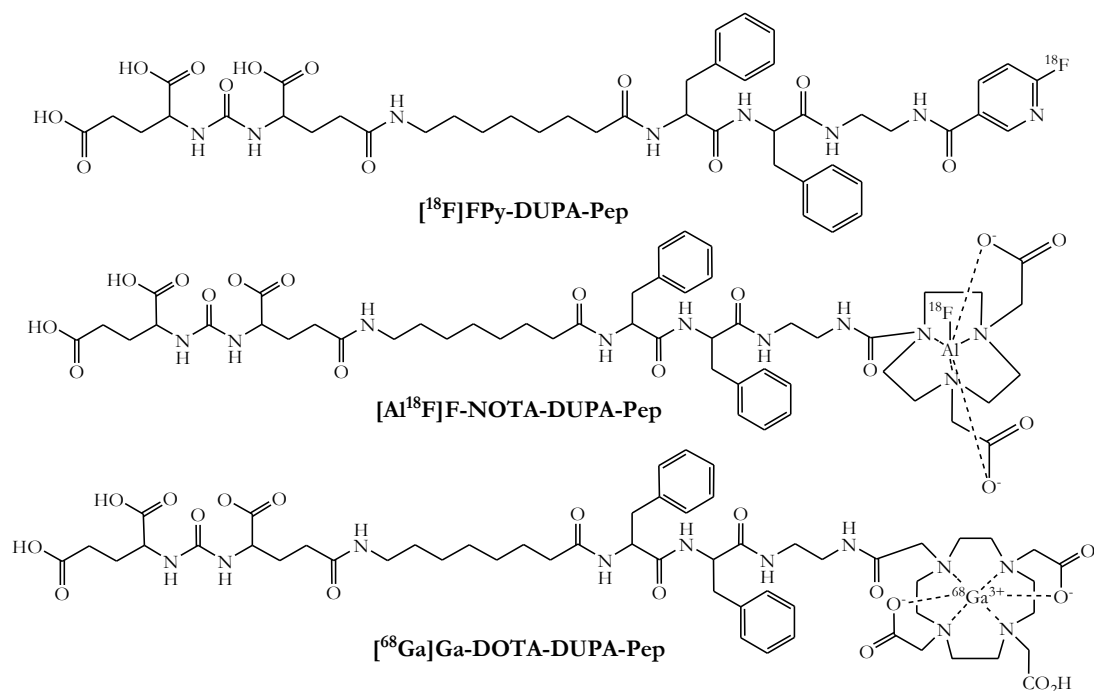
Figure 44. PSMA ligands.

Of particular interest is the radiotracer [^{68}Ga]Ga-DOTA-DUPA-Pep, used at the Nuclear Medicine of the Universitätsklinik of Ulm (Ulm – Germany). The interaction of the labelled peptide with PSMA was characterized in different cell lines (LNCaP, PC-3) and also in prostate carcinoma xenograft murine models. High specificity was demonstrated by significant binding affinities in PSMA-positive cell lines, HET-CAM xenografts and SCID mouse xenograft models. Immunohistochemical results of HET-CAM-model experiments clearly demonstrated specific binding to PSMA-positive cell lines, which was completely inhibited by 2-PMPA. Strong PSMA-affinity was shown by binding constants (K_D) of 21.6 ± 0.4 nM. In PSMA-positive SCID mouse xenografts, an uptake of 1.16 ± 0.22 % ID/g and a tumor-to-tissue ratio of 3.4 ± 1.8 were measured. Unspecific binding of 0.11 ± 0.04 % ID/g with a tumor-to-tissue ratio of 0.62 ± 0.50 was determined in PSMA-negative SCID mouse xenografts (Winter *et al.*, 2011). In clinical application, first *in vivo* experiments with [^{68}Ga]Ga-DOTA-DUPA-Pep showed very

promising results in detection of prostate carcinoma relapses and metastases with PET/CT, as shown in Figure 45.

Figure 45. A 70-year-old patient with a history of prostatectomy because of PCa 12 years before the examination, Gleason score 5+5, local radiation therapy and castration-resistant PCa at presentation, PSA 3 ng/ml.
[^{68}Ga]Ga-DOTA-DUPAPep showed large local recurrence and disseminated bone marrow metastases confirmed by MRI and a large local recurrence (arrow). Note normal tissue background mostly in blood pool, uptake in kidneys and urinary tract with some urine contamination (arrowhead) due to urinary conduit because of incontinence. Maximum intensity projection (MIP) of a PET image of the trunk acquired 1 h after injection of 85 MBq [^{68}Ga]Ga-DOTA-DUPA-Pep. (Source: Reske *et al.*, 2013).
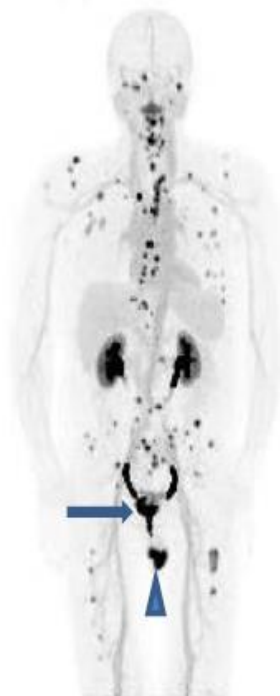
This PSMA-specific peptide provides a promising approach as agent for molecular imaging diagnostics of prostate carcinoma. The use of 1,4,7,10-tetraazacyclododecane-*N*,*N'*,*N''*,*N'''*-tetraacetic acid (DOTA) as chelating agent for ^{68}Ga required high temperatures and radiolabelling was carried out at 90°C and low pH.

In the present work, other analogues of DUPA-Pep were synthesized, conjugating DUPA-Pep to Desferrioxamine (Desferal; Df) and CHX-A´´-DTPA. Subsequent labelling with different radiometals, for both diagnosis and therapy, were performed. The ability to label Desferal and CHX-A´´-DTPA conjugated biomolecules at room temperature avoids unexpected heat-based side reactions.

5.3.1 Df-DUPA-Pep

5.3.1.1 Synthesis of Df-DUPA-Pep

Dupa-Pep has been synthesized and applied in preclinical and clinical using various chelating agents. Generally, the complexation requires high temperature, low pH or both these conditions. Desferal is an interesting chelating agent since it allows the incorporation of radiometal into molecules at room temperature and neutral pH. It is the chelating agent of choice for ^{89}Zr and it works also well with ^{68}Ga. Thus, Df-DUPA-Pep was synthesized. The synthesis is outlined in scheme 6.
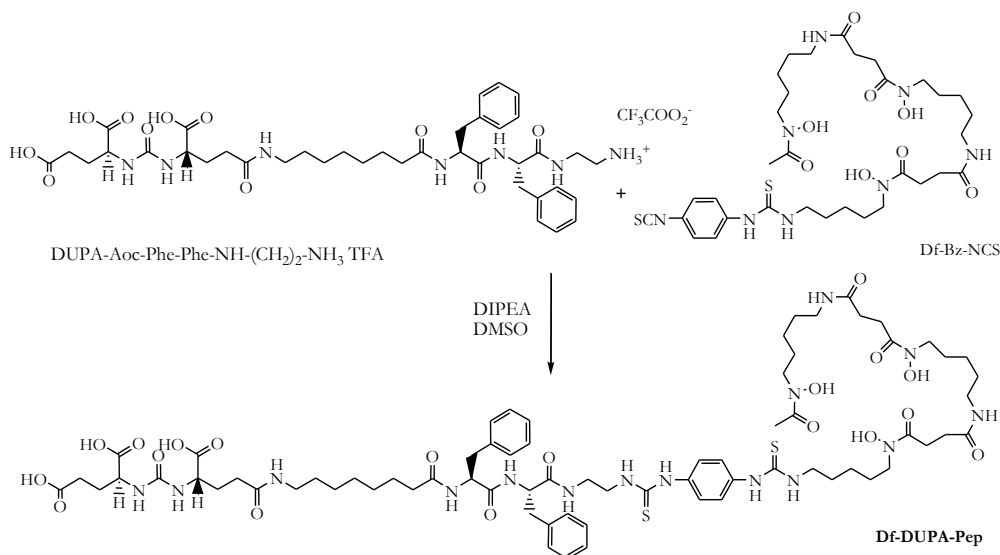
Scheme 6. Synthesis of Df-DUPA-Pep.

The Df-DUPA-Pep was prepared by reaction of *p*-isothiocyanatobenzyl-desferrioxamine (Df-Bz-NCS) with DUPA-Pep in DMSO in the presence of DIPEA as base. The reaction was carried out at room temperature overnight. The final compound was isolated and purified from the mixture by preparative HPLC using C18 column [Phenomonex Gemini 5u C18, 250x21.1mm, 5 μm] at a flow rate of 10 ml/min and a gradient elution (Table 23).

Table 23. Gradient elution for Df-DUPA-Pep purification.

	Gradient elution	
Time (min)	% MeCN, (0.1% TFA)	% Water, (0.1% TFA)
0-6	15	85
6-8	35	65
8-30	45	55
30-40	45	55

The peptide fraction was collected at a retention time of *ca.* 22.5 min to obtain Df-DUPA-Pep as a white powder, after lyophilisation, in 80 % yield and > 95 % purity (HPLC).

Figure 46. HPLC analytical chromatogram of Df-DUPA-Pep using reversed-phase column (Phenomenex Gemini, 5 μm, C18, 250 x 4.6 mm) and gradient elution of solvent A (water with 0.1 %TFA) and solvent B (MeCN with 0.1 %TFA), (85 % A for 4 min, 85-30 % A from 4-11 min, 30- 85 % A from 11-14 min, 85 % A from 14-16 min) at flow rate of 2 mL/min.

5.3.1.2   [^{89}Zr]Zr-Df-DUPA-Pep

5.3.1.2.1   Labelling of [^{89}Zr]Zr-Df-DUPA-Pep

Different conditions were tested in order to optimize the labelling of Df-DUPA-Pep with ^{89}Zr. Different zirconium intermediate could be applied for the labelling.

Although the [⁸⁹Zr]Zr-oxalate solution was suitable for complexation reactions involving the Df ligand, oxalic acid is highly toxic (decalcification of blood and acute renal failure due to the obstruction of kidney tubules by calcium oxalate) and must be removed before performing any *in vitro* or *in vivo* studies (Holland *et al.*, 2009). Therefore, [⁸⁹Zr]Zr-chloride has been investigated for the labelling Df-DUPA-Pep.

Increasing activity amount were applied on 50 µg precursor batches to study the effect of the excess on the radiochemical yield at 1, 3 and 24 hours. The results are reported below. The excess of peptide molecules with respect to the atom of radionuclide was calculated considering the specific activity of ⁸⁹Zr (16,615 TBq/mg).

$$Specific\ Activity\ \left(\frac{MBq}{mol}\right) = 16615\frac{TBq}{g} \cdot 89\frac{g}{mol} \cdot 10^6\frac{MBq}{TBq} = 1{,}48 \cdot 10^{12}\frac{MBq}{mol}$$

$$Number\ of\ atom\ for\ activity = \frac{N_A}{SA}$$

$$Number\ of\ atom\ for\ 1\ MBq\ activity\ = \frac{6{,}02 \cdot 10^{23}\text{mol}^{-1}}{1{,}48 \cdot 10^{12}\frac{\text{MBq}}{\text{mol}}} = 4{,}07 \cdot 10^{11}\text{MBq}^{-1}$$

Once calculated the number of atom of ⁸⁹Zr for 1 MBq, it was possible to calculate the excess of number of peptide molecules, considering that the molecular weight of Df-DUPA-Pep is 1550 g/mol, with respect to the numbers of atoms of the radionuclide.

$$Number\ of\ molecule\ of\ DfDUPAPep\ in\ 1\ g = \frac{6{,}02 \cdot 10^{23}\text{mol}^{-1}}{1550\frac{\text{g}}{\text{mol}}} = 3{,}99 \cdot 10^{23}\text{g}^{-1}$$

After incubation, 1 µL aliquots were withdrawn and analysed by RP-18 TLC using citrate buffer (0.1 M, pH 5) as a mobile phase solvent. Free ⁸⁹Zr formed complex with citrate and was eluted with the solvent front, whilst [⁸⁹Zr]Zr-Df-DUPA-Pep remained at the origin. TLC plates were determined by using phosphoimager. For an alternative

quantification method, the strips were cut in half and the γ-rays emissions at 909 keV were counted with a calibrated Packard Cobra™ II Auto-Gamma Counter using a dynamic energy window of 820 – 990 keV.

Table 24. Radiochemical yield at different excess of [89Zr]ZrCl4 measured at different time.

Amount (μg)	[89Zr]ZrCl4 Activity(MBq)	Excess	RCY (%)		
			1h	3h	24h
50	65,3	730	57	79	87
	30,5	1562	94	98	98
	18,7	2548	96,4	98	98
	9,3	5123	97,9	99	99
	4,6	10358	98,2	99	99
	2,3	20716	98,3	99	99
	0,98	48620	98,8	98	97
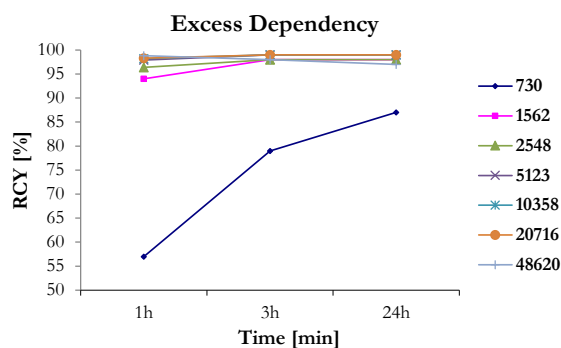
Figure 47. Radiochemical yields of Df-DUPA-Pep labelling with 89Zr in dependence on excess.

A more accurate study was then performed and the amount and time dependencies were considered, using different amounts of peptide with the same activity. 25 μl of [89Zr]ZrCl4 solution (2.1-2.2 MBq) were added to a solution of Df-DUPA-Pep dissolved in DMSO and 0.25 M HEPES buffer (pH=7.5; 500 μL). After brief shaking, the reaction was conducted at room temperature. Complexation of 89Zr and Df-DUPA-Pep was monitored at different times by y-counter measurements of TLC. The results are reported below.

Table 25. RCYs for the radiosynthesis of $[^{89}Zr]Zr$- Df-DUPA-Pep in dependence on concentration and time.

Amount (µg)	RCY (%)				
	1min	5min	10min	30min	60min
1	14.7±1.5	18.7±0.6	19.3±0.6	22.0±1.0	24.0±1.0
5	77.3±2.1	94.0±1.0	94.3±1.5	95.0±1.0	96.0±1.0
10	95.7±0.6	96.7±1.5	97.0±1.0	97.3±0.6	97.7±0.6
25	96.7±0.6	97.0±2.0	98.0±1.0	98.3±0.6	98.7±0.6
50	98.3±0.6	99.0±0.0	98.7±0.6	98.3±0.6	98.7±0.6

n=3
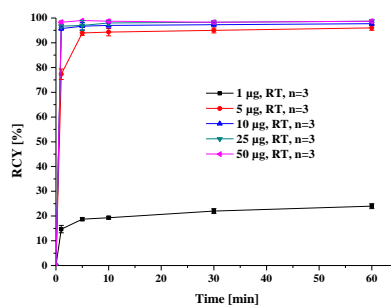
Figure 48. RCYs of Df-DUPA-Pep labelling with $[^{89}Zr]Zr\text{-}Cl_4$ in dependence on concentrations and time.

Considering the above mentioned excess, applying the same activity, the excess of peptide was 381 when using 1µg of peptide, that was found to be not sufficient to obtain a reasonable yield in the initial test; in fact, the RCYs were extremely low and did not overcome 30 % after 1h, confirming the data obtained in the initial evaluation. Increasing the amount of peptide to 5 and 10 µg, the excess raised to values that gave excellent results in the initial experiment at 1h measurement *i.e.* 1900 and 3800, respectively. As shown in the graph, apart from the 1 µg measurements, the complexation was extremely efficient, giving a high incorporation of the metal and all the reported RCYs raised up to more than 90 % within 5 minutes. The labelled peptide was analysed also by analytical radio-HPLC (Figure 49).
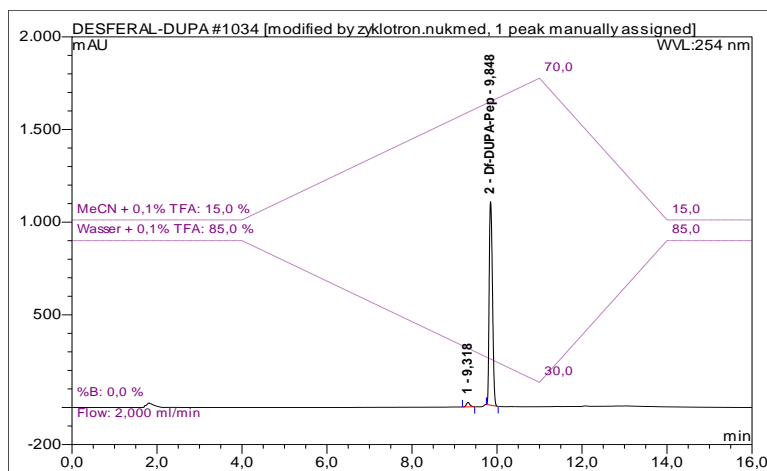
Figure 49. HPLC chromatograms of [^{89}Zr]Zr-Df-DUPA-Pep using reversed-phase column (Phenomenex Gemini, 5 μm, C18, 250 x 4.6 mm) and gradient elution of solvent A (water with 0.1 %TFA) and solvent B (MeCN with 0.1 %TFA), (85 % A for 5 min, 85-30 % A from 5-14 min, 30- 85 % A from 14-16 min) at flow rate of 2 mL/min (first peak being the total activity injected).

In all the reported experiments, the activity used was quite low, according to the ALARA (as low as reasonable achievable) concept. Thus, a study using highest activity was performed in order to get some information about labelling and complex stability. The amount of peptide used for this experiment was 100 μg, which is the maximum dose injectable according to the microdosing concept written in the EU Guideline (CPMP/SWP/2599/02/Rev 1). The appropriate amount of [^{89}Zr]ZrCl$_4$ solution (92 ± 10 MBq; 250-350 μl) was added to a solution of 100 μg Df-DUPA-Pep dissolved in DMSO (2 mg/ml) and 500 μL of 0.25 M HEPES buffer (pH=7.5). The mixture was reacted at room temperature. Complexation of ^{89}Zr and Df-DUPA-Pep were monitored at different time intervals by y-counter measurements of TLC. 95 % of the batch activity derived from the complex within 30 minutes and this percentage remained stable for 24 h, without a reduction of the incorporation.

Table 26. Radiochemical yield in dependence on time (starting activity: 92 ± 10 MBq; amount of peptide: 100 μg).

Amount (μg)	RCY %					
	5 min	**10 min**	**30 min**	**60 min**	**180 min**	**24 h**
100	76.7±8.4	89.4±4.4	95.7±0.7	95.6±1.9	95.4±1.9	95.4±1.5

n=3
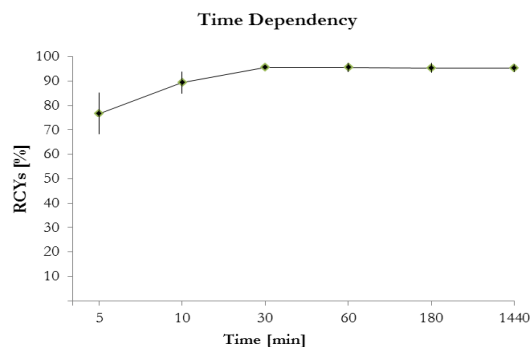
Figure 50. RCYs of Df-DUPA-Pep (100 μg) labelling with [^{89}Zr]Zr-Cl$_4$ (92 ± 10 MBq) in dependence on time.

5.3.1.3 [^{68}Ga]Ga-Df-DUPA-Pep

^{68}Ga is increasing popularity because it can be obtained from a commercially available ^{68}Ge/^{68}Ga generator system, independent from a cyclotron, which delivers the ^{68}Ga nuclide reliably for up to a year. However, few examples of ^{68}Ga-labelled proteins or other large biomolecules can be found in literature. This situation is mainly due to the fact that the chelator DOTA, which is predominantly used for radiometal nuclide complexation in nuclear medicine, requires high temperatures or long reaction times to form a complex with ^{68}Ga (Wadas *et al.*, 2010). Because proteins are susceptible to heat-induced disintegration, chelators requiring a heating step for complexation are not desirable for such a radiolabelling approach. Thus, the envisioned ^{68}Ga-labelling procedure for proteins should comprise only 1 simple, fast, and preferably quantitative labelling step at room temperature without the need for further purification.

5.3.1.3.1 Labelling of [^{68}Ga]Ga-Df-DUPA-Pep

After the preparation and purification of [^{68}Ga]GaCl$_3$ as previously described, the resulting [^{68}Ga]GaCl$_3$ solution (10-15 μl; 8-12 MBq) was added to a solution of Df-DUPA-Pep, dissolved in DMSO (1mg/ml), and 0.25 M HEPES buffer (pH 7.45, 500 μL); thereafter, the reaction was carried out at room temperature. 1 μL aliquots were withdrawn

at different time points and analyzed by RP-18 TLC using H_2O, 0.1 % TFA/MeOH (30/70) as mobile phase solvent. Using this eluent, the free gallium remained at the origin (Rf: 0.01) while the peptide was eluted with a Rf value of 0.7 (Figure 51). To calculate the corresponding Rf, low amount of activity was spotted at the solvent front, on the right part of the plate. TLC plates were determined by using phosphoimager.
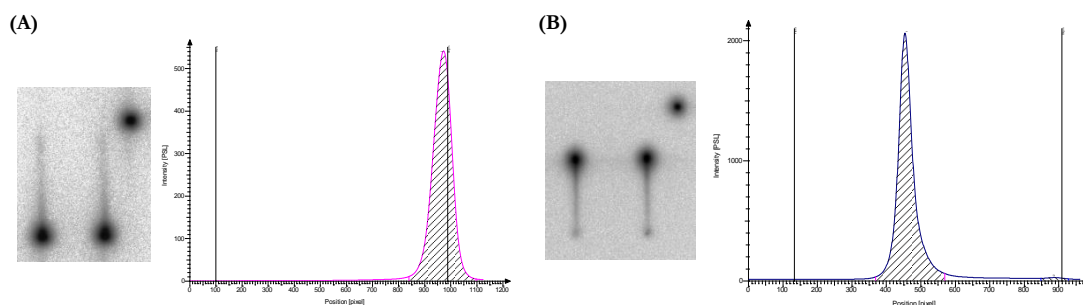
Figure 51. TLC plates developed in H2O, 0.1 % TFA/MeOH (30/70); (A) free gallium; (B) [^{68}Ga]GaDf-DUPA-Pep.

Labelling efficiency was determined in dependence on concentration of the peptide (1, 5 and 20 µg; 0.6, 3 and 13 nM) and on time (1, 5 and 10 min). When the lowest amount of Df-DUPA-Pep (1 µg) was used, a high RCY (93 $\pm$ 0.6 %) was obtained after 10 min. In the case of the highest concentration (20 µg), the RCY was >90 % after 1 min and increased up to 97 $\pm$ 1.6 % after 10 min.

Table 27. RCYs for the radiosynthesis of [^{68}Ga]Ga- Df-DUPA-Pep in dependence on concentration and time.

Amount (µg)	Volume (ml)	Conc. (µg/ml)	RCY %		
			1 min	5 min	10 min
1	0,516	1,94	77$\pm$2.5	90$\pm$1.0	93$\pm$0.6
5	0,520	9,62	89$\pm$2.6	92$\pm$1.0	95$\pm$0.4
20	0,532	37,59	91$\pm$0.7	94$\pm$0.6	97$\pm$1.6
n=3					
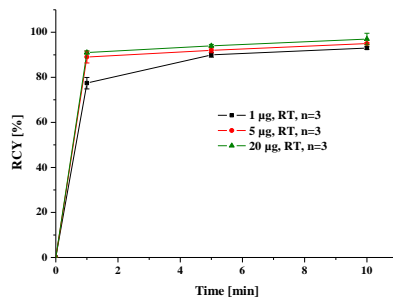
Figure 52. RCYs of Df-DUPA-Pep labelling with [^{68}Ga]Ga-Cl$_3$ in dependence on concentrations and time.

In the case of ^{68}Ga, the RCYs obtained were high also when using 1 μg of peptide. An explanation could be the fact that an activity of 1 MBq n.c.a. (no carrier added) of ^{68}Ga correlates to 5.87×10^{9} ^{68}Ga atoms, whereas 1 MBq of ^{89}Zr corresponds with 4.07×10^{11} ^{89}Zr atoms. Thus, comparing both reactions by statistical means (same activity) in case of ^{68}Ga-labelling there is a 69 fold higher excess in the relation of peptide to radionuclide compared to the use of ^{89}Zr. The radiolabelled peptide was analysed also by analytical radio-HPLC (Figure 53).
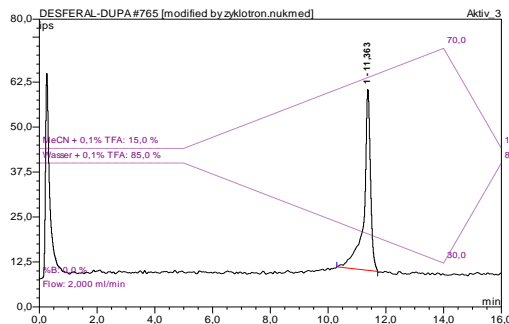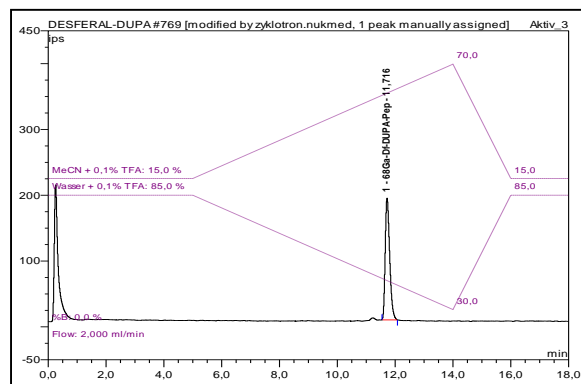

Figure 53. HPLC chromatogram of [^{68}Ga]Ga-Df-DUPA-Pep using reversed-phase column (Phenomenex Gemini, 5 μm, C18, 250 x 4.6 mm) and gradient elution of solvent A (water with 0.1 %TFA) and solvent B (MeCN with 0.1 %TFA), (85 % A for 5 min, 85-30 % A from 5-14 min, 30- 85 % A from 14-16 min, 85 % A from 16-18 min) at flow rate of 2 mL/min (first peak being the total activity injected).

Also in the case of [^{68}Ga]Ga-Df-DUPA-Pep, higher activity and bigger amount (≤100 μg) were tested. An average activity of 451 ± 50 MBq (ca. 300 μl) was tested with 100 μg, using the same reaction conditions above described, and the RCY was more than 95 % within 10 minutes (n=3). Thus, the amount of peptide was decreased to 20 μg, in

110

order to increase the specific activity. 352 ± 70 MBq of gallium (*ca.* 300 μl) were added to 20 μg of Df-DUPA-Pep in the same reaction conditions, but for longer time (15 minutes), and the incorporation still exceeded 95 %, with a specific activity of 25.3 ± 6 GBq/μmol (n=3).

5.3.1.4   *Stability studies of labelled Df-Dupa-Pep*

The stability of the labelled peptide in human serum and PBS buffer was verified via HPLC and TLC after 1, 5, 8, 24 and 48 hours for [^{89}Zr]Zr-Df-DUPA-Pep and after 30 min, 2, 4, 8 hours for [^{68}Ga]Ga-Df-DUPA-Pep. The radiochemical stability was determined by mixing [^{89}Zr]Zr-Df-DUPA-Pep with both serum and PBS buffer and incubating for 48 h. The same procedure was applied to [^{68}Ga]Ga-Df-DUPA-Pep. Incubation of both labelled compounds resulted in no detectable changes in the chromatograms.
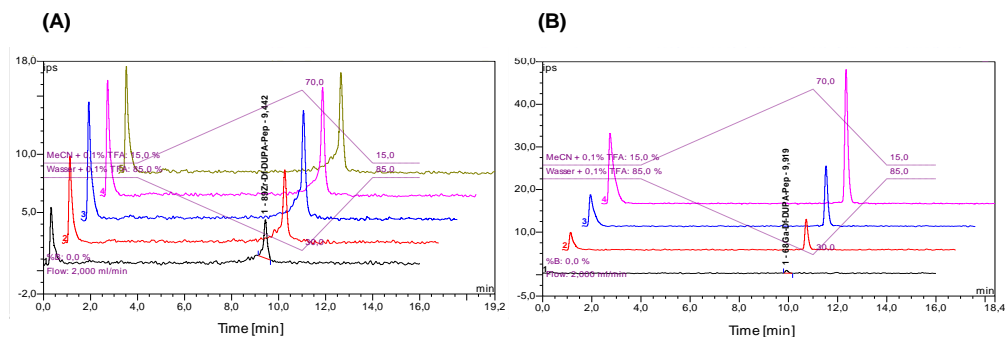
Figure 54. Stability studies of [^{89}Zr]Zr-Df-DUPA-Pep (A) and [^{68}Ga]Ga-Df-DUPA-Pep (B). (A): overlaid radio-HPLC chromatograms after 48h (1), 24h (2), 8h (3), 4h (4) and 1h (5); (B): Overlay of radio-HPLC chromatograms after 8h (1), 4h (2), 2h (3) and 30 min (4). The first peak shows always the total activity injected (detector bypass for recovery rate calculation).

5.3.1.5   *In vitro binding properties*

K_D values of cell binding in PSMA-positive cell lines (LNCaP C4-2 cells) were calculated for both radiotracers, using increasing concentration of [^{68}Ga]Ga-Df-DUPA-Pep and [^{89}Zr]Zr-Df-DUPA-Pep and defining nonspecific binding using a saturation dose

of 2-PMPA, a known inhibitor of PSMA, which completely abolished peptide binding, demonstrating the peptide-specificity for PSMA.

Table 28. Concentration K_D values calculated for both [^{68}Ga]Ga-Df-DUPA-Pep and [^{89}Zr]Zr-Df-DUPA-Pep in LNCaP C4-2 cell lines.

	[^{68}Ga]Ga-A	[^{89}Zr]Zr-A
K_D (nM)	42.04 ± 4.76	29.84 ± 4.82

n=3; A: -Df-DUPA-Pep
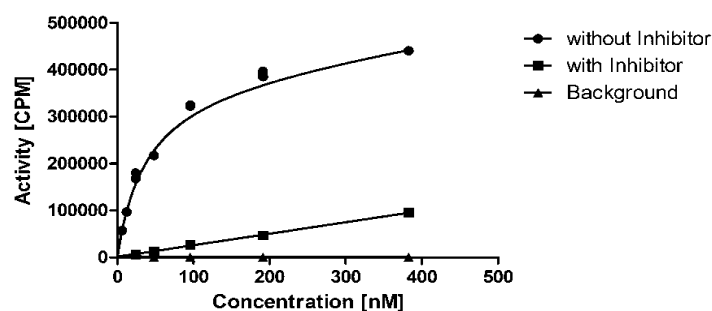
Figure 55. Binding of radioligand to LNCaP C4-2 cell lines in presence or absence of the inhibitor 2-PMPA.

5.3.1.6 In vivo biodistribution and tumor uptake

Prostate carcinoma cell lines LNCaP C4-2 (PSMA positive cells) and PC3 (PSMA negative cells) were implanted in different SCID mice on the shoulder. The radiotracers ([^{68}Ga]Ga-DfDUPA-Pep or [^{89}Zr]Zr-DfDUPA-Pep), formulated in 0.9 % NaCl solution, were injected into tumor-bearing mice through the tail vein. The radioactivity injected was between 2-12 MBq for the ^{89}Ga and less than 1 MBq for ^{89}Zr, due to the different half-life (~68 min and ~78 h, respectively). Accumulation of the labelled peptide was measured in PET/CT at various time points (1 to 3 h for ^{68}Ga and up to 24h for ^{89}Zr) (Figure 56). After the acquisition, the animals were sacrificed and the major organs, as well as the tumors, were recovered. The blood and tissue samples were weighed and activity was counted in the γ-counter. No radionuclide-dependent difference in binding affinity or

biological distribution was observed. PET/CT images depicted a specific accumulation in PSMA-positive tumor xenografts. Further uptake was detected in kidney, bladder and spleen. An average tumor-to-tissue ratio of 26.75 ± 10.4 was calculated in PSMA-positive tumors. PSMA-negative xenografts showed a tumor-to-tissue ratio of 1.15 ± 0.28.
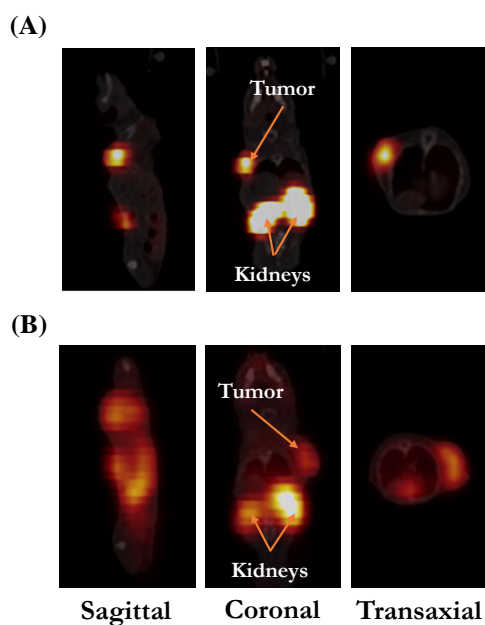
Figure 56. Whole-body PET-images of rats bearing LNCaP C4-2 tumor xenografts, injected with **(A)** [^{89}Zr]Zr-Df-DUPA-Pep and **(B)** [^{68}Ga]Ga-Df-DUPA-Pep. The acquisitions were performed after 24h and 1h after administration, respectively. Organs imaged are kidneys and tumor, where there was a great uptake of the radiotracer.

The animal studies were performed in accordance with the NIH guidelines for the human use of animals and all procedures were reviewed and approved by the National Cancer Institute Animal Care and Use Committee.

5.3.2 CHX-A´´-DTPA-DUPA-Pep

5.3.2.1 Synthesis of CHX-A´´-DTPA-DUPA-Pep

Once evaluated the uptake of Df-DUPA-Pep, it was decided to conjugate the molecule with another chelating agent in order to complex radiometals for therapeutic purposes (^{90}Y and ^{177}Lu). CHX-A´´-DTPA is the selected chelating agent, the cyclohexyl derivative of DTPA, which shows higher steric rigidity compared to the parent structure that conferred stability to the complex. The synthesis of CHX-A´´-DTPA-DUPA-Pep is outlined in scheme 7.

DUPA-Aoc-Phe-Phe-NH-(CH$_2$)$_2$-NH$_3$ TFA   p-SCN-Bn-CHX-A´´-DTPA

DIPEA
DMSO
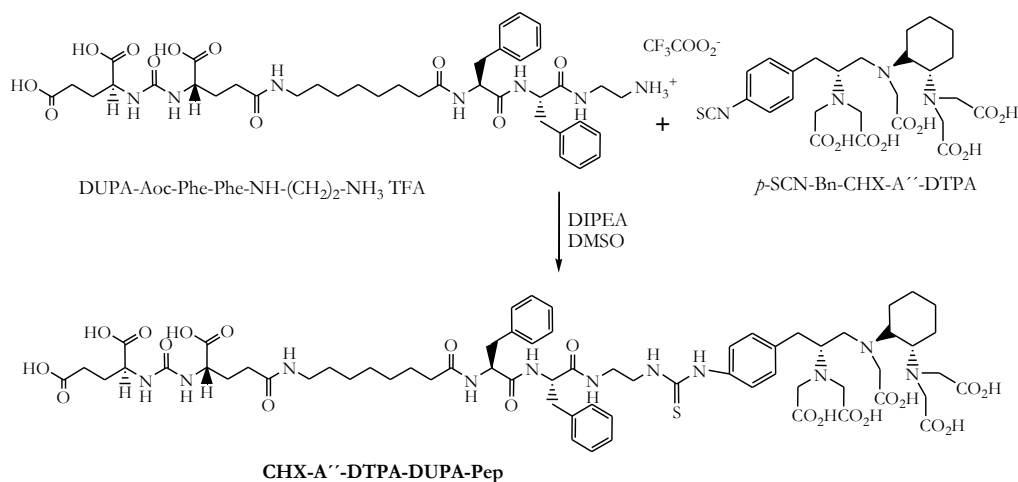
CHX-A´´-DTPA-DUPA-Pep

Scheme 7. Synthesis of CHX-A´´-DTPA-DUPA-Pep.

The CHX-A´´-DTPA-DUPA-Pep was prepared by reaction of p-SCN-Bn-CHX-A´´-DTPA with DUPA-Pep Trifluoroacetate in DMSO in presence of DIPEA as base. The reaction was kept at room temperature overnight. The final compound was isolated and purified from the mixture by preparative HPLC using C18 column [Phenomonex Gemini 5u C18, 250x21.10mm, 5 micron] at a flow rate of 7 ml/min and a gradient elution carried out as reported below.

Table 29. Gradient elution for CHX-A´´-DTPA-DUPA-Pep purification.

Gradient elution		
Time (min)	% MeCN, (0.1% TFA)	% Water, (0.1% TFA)
0-3	20	80
3-15	40	60
15-30	40	60

The product fraction was collected at a retention time of 23.2 min to give CHX-A´´-DTPA-DUPA-Pep as a white powder, after lyophilization, in 70 % yield and > 95 % purity (HPLC).
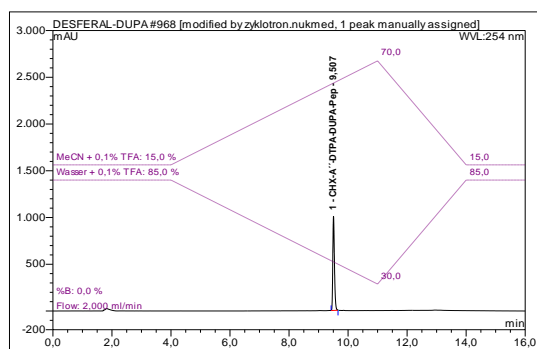
Figure 57. Analytical HPLC chromatogram of CHX-A´´-DTPA-DUPA-Pep using reversed-phase column (Phenomenex Gemini, 5 μm, C18, 250 x 4.6 mm) and gradient elution of solvent A (water with 0.1% TFA) and solvent B (MeCN with 0.1% TFA), (85 % A for 4 min, 85-30 % A from 4-11 min, 30- 85 % A from 11-14 min, 85 % A from 14-16 min) at flow rate of 2 mL/min.

5.3.2.2 [^{89}Zr]Zr-CHX-A´´-DTPA-DUPA-Pep

5.3.2.2.1 Labelling of [^{89}Zr]Zr-CHX-A´´-DTPA-DUPA-Pep

Complexation of ^{89}Zr and CHX-A´´-DTPA-DUPA-Pep was monitored at different time intervals to study the dependency of RCY on amount and time, as in the case of Df-DUPA-Pep. 16 μl of [^{89}Zr]ZrCl$_4$ solution (3.95 MBq – 4.01 MBq), at pH 7, were added to a solution of CHX-A´´-DTPA-DUPA-Pep dissolved in DMSO (1 mg/ml) and 500 μL of 0.25 M HEPES buffer (pH=7.4). The reaction was carried out at room temperature.

Complexation of ^{89}Zr and CHX-A´´-DTPA-DUPA-Pep was monitored by y-counter measurements of TLC. TLC plates were run using as eluent citrate 0.1 M at pH 5. The results are reported below.

Table 30. RCYs for the radiosynthesis of [^{89}Zr]Zr-CHX-A´´-DTPA-DUPA-Pep in dependence on concentration and time.

Amount (µg)	RCY %				
	1 min	5 min	10 min	30 min	60 min
100	19.3±0.6	39.0±1.0	56.7±0.6	89.7±0.6	98.7±0.6
50	12.7±0.6	27.7±0.6	42.7±1.5	80.0±1.0	96.0±1.0
25	9.3±1.5	18.7±0.6	27.0±1.0	56.3±0.6	82.7±0.6

n=3

The obtained results were not satisfactory. After 30 minutes, the RCY did not reach 95 %, even with the highest amount (100 µg). After 60 min, the incorporation exceeded this limit (95 %) with amount ≥50 µg but, as the initial activity used in these preliminary tests was quite low, possible future application with highest activity were not achievable without a further purification. Actually, these results can be in accordance with the fact that CHX-A´´-DTPA is not the chelating agent of choice for ^{89}Zr, rather for other radiometals as ^{90}Y, ^{86}Y, ^{177}Lu, ^{111}In and also for ^{68}Ga (Wei *et al.*, 2009).
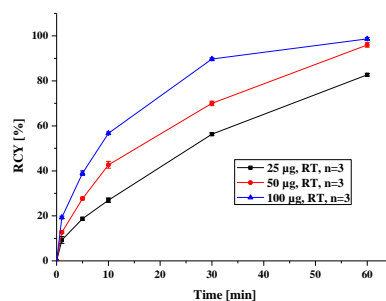
Figure 58. RCYs of CHX-A´´-DTPA-DUPA-Pep labelling with [^{89}Zr]Zr-Cl$_4$ in dependence on concentrations and time.

5.3.2.3 [^{68}Ga]Ga-CHX-A´´-DTPA-DUPA-Pep

5.3.2.3.1 Labelling of [^{68}Ga]Ga-CHX-A´´-DTPA-DUPA-Pep

[^{68}Ga]GaCl$_3$ solution (13 μl; 9.3 – 9.6 MBq) was added to a solution of CHX-A´´-DTPA-DUPA-Pep, dissolved in DMSO (1mg/ml), and 0.25 M HEPES buffer (pH 7.45, 500 μL); thereafter, reaction was carried out at room temperature. At different time points, 1 μL aliquots were withdrawn and analysed under the same condition as in [^{68}Ga]Ga-Df-DUPA-Pep; the Rf of the labelled peptide was 0.72, quite the same as for [^{68}Ga]Ga-Df-DUPA-Pep (0.70). Labelling efficiency was determined in dependence on concentration of the peptide (1, 10, 25, 50 and 100 μg; 0.72, 7.18, 17.95, 35.91 and 71.81 nM) and on time (1, 5, 10, 30 and 60 min). The results are reported below and showed higher incorporation in less time compared with the data obtained with ^{89}Zr.

Table 31. RCYs for the radiosynthesis of [^{68}Ga]Ga-CHX-A´´-DTPA-DUPA-Pep in dependence on concentration and time.

Amount (μg)	RCY %				
	1 min	5 min	10 min	30 min	60 min
100	95.1±0.3	95.8±0.1	96.1±0.1	97.3±0.1	97.7±0.6
50	69.4±0.9	95.4±0.4	96.6±0.6	96.6±0.2	97.2±0.7
25	29.0±1.5	70.0±1.3	85.6±0.8	96.61±0.3	97.1±0.6
10	3.7±0.3	14.0±0.3	21.9±0.8	41.3±4.0	56.5±5.8
1	0.2±0.1	0.2±0.0	0.3±0.1	0.5±0.1	0.6±0.1

n=3
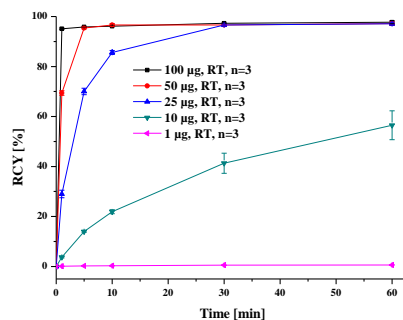
Figure 59. RCYs of CHX-A´´-DTPA-DUPA-Pep labelling with [^{68}Ga]Ga-Cl$_3$ in dependence on concentrations and time.

In case of the highest concentration (100 μg), the RCY was >90 % after 1 min and increased up to 97.3 ± 0.1 % after 30 min. Also using 50 and 25 μg, the RCY exceeded 95 %, after 5 min and 30 min respectively. The lowest amount of CHX-A´´-DTPA-DUPA-Pep used was 1 μg and, under this condition, the labelling did not occur, while going up to 10 μg the incorporation of the radiometal started to take place but without reaching the high RCY obtained using more amount of peptide. Thus, fast complexation and high yield were achieved using 100 μg of peptide. Lower amount of peptide could be applied to get a better specific activity but not less than 25 μg without need to purify the reaction solution.

5.3.2.4 [^{90}Y]Y-CHX-A´´-DTPADUPA-Pep

[^{90}Y]YCl$_3$ solution in 0.04 M HCl (5 μl – 5.55 MBq), purchased from Eckert Ziegler, were added to a solution of 100 μg of CHX-A´´-DTPA-DUPA-Pep dissolved in DMSO (2 mg/ml) and 500 μL of 0.25 M NH$_4$OAc buffer (pH=5.5). The reaction was carried out at room temperature for 30 min and then checked using 2-solvent systems for RP-18 thin layer chromatography (TLC), tri-sodium citrate dihydrate 0.1 M, for inorganic compounds, and H$_2$O, 0.1 % TFA/MeOH (30/70), for organic compounds. Using the first eluent, the organic compounds remained at the starting point whilst the inorganic free yttrium-90 run to the front of the solvent; in the second eluent, free ^{90}Y^{3+} remained at the starting point and the organic compounds run. TLC studies confirmed the production of a single labelled compound at the Rf. 0.72, showing incorporation greater than 95 % within 30 min, while ^{90}Y^{3+} remained at lower Rf due to the polarity. The results are reported below.
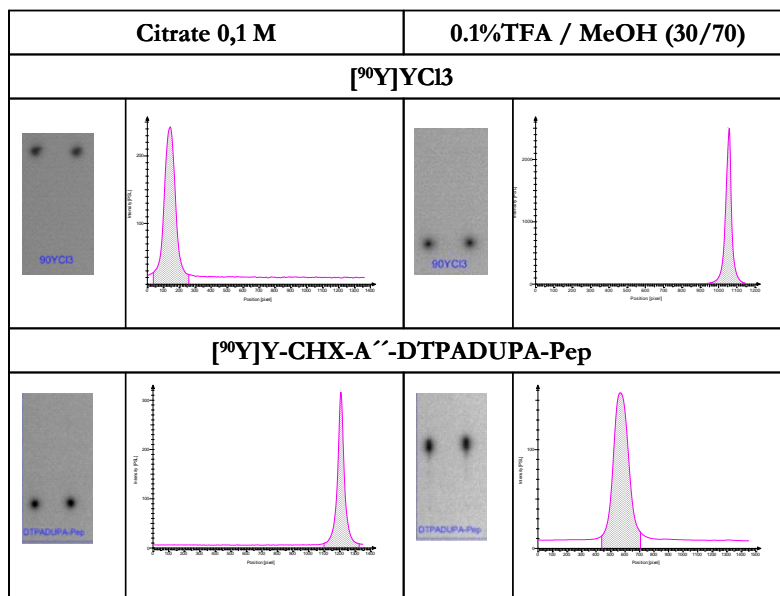
Figure 60. TLC of ^{90}Y, free and complexed onto CHX-A´´-DTPA-DUPA-Pep, developed using two different eluents and monitored by phosphoimager.

Thus, study of concentration and time dependencies were performed using different amount of peptide (25, 50, 100 µg; 17.95, 35.91 and 71.81 nM) and diverse time points for analysis (5, 10, 30 and 60 min). The analysis was conducted as previously performed in the case of ^{68}Ga and ^{89}Zr and the results are reported below. The incorporation was quantitative, more than 95 % within 5 min at every concentration level, rendering the purification not necessary.

Table 32. RCYs for the radiosynthesis of [^{90}Y]Y-CHX-A´´-DTPA-DUPA-Pep in dependence on concentration and time.

Amount	RCY %			
(µg)	5 min	10 min	30 min	60 min
100	98.4±0.4	98.2±0.2	99.3±0.2	99.0±0.1
50	98.6±0.1	982±0.2	98.5±0.3	99.0±0.1
25	98.2±0.2	97.3±1.0	98.7±0.2	97.9±0.1

n=3
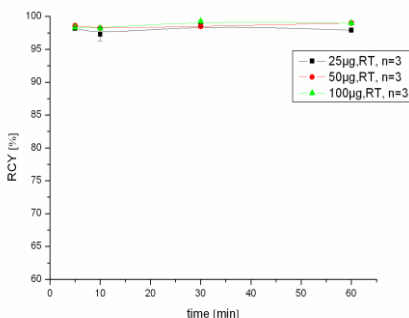
Figure 61. RCYs of CHX-A´´-DTPA-DUPA-Pep labelling with [^{90}Y]Y-Cl$_3$ in dependence on concentrations and time.

5.3.2.5 [^{177}Lu]Lu-CHX-A´´-DTPADUPA-Pep

^{177}Lu is an interesting radiometal applicable for radiotherapy, which offers the possibility to image, thanks to the γ-emission, and a lower toxicity compared with ^{90}Y. Also in this case, a time and concentration dependency study was performed. The same condition used for the analysis in the case of the other radiometals were suitable for ^{177}Lu. A solution of the peptide (10, 25, 50 and 100 μg) in DMSO was diluted with 0.5 ml of 0.5 M NH$_4$OAc buffer (pH = 5.5) and mixed. After that, [^{177}Lu]LuCl$_3$ was added (5 μL in 0.04 M HCl; 6.3-6.7 MBq). The reaction solutions were kept at room temperature and an aliquot was withdrawn at every time points on a TLC and analysed via phosphoimager.

Table 33. RCYs for the radiosynthesis of [^{177}Lu]Lu-CHX-A´´-DTPA-DUPA-Pep in dependence on concentration and time.

Amount (μg)	RCY %			
	5 min	10 min	30 min	60 min
100	98.4±0.1	98.6±0.3	99.3±0.2	99.6±0.2
50	95.4±0.1	96.7±0.2	98.5±0.4	98.4±0.7
25	95.7±0.5	97.2±0.7	93.4±0.4	96.1±1.1
10	96.2±1.0	95.2±0.8	98.6±0.4	96.7±0.3

n=3
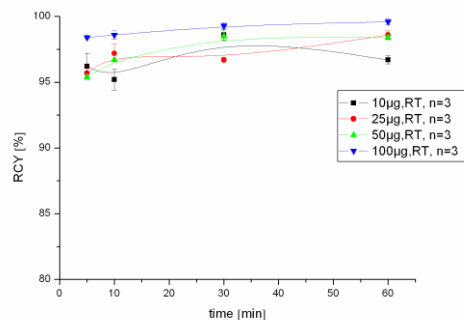
Figure 62. RCYs of CHX-A´´-DTPA-DUPA-Pep labelling with [^{177}Lu]Lu-Cl$_3$ in dependence on concentrations and time.

The incorporation was excellent as in case of ^{90}Y, with a RCY higher than 90 % also after 5 minutes.

4.2.2.6 Stability of labelled CHX-A´´-DTPA-DUPA-Pep

The stability of the labelled peptide in human serum and PBS buffer was verified via HPLC and TLC after 30 min, 2, 4, 8 hours for [^{68}Ga]Ga-CHX-A´´-DTPA-DUPA-Pep. The radiochemical stability was determined by mixing [^{68}Ga]Ga-CHX-A´´-DTPA-DUPA-Pep with both human serum and PBS buffer and incubating maintained at 37°C for 8 h. Periodically, samples were removed for the analysis in radio-TLC and radio-HPLC. Incubation resulted in no detectable changes in the chromatograms.
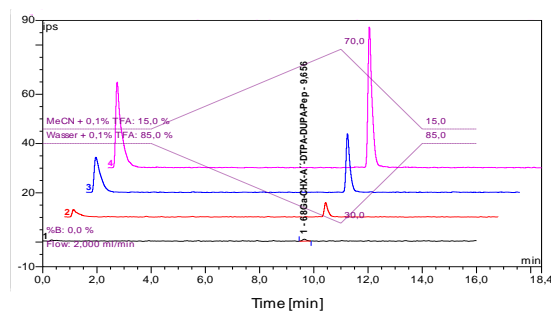
Figure 63. Stability study of [^{68}Ga]Ga-CHX-A´´-DTPA-DUPA-Pep. Overlay of radio-HPLC chromatograms after 8h (1), 4h (2), 2h (3) and 30 min (4). The first peak shows always the total activity injected (detector bypass for recovery rate calculation).

121

Studies of [^{90}Y]Y-CHX-A´´-DTPA-DUPA-Pep and [^{177}Lu]Lu-CHX-A´´-DTPA-DUPA-Pep stability will be concluded in the next experiments. The capacity of effectively retaining radiometals under physiological conditions is particularly important, especially with ^{90}Y, given its propensity to localize to bone, causing unacceptable bone marrow toxicity.

5.3.2.1 In vitro binding properties

K_D values and cellular uptake in PSMA-positive cell lines (LNCaP C4-2 cells) of [^{68}Ga]Ga-CHX-A´´-DTPA-DUPA-Pep and [^{177}Lu]Lu-CHX-A´´-DTPA-DUPA-Pep were calculated, using increasing concentration of radiotracer and defining nonspecific binding using a saturation dose of 2-PMPA, a known inhibitor of PSMA, which completely abolished peptide binding, demonstrating the peptide-specificity for PSMA.

Table 34. K_D values calculated for both [^{68}Ga]Ga-CHX-A´´-DTPA-DUPA-Pep, [^{177}Lu]Lu-CHX-A´´-DTPA-DUPA-Pep in LNCaP C4-2 cell lines.

	[^{68}Ga]Ga-A	[^{177}Lu]Lu-A
K_D (nM)	12.25 ± 0.41	13.79 ± 0.87

n=3; A: -CHX-A´´-DTPA-DUPA-Pep
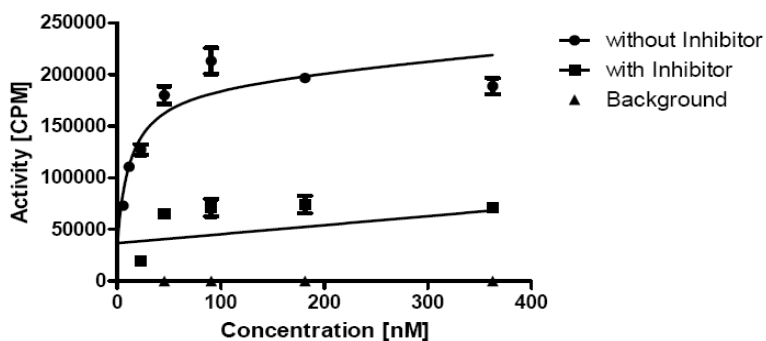
Figure 64. Binding of radioligand [^{68}Ga]Ga-CHX-A´´-DTPA-DUPA-Pep to LNCaP C4-2 cell lines in presence or absence of the inhibitor 2-PMPA.

5.3.2.2 Future perspective

CHX-A´´-DTPA-DUPA-Pep could be a potential candidate for the treatment of prostate cancer and metastatic lesion derived from PCa.

Further experiments still remain to be performed. First, it is necessary to complete the stability studies and to evaluate the K_D values of the remaining labelled molecules. Once the stability of radiotracers in both PBS and HS will be confirmed, PET/CT needs to be performed in tumor bearing mice for assessing tumor uptake and biodistribution of the radiotracer. Extremely important is the evaluation of tracer's retention in the different organs, in order to define the therapeutic system. Indeed, as Df-DUPA-Pep was cleared by kidneys, it is highly probable that also CHX-A´´-DTPA-DUPA-Pep will be eliminated via renal clearance. The high and persistent localization of radiolabelled molecules in the kidneys creates concern about potential renal radiation toxicity, thus compromising therapeutic effectiveness. In general, the risk of toxicity seems to depend on the characteristics of the oncophilic molecule, such as the molecular weight, electric charges and clearance pathways, as well as the chemical and physical characteristics of the applied radionuclide. In the case of radiolabelled peptides for NETs therapy (DOTATOC and DOTATATE, labelled with ^{177}Lu or ^{90}Y) co-infusion of positively charged amino acids gave encouraging results for the prevention of radiation-induced renal damage (Lambert *et al.*, 2004). Hence, further studies have to be conducted to better understanding the potential of these radiotracers.

5.4 Mesoporous Nanoparticles (MSNPs)

Mesoporous nanoparticles constitute a new generation of materials which show ordered arrangements of channels and cavities of different geometry built up from SiO_2 units. The pore size is variable (2 nm < Dp < 50 nm) and can be controlled and modified, in a reasonable range, using *in situ* and *ex situ* synthetic strategies. The feasibility of obtaining different pore sizes and geometries offers a wide range of possibilities for

hosting molecules larger than the ones exhibited for classic microporous materials, such as zeolites.

MSNPs were synthesized by the research group of Lindén, according to previously published procedures (Kim M.-H. *et al.*, 2011). For further derivatization, primary amino groups were introduced using 3-aminopropyltriethoxysilane (APTES) through a post-grafting method; the degree of amination on the surface was 1.5 mmol/g and the amino group was then used for the introduction of Desferal. After modification, the physical and chemical properties of SiNPs were characterized and are reported in the table below.

Table 35. Characteristics of Df-MSNPs.

Characteristics of the particles Df24-1	
Diameter	200 nm
Surface area	260 m^2/g
Pore volume	0.7 ml/g
Pore diameter	8 nm
Amino groups	1.5 mmol/g
Df loading	16 wt%

The main aim of this project is, by attaching a radiolabel to the particle surface, to sensitively define the clinical potential of these nanoparticles, which could be easily molecularly targeted probes. The focal criteria that need to be satisfied are:

1. favourable distribution;
2. efficient renal clearance;
3. extended circulation (blood residence) times;
4. improved tumoral penetration

The initial part of this project foresaw the study of the labelling reaction and then their stability in dispersion using different media.

5.4.1 Df-MSNPs

5.4.1.1 [^{89}Zr]Zr-Df-MSNPs

Labelling of MSNPs gives the unique opportunity for a non-invasive study of their biodistribution after injection. First, concentration and time dependencies study was performed in order to verify the feasibility and best reaction conditions for the labelling. Different amounts of Df-MSNPs in DMSO (5, 10, 25 μg) were added, after being vortexed, to NH$_4$OAc 0.25 M, pH 7.8 (1 ml) and dispersed. [^{89}Zr]ZrCl$_4$ (25 μl – 2.18 MBq) was added and the reaction was mixed at room temperature with a vertical lab rotator. 1 μl of this suspension was withdrawn at different time points and spotted on a TLC and subsequently developed using as eluent citrate buffer (0.1 M, pH 5), which elutes free ^{89}Zr with the solvent front. Nanoparticles cannot move and remain on the origin, so this mobile phase is the only feasible in these experiments. From amounts > 25 μg, the RCY quickly reached high value of incorporation of the radiometal.

Table 36. RCY of [^{89}Zr]Zr-Df-MSNPs labelling reaction in dependence on concentration and time.

Amount (μg)	RCY %		
	1 min	5 min	10 min
25	94.7±0.6	97.3±1.2	97.7±0.6
10	41.3±2.1	62.7±1.5	71.0±2.0
5	22.7±1.5	25.7±4.7	27.7±4.2

n=3
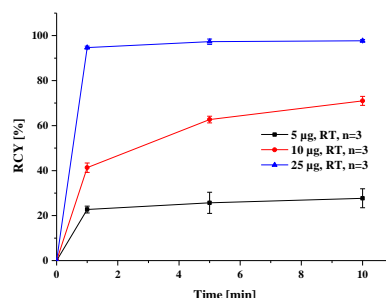
Figure 65. Radiochemical yield of Df-Nanoparticles labelling with [^{89}Zr]ZrCl$_4$ in dependence on concentration and time, without further washing.

5.4.1.2   *Study of dispersibility of [^{89}Zr]Zr-Df-MSNPs*

Df-MSNPs need to be formulated in an appropriate medium for subsequent injection into mice. The *media* considered were:

- ✓   0.9 % NaCl
- ✓   10 % FCS
- ✓   100 mM KCl
- ✓   Medium
- ✓   Water (WFI)

The behaviour of labelled nanoparticles in these different media was monitored through dynamic measurements in the Biograph mCT (Siemens Healthcare Global) according to the following schedule: 18 frames of 10 minutes each (total 180 minutes) and one frame of 10 minutes after 20 h. Images obtained from PET studies were corrected for radioactivity decay, calibrated and radioactivity concentration data were expressed as activity concentration (Bq/ml). Regions of Interest (ROIs) were performed drawing circular ROIs on the bottom and upper part of the vials. 100 μg of Df-MSNPs were labelled with [^{89}Zr]ZrCl$_4$ (30 MBq), as previously described. The batch was divided into five vials (5.5 MBq each), keeping all the vials into ultrasound bath. After 5 minutes, the vials were positioned into Biograph mCT and the final data were reported below. During time, the tendency of nanoparticles was to distribute on the bottom part in each medium but with different speed. 0.9 % NaCl and WFI were comparable and the sedimentation started almost after 30 minutes, while in the case of 10 % FCS and medium the sedimentation started at 50 minutes. 100 mM KCl was the better medium and the sedimentation was delayed at almost 70 minutes with an inferior slope compared with the other media. For further application, PEGylation of nanoparticles and binding of DUPA moiety to the surface are taken into account. The first modification may enhance the solubility of nanoparticles in aqueous medium and, in a second time, prolong the plasma serum half-life of proteins by increasing their hydrodynamic volume and hence decreasing their renal clearance. Regarding the second modification, DUPA moiety can selectively drive nanoparticles to PSMA tumor bearing cells, reducing eventual side effects and

making nanoparticles a selective and suitable vehicle for diagnostic and therapeutic molecules.
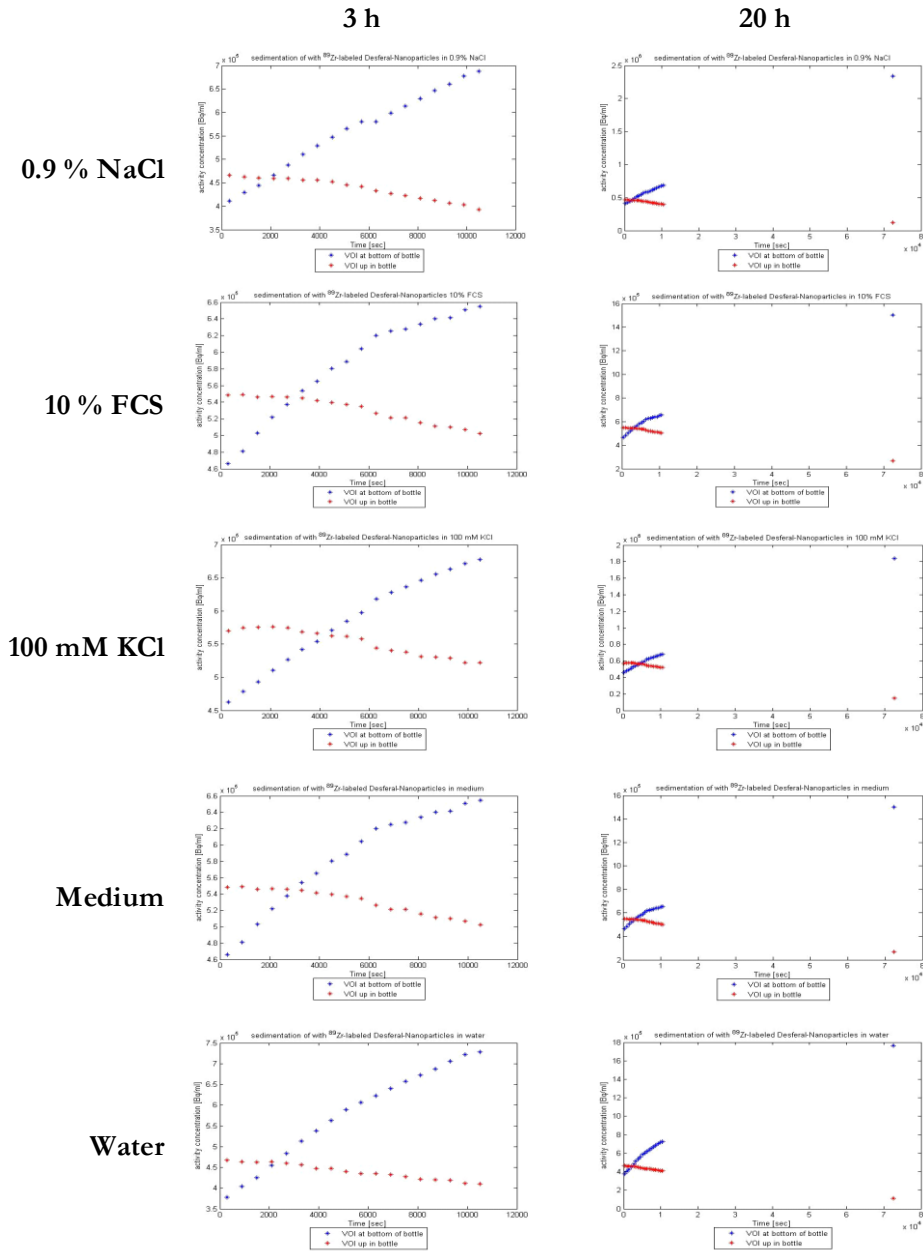
Figure 66. Dispersibility of [⁸⁹Zr]Zr-Df-Nanoparticles in dependence on medium and time (blue dot: bottom; red dot: upper part of the vial).

127

6 CONCLUSIONS

In conclusion, new biomolecules specifically conceived for two different targets, *i.e.* COX-2 and PSMA, have been developed.

COX-2, the first target under investigation, is an inducible enzyme, which plays an important role in inflammation. Elevated COX-2 levels are correlated not only with inflammation but also with premalignancy/cancer progression and neurodegenerative diseases. Thus, non-invasive monitoring of COX-2 functional expression would definitely facilitate efforts to understand COX-2 pharmacology *in vivo*.

VA426, a specific COX-2 inhibitor, was labelled with carbon-11 for COX-2 *in vivo* imaging. [^{11}C]VA426 was prepared by O-methylation of the corresponding alcohol VA425, in presence of NaH (60 % dispersion in mineral oil) (1:10), with [^{11}C]CH$_3$I. The radiochemical yield was 21 ± 1.67 % (decay-corrected, based on [^{11}C]CH$_3$I) (n = 3) with a specific activity of 90 ± 54 GBq/μmol (n = 3). Total synthesis time was 30 min from end of bombardment, with an average final activity of 2.0 ± 0.2 GBq (n=3). Quality control confirmed excellent chemical and radiochemical purity (>95 %). Preliminary PET studies were performed in BL/6 female mice with a sterile inflammation, induced by intraperitoneal lipopolysaccharide (LPS) injection. Mice treated with LPS, compared with the control, showed more intense uptake at the injection site of the toxin. In particular, it was possible to notice a major distribution in the liver and intestine, which are sites normally characterized by high uptake of this type of tracers. [^{11}C]VA426 was excreted via hepatobiliary clearance. Further studies are planned in order to evaluate the potential of this tracer for COX-2 *in vivo* visualization. It is worthy to consider the principal problems previously encountered during potential COX-2 tracers development. The main causes of deficiency of COX-2 tracers are non-specificity of COX-2 binding, poor *in vivo* stability and/or high blood retention. In particular, the long residency time in bloodstream is likely to be an effect of carbonic anhydrase binding. Carbonic anhydrase is a metallopeptidase highly expressed in blood cells and COX-2 inhibitors are carbonic anhydrase inhibitors, especially the sulphonamide-based COX-2 inhibitors. Nevertheless, sulphonamide or methylsulfone group is essential for COX-2 binding and, therefore, imaging. VA426 owns a methylsulfone group, which guarantees the proper structure for selective binding but

may reduce the blood retention. Thus, further investigations on cell lines expressing COX-2 (*e.g.* colorectal cancer cell lines) will be exploited, including blocking and metabolic studies, in order to evaluate the potential use of [^{11}C]VA426 as a marker for COX-2 distribution with PET.

The second target studied is the prostate-specific membrane antigen (PSMA). PSMA is a cell surface protein overexpressed in prostate cancer. Due to its specificity of expression, PSMA is considered a cancer marker and a good target for imaging agents and therapy.

Dupa-Pep, a known specific PSMA ligand, was conjugated with different chelating agent or prosthetic group in order to label it with radiometals or other radionuclides (*e.g.* ^{18}F). The obtained results were satisfactory although the syntheses were time-consuming or the complexation required activation energy (higher reaction temperature) and/or long reaction times. Thus, in the attempt to develop simple, fast and quantitative labelling step at room temperature, different chelator approaches have been investigated. In particular, the choice of appropriate chelators allows the use of different radiometals, for both diagnostic and, more importantly, therapeutic purposes.

In this project, Dupa-Pep was conjugated with both *p*-isothiocyanatobenzyl-desferrioxamine (Df-Bz-NCS) and *p*-isothiocyanatobenzyl-*trans*-cyclohexyldiethylene triaminepenta-acetic acid (CHX-A´´-DTPA-NCS), to get Df-DUPA-Pep and CHX-A´´-DTPA-DUPA-Pep in high chemical yields (80 % and 70 %, respectively) and purity (>95 %). Df-DUPA-Pep was labelled with ^{68}Ga and ^{89}Zr for PET imging and CHX-A´´-DTPA-DUPA-Pep with ^{68}Ga and ^{89}Zr for imaging, and with ^{90}Y and ^{177}Lu for therapeutic applications. Studies of time and concentration dependency were performed for all the labelling reactions.

[^{68}Ga]Ga-Df-DUPA-Pep and [^{89}Zr]Zr-Df-DUPA-Pep were successfully synthesized at room temperature and pH of 7.5. The radiosyntheses proceeded in high radiochemical yields of 95 % in a reaction time of 10 min. A final purification procedure was dispensable, as the radiotracers were directly applicable for further utilization. The stability of the labelled peptides was confirmed in human serum (HS) and PBS buffer at

37°C. K_D values for both compounds are within nanomolar concentration range. PET/CT images depicted a specific accumulation in PSMA-positive tumor xenografts, with an average tumor-to-tissue ratio of 26.75 ± 10.4. Further uptake was detected in kidney, bladder and spleen.

Regarding CHX-A´´-DTPA-DUPA-Pep, labelling with ^{68}Ga proceeded faster and with higher RCYs than ^{89}Zr, in accordance with the fact that CHX-A´´-DTPA is not the chelating agent of choice for ^{89}Zr, but for other radiometals as ^{90}Y, ^{86}Y, ^{177}Lu, ^{111}In and ^{68}Ga. The incorporation level of ^{68}Ga was more than 95 % within 10 min. The stability of the ^{68}Ga labelled compound was confirmed in both HS and PBS at 37°C for 8 h. The labelling with the therapeutic radiometals ^{90}Y and ^{177}Lu was performed at room temperature and pH of 5.5. The high labelling efficiencies for both radiometals avoid the need of post-labelling purification. K_D values were evaluated for [^{68}Ga]Ga-CHX-A´´-DTPA-DUPA-Pep and [^{177}Lu]Lu-CHX-A´´-DTPA-DUPA-Pep and found to be, also with these compounds, within nanomolar concentration range. K_D value of [^{90}Y]Y-CHX-A´´-DTPA-DUPA-Pep has to be evaluated. Further experiments have to be executed for verifying the actual applicability of these complexes in nuclear medicine as diagnostic and therapeutic agents, with particular regard to *in vivo* bioavailability and stability. Moreover, high priority has to be devoted to the evaluation of tracer's retention in the different organs, in order to define the therapeutic system. In fact, the high and persistent localization of radiolabelled molecules in the kidneys can lead to potential renal radiation toxicity, compromising therapeutic effectiveness, depending on the characteristics of the tracers. Hence, further studies should be conducted to better understanding the potential of these radiotracers for therapeutic purposes.

As a subset of PCa DUPA-Pep project, application of particular nanoparticles have been investigated. Mesoporous nanoparticles (MSNPs) constitute a new generation of materials, which offer the possibility for hosting and delivering molecules (*e.g.* anti-cancer drugs) within the bloodstream to diseased organs and tissues. Specific modifications of MSNPs allow selective binding to cell surface receptors overexpressed in diseases. In the first section of this research project, MSNPs were conjugate with desferal and labelled

with [89]Zr. Labelling feasibility has been confirmed and optimal reaction conditions were evaluated through concentration and time dependency studies. Starting from 25 μg of Df-MSNPs, the RCYs quickly reached high values of incorporation of the radiometal. The behaviour of labelled Df-MSNPs in different *media* was monitored through dynamic PET measurements. 100 mM KCl proved to be the better medium to formulate these nanoparticles for further experiments. Future development will be PEGylation of nanoparticles and binding of DUPA moiety to the surface. These modifications might lead to enhance nanoparticles solubility in aqueous medium, to prolong their plasma serum half-life and to selectively drive nanoparticles to PSMA tumor bearing cells, reducing eventual side effects and making nanoparticles a selective and suitable vehicle for diagnostic and therapeutic molecules.

7   REFERENCES

Abou D.S., Ku T. and Smith-Jones P.M. In vivo biodistribution and accumulation of ^{89}Zr in mice. *Nucl Med Biol.* 2011;38:675–681

Almansa C, Alfón J., de Arriba A.F., Cavalcanti F.L., Ecamilla I., Gómez L.A., Miralles A., Soliva R., Bartrolí J., Carceller E., Merlos M., García-Rafanell J. Synthesis and Structure-Activity Relationship of a New Series of COX-2 Selective Inhibitors: 1,5-Diarylimidazoles. *Journal of Medicinal Chemistry* 2003;46(16):3463–3475

Al-Momani E., Malik N., Machulla H.J., Reske S.N., and Solbach C. Radiosynthesis of [^{18}F]FEt-Tyr-urea-Glu ([^{18}F]FEtTUG) as a new PSMA ligand. *J Radioanal Nucl Chem.* 2013;295(3):2289–2294

Ambrogio M.W., Thomas C.R., Zhao Y.-L., Zink J. I., and Fraser Stoddart J. Mechanized silica nanoparticles: A new frontier in theranostic nanomedicine. *Acc. Chem. Res.* 2011;44:903–913

Anzini M., Rovini M., Cappelli A., Vomero S., Manetti F., Botta M., Sautebin L., Rossi A., Pergola C., Ghelardini C., Norcini M., Giordani A., Makovec F., Anzellotti P., Patrignani P., and Biava M. Synthesis, Biological Evaluation, and Enzyme Docking Simulations of 1,5-Diarylpyrrole-3-Alkoxyethyl Ethers as Selective Cyclooxygenase-2 Inhibitors Endowed with Anti-inflammatory and Antinociceptive Activity. *J. Med. Chem.* 2008;51:4476–4481

Barinka C., Šácha P., Sklenář J., Man P., Bezouška K., Slusher B.S., and Konvalinka J. Identification of the *N*-glycosylation sites on glutamate carboxypeptidase II necessary for proteolytic activity. *Protein Science.* 2004;13:1627–1635

Beck J.S., Vartuli J.C., Roth W.J., Leonowicz M.E., Kresge C.T., Schmitt K.D., Chu C.T.W., Olson D.H., Sheppard E.W., McCullen S.B., Higgins J.B., and Schlenkert J.L.A. New Family of Mesoporous Molecular Sieves Prepared with Liquid Crystal Templates. *J. Am. Chem. Soc.* 1992;114:10834–10843

Belloli S., Jachetti E., Moresco R.M., Picchio M., Lecchi M., Valtorta S., Freschi M., Michelini R.H., Bellone M., Fazio F. Characterization of preclinical models of prostate cancer using PET-based molecular imaging. *Eur J Nucl Med Mol Imaging.* 2009;36:1245–1255

Benezra M., Penate-Medina O., Zanzonico P.B., Schaer D., Ow H., Burns A., DeStanchina E., Longo V., Herz E., Iyer S., Wolchok J., Larson S.M., Wiesner U., Bradbury M.S. Multimodal silica nanoparticles are effective cancer-targeted probes in a model of human melanoma. *J Clin Invest.* 2011;121(7):2768–80

Berger U.V., Carter R.E., McKee M., and Coyle, J.T. N-acetylated alpha-linked acidic dipeptidase is expressed by non-myelinating Schwann cells in the peripheral nervous system. *J. Neurocytol.* 1995;24:99–109

Boswell C.A., Regino C.A.S., Baidoo K.E., Wong K.J., Bumb A., Xu H., Milenic D.E., Kelley J.A., Lai C.C., and Brechbiel M.W. Synthesis of a Cross-Bridged Cyclam Derivative for Peptide Conjugation and ^{64}Cu Radiolabeling. *Bioconjugate Chem.* 2008;19:1476–1484

Brechbiel M.W. Bifunctional Chelates for Metal Nuclides. *Q J Nucl Med Mol Imaging.* 2008;52(2):166–173

Breeman W.A., de Jong M., de Blois E., Bernard B.F., Konijnenberg M., and Krenning E.P. Radiolabelling DOTA peptides with ^{68}Ga. *Eu. J. Nucl. Med. Mol. Imaging.* 2005;32(4):478

Brunberg J.A., Frey K.A., Horton J.A., Deveikis J.P., Ross D.A., and Koeppe R.A. [^{15}O]H$_2$O positron emission tomography determination of cerebral blood flow during balloon test occlusion of the internal carotid artery. AJNR Am J Neuroradiol. 1994;15(4):725–32

Carter E.A., Paul K., Barrow S.A., Fischman A.J., and Tompkins R.G. Previous Burn Injury Predisposes Mice to Lipopolysaccharide (LPS) Induced Changes in Glucose Metabolism. J Burn Care Res. 2012;33(5):683–689

Catalona W.J., Smith D.S., Ratliff T.L., *et al.* Measurement of prostate-specific antigen in serum as a screening test for prostate cancer. *N Engl J Med.* 1991;324:1156–61

Chinol M. and Hnatowich D.J. Genrator-Produced Yttrium-90 for Radioimmunotherapy. J. Nucl. Med. 1987;28:1465–1470

Comar D., Mazière M., and Crouzel C. Synthèse et métabolisme de molecules radiopharmaceutiques marquees au carbon-11-I-iodomethylate de chlorpromazine-[11]C. *Radiopharmaceuticals and Labelled compounds*. 1974. Vol. I. IAEA, Vienna.

Correia J.D.G., Paulo A., Raposinho P.D., and Santos I. Radiometallated peptides for molecular imaging and targeted therapy. *Dalton Trans.* 2011;40:6144–6167

Chakravarty R., Pandey U., Manolkar R.B., Dash A., Venkatesh M., Pillai M.R.A. Development of an electrochemical 90Sr-90Y generator for separation of 90Y suitable for targeted therapy. Nucl. Med. Biol. 2008;35:245–253

Chandrasekharan N.V., Dai H., Roos K.L., Evanson N.K., Tomsik J., Elton T.S., and Simmons D.L. From the cover: COX-3, a cyclooxygenase-1 variant inhibited by acetaminophen and other analgesic/antipyretic drugs: Cloning, structure, and expression. Proc. Natl. Acad. Sci. USA 2002;99:13926–13931

Chen Y., Pullambhatla M., Foss C.A., Byun Y., Nimmagadda S., Senthamizhchelvan S., Sgouros G., Mease R.C., and Pomper M.G. 2-(3-{1-Carboxy-5-[(6-[^{18}F]Fluoro-Pyridine-3-Carbonyl)-Amino]-Pentyl}-Ureido)-Pentanedioic Acid, [^{18}F]DCFPyL, a PSMA-Based PET Imaging Agent for Prostate Cancer. *Clin Cancer Res.* 2011;17:7645–7653

Chopra A. ^{123}I-Labeled (S)-2-(3-((S)-1-carboxy-5-(3-(4-iodophenyl)ureido)pentyl)ureido)pentanedoic acid. *Molecular Imaging & Contrast Agent Database*

CPMP/SWP/2599/02/Rev 1. Committee for Medicinal Products for Human use (CHMP). Position Paper on Non-Clinical Safety Studies to Support Clinical Trials with a Single Microdose

Czarneckia A. and Karshenboimb S.G. Decays of Positronium. hep-ph/9911410. 1999

Danhier F., Feron O., Préat V. To exploit the tumor microenvironment: passive and active tumor targeting of nanocarriers for anti-cancer drug delivery. *J Controlled Release.* 2010;148:135–146

Dannhardt G. and Laufer S. Structural Approaches to Explain the Selectivity of COX-2 Inhibitors: Is There a Common Pharmacophore? *Current Medicinal Chemistry.* 2000;7:1101–1112

De Vries E.F.J., van Waarde A., Buursma A.R., Vaalburg W. Synthesis and in vivo evaluation of ^{18}F-desbromo-DuP-697 as a PET tracer for cyclooxygenase-2 expression. *J Nucl Med.* 2003;44:1700–6

De Vries E.F.J., Doorduin J., Dierckx R.A., van Waarde A. Evaluation of [11C]rofecoxib as PET tracer for cyclooxygenase 2 overexpression in rat models of inflammation. *Nuclear Medicine and Biology.* 2008;35:35–42

Doble, A. The role of excitotoxicity in neurodegenerative disease: Implications for therapy. *Pharmacol. Ther.* 1999;81:163–221

Eisinger A.L., Prescott S.M., Jones D.A., Stafforini D.M. The role of cyclooxygenase-2 and prostaglandins in colon cancer. *Prostaglandins & Other Lipid Mediat.* 2007;82:147–154

Fletcher J.W., Djulbegovic B., Soares H.P., Siegel B.A., Lowe V.J., Lyman G.H., Coleman R.E., Wahl R., Paschold J.C., Avril N., Einhorn L.H., Suh W.W., Samson D., Delbeke D., Gorman M., and Shields A.F. Recommendations on the Use of ^{18}F-FDG PET in Oncology. *J Nucl Med.* 2008;49:480–508

Foss C.A., Mease R.C., Fan H., Wang Y., Ravert H.T., Dannals R.F., Olszewski R.T., Heston W.D., Kozikowski A.P., and Pomper M.G. Radiolabeled Small-Molecule Ligands for Prostate-Specific Membrane Antigen: In vivo Imaging in Experimental Models of Prostate Cancer. *Clin Cancer Res.* 2005;11:4022–4028

Garavito R.M., Malkowski M.G., DeWitt D.L. The structures of prostaglandin endoperoxide H synthases-1 and -2. *Prostaglandins Other Lipid Mediat.* 2002;68–69:129–52

Ghosh A., Heston W.D.W. Tumor target prostate specific membrane antigen (PSMA) and its regulation in prostate cancer. *J Cell Biochem.* 2004;91(3):528–39

Goodman Jr. O.B., Barwe S.P., Ritter B., McPherson P.S., Vasko A.-J., Keen J.H., Nanus D.M., Bander N.H., Rajasekaran A.K. Interaction of prostate specific membrane antigen with a highly specific antibody against the clathrin and the adaptor protein complex-2. *Int. J. Oncol.* 2007;31(5):1199–1203

Greene M.W., Tucker W.D. An improved gallium-68 cow. Int J Appl Radiat *Isot.*1961;12:62–63

Grün M., Lauer I., and Unger K.K. The synthesis of micrometer- and submicrometer-size spheres of ordered mesoporous oxide MCM-41. *Advanced Materials.* 1997;9(3):254–257

Hankey B.F., Feuer E.J., Clegg L.X., *et al.* Cancer surveillance series: interpreting trends in prostate cancer-part I: evidence of the effects of screening in recent prostate cancer incidence, mortality, and survival rates. *J Natl Cancer Inst.* 1999;91:1017–24

Hao G., Zhou J., Guo Y., Long M.A., Anthony T., Stanfield J., Hsieh J.-T., Sun X. A cell permeable peptide analog as a potential-specific PET imaging probe for prostate cancer detection. *Amino Acids.* 2011;41:1093–1101

Happel S., Streng R., Vater P., Ensinger W. Sr/Y separation by supported liquid membranes based on nuclear track micro filters. Radiat. Meas. 2003;36:761–766

Hara T., Kosaka N., and Kishi H. PET imaging of prostate cancer using carbon-11-choline. *J Nucl Med.*1998;39(6):990–5

Hawkey C.J. COX-2 inhibitors. *Lancet* 1999;353:307–14

Hillier S.M., Maresca K.P., Femia F.J., Marquis J.C., Foss C.A., Nguyen N., Zimmerman C.N., Barrett J.A., Eckelman W.C., Pomper M.G., Joyal J.L., and Babich J.W. Preclinical Evaluation of Novel Glutamate-Urea-Lysine Analogues That Target Prostate-Specific Membrane Antigen as Molecular Imaging Pharmaceuticals for Prostate Cancer. *Cancer Res.* 2009;69(17):6932–40

Holland J.P., Phil D., Sheh Y., and Lewis J.S. Standardized methods for the production of high specific-activity zirconium-89. *Nucl Med Biol.* 2009;36(7):729–739

Holland J.P., Divilov V., Bander N.H., Smith-Jones P.M., Larson S.M., and Lewis JS. ^{89}Zr-DFO-J591 for ImmunoPET of Prostate-Specific Membrane Antigen Expression In Vivo. *J Nucl Med.* 2010;51:1293–1300

Holland J.P., Williamson M. J., and Lewis J.S. Unconventional Nuclides for Radiopharmaceuticals. *Molecular Imaging.* 2010;9(1):1–20

Hsieh B.T., Ting G., Hsieh H.T., Shen L.H. Preparation of carrier-free yttrium-90 for medical applications by solvent extraction chromatography. Appl. Radiat. Isot. 1993:44:1473–1480

IAEA-TECDOC-1340, 2003. Manual for reactor produced radioisotopes

Ikeda M., Ochi R., Wada A., and Hamachi I. Supramolecular hydrogel capsule showing prostate specific antigen-responsive function for sensing and targeting prostate cancer cells. *Chem Sci*. 2010;1:491–498

Jackson G.E. and Byrne M.J. Metal Ion Speciation in Blood Plasma: Gallium-67-Citrate and MRI Contrast Agents. *J Nucl Med.* 1996;37:379-386

Ketring A.R., Ehrhardt G.J., Embree M.F., Bailey K.D., Tyler T.T., Gawenis J.A., Jurisson S.S., Engelbrecht H.P., Smith C.J., and Cutler C.S. Production and Supply of High Specific Activity Radioisotopes for Radiotherapy Applications. Alasbimn Journal 2003;19:Article N° AJ19-2

Kresge C.T., Leonowicz M.E., Roth W.J., Vartuli J.C., and Beck J.S. Ordered mesoporous molecular sieves synthesized by a liquid-crystal template mechanism.*Nature.* 1992;359:710–712

(a) Kularatne A.S., Wang K., Santhapuram H.K.R., and Low P.S. Prostate-Specific Membrane Antigen Targeted Imaging and Therapy of Prostate Cancer Using a PSMA Inhibitor as a Homing Ligand. *Mol Pharmaceutics*.2009;6(3):780–789

(b) Kularatne A.S., Zhou Z., Yang J., Post C.B., and Low P.S. Design, Synthesis, and Preclinical Evaluation of Prostate-Specific Membrane Antigen Targeted ^{99m}Tc-Radioimaging Agents. *Mol Pharmaceutics.* 2009;6(3):790–800

Lambert B., Cybulla M., Weiner S.M., Van De Wiele C., Ham H., Dierckx R.A., and Otte A. Renal Toxicity after Radionuclide Therapy. Radiation Research. 2004;161(5):607–611

Li Z., Barnes J.C., Bosoy A., Fraser Stoddart J., and Zink J.I. Mesoporous silica nanoparticles in biomedical applications. *Chem Soc Rev.* 2012;41:2590–2605

Maeda H., Sawa T., and Konno T. Mechanism of tumor-targeted delivery of macromolecular drugs, including the EPR effect in solid tumor and clinical overview of the prototype polymeric drug SMANCS. *J Controlled Release.* 2001;74:47–61

Malik N., Machulla H.J., Solbach C., Winter G., Reske S.N., and Zlatopolskiy B. Radiosynthesis of a new PSMA targeting ligand ([^{18}F]FPy-DUPA-Pep). *Appl Radiat Isotopes.* 2011;69(7):1014–1018

Malik N., Zlatopolskiy B., Machulla H.J., Reske S.N., and Solbach C. One pot radiofluorination of a new potential PSMA ligand [Al^{18}F]NOTA-DUPA-Pep. *J Label Compd Radiopharm.* 2012;55:320–325

McCarthy T.J., Sheriff A.U., Graneto M.J., Talley J.J., Welch M.J. Radiosynthesis, in vitro validation, and in vivo evaluation of ^{18}F-labeled COX-1 and COX-2 inhibitors. *J Nucl Med.* 2002;43:117–24

Meijs W.E., Herscheid J.D.M., Haisma H.J., Wijbrandts R., van Langevelde F., van Leuffen P.J., *et al.* Production of highly pure no-carrier added ^{89}Zr for the labelling of antibodies with a positron emitter. *Appl Radiat Isotopes.* 1994;45:1143–7

Meyer G.J., Mäcke H., Schuhmacher J., Knapp W.H., and Hofmann M. ^{68}Ga-labelled DOTA-derivatised peptide ligands. *Eur J Nucl Med Mol Imaging.* 2004;31:1097–1104

Moerlein S.M., Laufer P., and Stöcklin G. Effect of lipophilicity on the in vivo localization of radiolabelled spiperone analogues. *Int J Nucl Med Biol.* 1985;12(5):353–6

Nolting D.D., Nickels M.L, Guo N., Pham W. Molecular imaging probe development: a chemistry perspective. *Am J Nucl Med Mol Imaging.* 2012;2(3):273–306

Olson W.C., Heston W.D.W. and Rajasekaran A.K. Clinical Trials of Cancer Therapies Targeting Prostate-Specific Membrane Antigen. *Rev Recent Clin Trials.* 2007;2(3):182–190

Ostrov D.A. and Contag C.H. Molecular Imaging of Inflammation and Carcinogenesis. *Cancer Prev Res* 2011;4:1523–1526

Oyama N., Miller T.R., Dehdashti F., Kibel A.S., Michalski J.M., Fischer K.C., Picus J., Siegel B.A., Andriole G.L., Welch M.J. Carbon-11-acetate PET imaging of recurrent prostate cancer. *J Urol.* 2002;167(4):173–174

Oyama N., Ponde D.E., Dence C., Kim J., Tai Y.C., Welch M.J. Monitoring of therapy in androgen-dependent prostate tumor model by measuring tumor proliferation. *J Nucl Med.* 2004;45(3):519–525

Pascali C., Bogni A., Crippa F., and Bombardieri E. Concetti generali sulla produzione di Radiofarmaci emettitori di positroni. *Milano: Aretrè editore.*1999.

Peer D., Karp J.M., Hong S., Farokhzad O.C., Margalit R., and Langer R. Nanocarriers as an emerging platform for cancer therapy. *Nat Nanotechnol.* 2007;2:751–60

Perk L.R., Vosjan M.J.W.D., Visser G.W.M., Budde M., Jurek P., Kiefer G.E., and van Dongen G.A. M. S.*p*-Isothiocyanatobenzyl-desferrioxamine: a new bifunctional chelate for facile radiolabeling of monoclonal antibodies with zirconium-89 for immuno-PET imaging. *Eur J Nucl Med Mol Imaging.* 2010;37:250–259

Phelps M.E. PET: The Merging of Biology and Imaging into Molecular Imaging. *J NuclMed.* 2000;41:661–681

Ponsky L.E., Cherullo E.E., Starkey R., Nelson D., Neumann D., Zippe C.D. Evaluation of preoperative ProstaScint scans in the prediction of nodal disease. *Prostate Cancer Prostatic Dis.* 2002;5:132–135

Prabhakaran J., Majo V.J., Simpson N.R., Van Heertum R.L., Mann J.J., Kumar J.S.D. Synthesis of [C-11]celecoxib: a potential PET probe for imaging COX-2 expression. *J Label Compd Radiopharm.* 2005;48:887–95

Prenant C. and Crouzel C. A new simple and attractive method of [^{11}C]halogenomethanes production. *J Label Compd Radiopharm.* 1991;30:125–131

Price E.W., Cawthray J.F., Bailey G.A., Ferreira C.L., Boros E., Adam M.J., and Orvig C. H$_4$octapa: An Acyclic Chelator for ^{111}In Radiopharmaceuticals. *J. Am. Chem. Soc.* 2012;134:8670−8683

Radu D.R., Lai C.Y., Jeftinija K., Rowe E.W., Jeftinija S., Lin V.S.Y.A. Polyamidoamine Dendrimer-Capped Mesoporous Silica Nanosphere-Based Gene Transfection Reagent. *J. Am. Chem. Soc.* 2004;126:13216–13217

Rajasekaran, A.K, Anilkumar G., and Christiansen J.J. Is prostate-specific membrane antigen a multifunctional protein? *Am J Physiol Cell Physiol.* 2005;288(5):975–981

Ramogida C.F. and Orvig C. Tumour targeting with radiometals for diagnosis and therapy. *Chem. Commun.*2013;49:4720–4739

Robinson M.B., Blakelys R.D., Couto R., and Coyle J.T. Hydrolysis of the Brain Dipeptide N-Acetyl-L-aspartyl-L-glutamate. Journal of Biological Chemistry. 1987;262(25):14498–14506

Salutsky R. and Kirly M. Preparation and half-life of carrier-free yttrium-90. Anal. Chem. 1955;27:567–569.

Sandford G. Elemental fluorine in organic chemistry (1997–2006). *Journal of Fluorine Chemistry.* 2007;128(2):90–104

Schuhmacher J., Maier-Borst W. A new ^{68}Ge/^{68}Ga radioisotope generator system for production of ^{68}Ga in dilute HCl. *Int J Appl Radiat Isotopes.* 1981;32:31–36

Shannon R.D. Revised Effective Ionic Radii and Systematic Studies of Interatomie Distances in Halides and Chaleogenides. *Acta Cryst.* 1976; A32, 751–767

Shreve P.D., Grossman H.B., Gross M.D., Wahl R.L. Metastatic prostate cancer: initial findings of PET with 2-deoxy-2-[F-18]fluoro-D-glucose. *Radiology.* 1996;199(3):751–756

Shields A.F., Grierson J.R., Dohmen B.M., Machulla H.J., Stayanoff J.C., Lawhorn-Crews J.M., Obradovich J.E., Muzik O., and Mangner T.J. Imaging proliferation in vivo with [F-18]FLT and positron emission tomography. *Nature Medicine.* 1998;4(11):1334–1336

Shokeen M. and Wadas T.J. The development of Copper Radiopharmaceuticals for Imaging and Therapy. *Med Chem.* 2011;7:413–429

Sinusas A.J., Bengel F., Nahrendorf M., Epstein F.H., Wu J.C., Villanueva F.S., Fayad Z.A., and Gropler R.J. Multimodality Cardiovascular Molecular Imaging, Part I. *Circ Cardiovasc Imaging.* 2008;1:244–256

Skraba W.J., Arino H., Kramer H.H. A new 90Sr/90Y radioisotope generator. Int. J. Appl. Radiat. Isot. 1978 ;29 :91–96

Smith W.L., DeWitt D.L., and Garavito R.M. CYCLOXYGENASES: Structural, Cellular, and Molecular Biology. *Annu. Rav. Biochem.* 2000;69:145–82

Smith W.L. Nutritionally essential fatty acids and biologically indispensable cyclooxygenases.*Trends in biochemical sciences.* 2008;33(1):27–37

Soloviev D., Fini A., Chierichetti F., Al-Nahhas A., Rubello D. PET imaging with ^{11}C-acetate in prostate cancer: a biochemical, radiochemical and clinical perspective. European Journal of Nuclear Medicine and Molecular Imaging. 2008;35(5):942–949

Strickley R.G. Solubilizing Excipients in Oral and Injectable Formulations. Pharmaceutical Research. 2004;21(2):201–230

Townsend D.W. Physical principles and technology of clinical PET imaging. *Ann Acad Med Singapore.* 2004;33:133–145

Tricoli J.V., Schoenfeldt M., Conley B.A. Detection of prostate cancer and predicting progression: Current and future diagnostic markers. *Clin Cancer Res.* 2004;10:3943–53

Tsujii M., Kawano S., and Dubois R.N. Cyclooxygenase-2 expression in human colon cancer cells increases metastatic potential. Proc. Natl. Acad. Sci. USA 1997;94:3336–3340

Uddin J., Crews B. C., Ghebreselaise K., Huda I., Kingskey P.J., Sib Ansan M., Tantawy M.N., Reese J., Marnett L.J. Fluorinated COX-2 Inhibitors as Agents in PET Imaging of Inflammation and Cancer. *Cancer Prev. Res.* 2011;4:1536–1545

U.S. Department of Commerce, 1959. Maximum permissible body burden and maximum permissible concetrations of radionuclides in air and water for occupational exposure. National Bureau of Standards Handbook. 69, AFP 160-67, p.38

Vecchio A.J. and Malkowski M.G. The structure of NS-398 bound to cyclooxygenase-2. J Struct Biol. 2011;176(2):254–258

Verel I., Visser G.W.M., Boellaard R., Stigter-van Walsum M., Snow G.B., and van Dongen G.A.M.S. [89]Zr-immuno-PET: Comprehensive procedures for the production of 89Zr-labeled monoclonal antibodies. *J Nucl Med.* 2003;44:1271–81.

Vivero-Escoto J.L., Slowing I.I., Trewyn B.G., and Lin V.S.-Y. Mesoporous Silica Nanoparticles for Intracellular Controlled Drug Delivery. *Small.* 2010;6:1952–1967

Volterrani D., Erba P.A., Mariani G. Fondamenti di medicina nucleare: tecniche e applicazioni. Springer-Verlag Italia. 2010

Wadas T.J., Wong E.H., Weisman G.R., Anderson C.J. Coordinating Radiometals of Copper, Gallium, Indium, Yttrium and Zirconium for PET and SPECT Imaging of Disease. *Chem Rev.* 2010;110(5):2858–2902

Wei L., Zhang X., Gallazzi F., Miao Y., Jin X., Brechbiel M.W., Xu H., Clifford T., Welch M.J., Lewis J.S., and Quinn T.P. Melanoma Imaging using ^{111}In, [86]Y and ^{68}Ga labelled CHX-A´´-Re(Arg[11])CCMSH. Nucl Med Biol. 2009;36(4):345–354

Wike J.S., Guyer C.E., Ramey D.W., Phillps B.P. Chemistry for commercial scale production of yttrium-90 for medical research. Appl. Radiat. Isot. 1990;41:861–865

Winter G., Zlatopolskiy B., Kull T., Bertram J., Genze F., Cudek G., Machulla H.-J., and Reske S.N. ^{68}Ga-DOTA-DUPA-Pep as a new peptide conjugate for molecular imaging of prostate carcinoma. J Nucl Med 2011;52(Suppl 1):1597

Zarghi A. and Arfaei S. Selective COX-2 Inhibitors: A Review of Their Structure-Activity Relationships. *Iranian Journal of Pharmaceutical Research* 2011;10(4):655–683

Zeglis B.M. and Lewis J.S. A practical guide to the construction of radiometallated bioconjugates for positron emission tomography. Dalton Trans. 2011;40:6168–6195

Zhang Q., Liu F., Truc Nguyen K., Ma X., Wang X., Xing B., and Zhao Y. Multifunctional Mesoporous Silica Nanoparticles for Cancer-Targeted and Controlled Drug Delivery. *Adv Funct Mater.* 2012;22:5144–5156

Zhernosekov K.P., Filosofov D.V., Baum R.P., Aschoff P., Bihl H., Razbash A.A., Jahn M., Jennewein M., and Rösch F. Processing of Generator-Produced ^{68}Ga for Medical Application. *J Nucl Med.* 2007;48(10):1741–1748